CHEMICAL CHARACTERIZATION AND SOURCE APPORTIONMENT OF ORGANIC AEROSOL AT URBAN AND RURAL SITES IN THE SOUTHEASTERN UNITED STATES

Weruka Rattanavaraha

A dissertation submitted to the faculty of the University of North Carolina at Chapel Hill in partial fulfillment of the requirements for the degree of Doctor of Philosophy in the Department of Environmental Sciences and Engineering in the Gillings School of Global Public Health.

Chapel Hill
2016

Approved by:

Jason D. Surratt

Richard M. Kamens

Avram Gold

Kenneth G. Sexton

Manjula Canagaratna

ABSTRACT

Weruka Rattanavaraha: Chemical Characterization and Source Apportionment of Organic Aerosol at Urban and Rural Sites in the Southeastern United States
(Under the direction of Jason D. Surratt)

Atmospheric fine aerosol ($PM_{2.5}$) adversely affects human health and air quality as well as plays a critical role in Earth's climate. Organic aerosol (OA) contributes a substantial fraction to $PM_{2.5}$ mass. In order to investigate the formation, sources and behavior of OA in the Southeastern U.S., the Aerodyne Aerosol Chemical Speciation Monitor (ACSM) was deployed at a rural (Centreville, AL (CTR)) and an urban site (Jefferson Street (JST) in Atlanta, GA) for 1 year. The JST and CTR sites are part of the Southeastern Aerosol Research and Characterization (SEARCH) network. In addition to the continuous SEARCH measurements, high-volume filter samplers were periodically operated to collect $PM_{2.5}$, aiding in the identification of OA sources. At CTR, multilinear engine (ME-2) was applied to the yearlong OA mass spectral data in order to resolve OA sources. ME-2 resolved six factors: hydrocarbon-like organic aerosol (HOA), biomass burning organic aerosol (BBOA), low-volatility oxygenated organic aerosol (LV-OOA), semi-volatile oxygenated organic aerosol (SV-OOA), isoprene-epoxydiol organic aerosol (IEPOX-OA), and 91Fac. At JST, positive matrix factorization (PMF) and ME-2 were applied to yearlong and seasonal datasets to more clearly resolve certain OA sources and reasonably estimate mass contributions of each factor. The results indicate that the sum of LV-OOA and SV-OOA dominated the mass fraction of OA in all seasons (46-70%) at both sites. HOA was

higher at JST than CTR. BBOA contributed a larger fraction of OA in colder seasons at both sites, particularly at JST where BBOA was related to residential burning. At both sites, IEPOX and 91Fac were highest in summer and were associated with the atmospheric chemistry of isoprene emissions. Thus, the last project was conducted in summer at another urban site of the SEARCH network, Birmingham, AL (BHM), during the 2013 Southern Oxidant Aerosol Study (SOAS) in order to investigate the impact of anthropogenic pollution on isoprene-derived secondary organic aerosol (SOA). The results reveal a moderate correlation (r^2 = 0.57) of methacrylic acid epoxide and hydroxymethly-methyl-α-lactone-derived SOA tracers with nighttime nitrate radical production and strong correlation (r^2 = 0.72) with ozone during the daytime, confirming previous studies that anthropogenic pollutants enhance isoprene-derived SOA formation.

ACKNOWLEDGEMENTS

This dissertation could not have been accomplished without the supervision of Dr. Jason Surratt. I would like to express my immeasurable appreciation to him for his support, assistance and encouragement throughout my study at the UNC, Chapel Hill. Dr. Surratt is not only my wonderful advisor, but also my big brother who always gave a good care to me when we traveled together for the field studies. He is my role model on both characteristics of scientist and human being. I would also like to thank my dissertation committee members: Professor. Richard M. Kamens, Dr. Avram Gold, Dr. Kenneth G. Sexton and Dr. Manjula Canagaratna. I thank Prof. Kamens for inspiring me to pursue PhD. His vision emphasized me the importance of PhD study for my future career in my home country (Thailand). I am deeply thankful to Dr. Gold and Dr. Sexton for their insightful suggestions on both research and manuscript writing. I truly appreciate technical explanation about factor analysis techniques via detailed emails from Dr. Canagaratna. I would like to thank Dr. Zhenfa Zhang for making organic synthesis used in this dissertation.

I am gratitude to all of the great collaborators including: Dr. Eric Edgeton, Dr. Karsten Baumann, Jerry Brown, John Simpson, Dennis Stripling from Atmospheric Research & Analysis, Inc. (ARA), Dr. Phil Croteau from Aerodyne Research, Inc. (ARI), Fred Brechtel from Brechtel Manufacturing, Inc. (BMI), Dr. Stephanie Shaw and Dr. Eladio Knipping from Electric Power Research Institute (EPRI).

I am extremely thankful to Dr. Ying-Hsuan Lin for being my mentor, colleague, and best friend. I would like to thank Surratt/Turpin group members: Dr. Sri Hapsari Budisulistiorini, Dr. Matthieu Riva, Dr. Theran Riedel, Kevin Chu, Tianqu Cui, Sara Duncan, Xinxin Li, Maiko Arashiro, Vineet Raja Gopinathan, Tashana Detwiler, Yuzhi Chen, Hang Xu, Thais Barbosa, Michael Williams, Rachel Long and Hilary Green for their assistance and friendship. My student life was fulfilled with happiness because of them.

Special thanks to Jack Whaley and Wakefield Harper for providing very helpful information along the way to align my research plan with the graduation timeline. My appreciation is extended to all professors, staff and friends in the Department of Environmental Sciences and Engineering for making my learning experiences very memorable.

I acknowledge SCG Chemicals, Inc, Thailand for funding me to study at UNC, Chapel Hill and EPRI for funding research projects in this dissertation.

Finally, I would like to express my deepest gratitude to my family. Thanks my parents, Mr. Wirat and Mrs. Krongkaew Rattanavaraha for always being beside me no matter how hard the situation is. Thanks my life-time partner, Sarakorn Yoonton, for his unconditional love and support. Thanks my sister, Waranya Rattanavarha, and my brother, Weerapat Rattanavarha, for sharing many great things as we are sibling. My success story could not have been made without them.

TABLE OF CONTENTS

LIST OF TABLES

LIST OF FIGURES

LIST OF ABBREVIATIONS

ACSM	aerosol chemical speciation monitor
AMS	aerosol mass spectrometer
BBOA	biomass burning aerosol
BC	black carbon
BHM	Birmingham
BVOC	biogenic volatile organic compounds
CE	collection efficiency
CMB	chemical mass balance
COA	cooking organic aerosol
CTR	Centreville
DMA	differential mobility analyzer
EC	elemental carbon
GC/EI-MS	gas chromatography/electron ionization quadrupole mass spectrometry
HOA	hydrocarbon-like organic aerosol
IE	ionization efficiency
IEPOX	isoprene epoxydiols
JST	Jefferson Street

LRK	Look Rock
LV-OOA	low volatility oxygenated organic aerosol
LWC	liquid water content
NR-PM_1	non-refractory particulate matter with aerodynamic diameter less than 1 μm
OA	organic aerosol
OC	organic carbon
OM	organic matter
OOA	oxygenated organic aerosol
MCPC	mixing condensation particle counter
ME-2	multilinear engine
MFC	mass flow controllers
PM	particulate matter
PM_1	particulate matter with aerodynamic diameter less than 1 μm
$PM_{2.5}$	particulate matter with aerodynamic diameter less than 2.5 μm
PMF	positive matrix factorization
POA	primary organic aerosol
Q-AMS	quadrupole aerosol mass spectrometer
RF	response factor

RH	relative humidity
RIE	relative ionization efficiency
SEARCH	Southeastern Aerosol Research and Characterization
SEM	secondary electron multiplier
SEMS	scanning electrical mobility system
SOA	secondary organic aerosol
SOAS	Southern Oxidant Aerosol Study
SV-OOA	semi-volatile oxygenated organic aerosol
UPLC/ESI-HR-QTOFMS	ultra-performance liquid chromatography/electrospray ionization high-resolution quadrupole time-of-flight mass spectrometry
VOC	volatile organic compounds
WSOC	water-soluble organic carbon

CHAPTER I:
INTRODUCTION

Ambient fine aerosol ($PM_{2.5}$, aerosol with aerodynamic diameter $\leq$ 2.5 μm) and submicron aerosol (PM_1, aerosol with aerodynamic diameter $\leq$ 1 μm) play a key role in physical and chemical atmospheric processes. They influence climate patterns both directly, through the absorption and scattering of solar and terrestrial radiation, and indirectly, through cloud formation (Kanakidou et al., 2005). In addition to climatic effects, $PM_{2.5}$ and PM_1 has been demonstrated to pose a human health risk through inhalation exposure (Pope and Dockery, 2006; Hallquist et al., 2009). The composition of $PM_{2.5}$ and PM_1 is of particular interest due to the fact that different chemical constituents may cause unequal toxicity to human health as well as uncertain climatic effects. Organic material accounts for substantial fractions of $PM_{2.5}$ and PM_1, thus playing an important role in determining the aerosol chemical and physical properties (Seinfeld and Pankow, 2003; Kanakidou et al., 2005; Zhang et al., 2007). Organic aerosol (OA) is ubiquitous and can be emitted directly as primary organic aerosol (POA) and indirectly as secondary organic aerosol (SOA). The latter is formed the atmospheric oxidation of volatile organic compounds (VOCs), resulting in lower volatility products that either condense or undergo multiphase chemistry to produce SOA (Hallquist et al, 2009; Nozière et al., 2015). Depending upon location, approximately 50 – 85% of the total OA can be derived from SOA sources (Hallquist et al., 2009; Nozière et al., 2015). While major advances have been made in our knowledge of atmospheric SOA formation and evolution over the last decade (Nozière et al.,

2015), there remain significant uncertainties in these chemical processes that yield inaccurate estimates of atmospheric SOA levels (Nozière et al., 2015). Chemical characterization of atmospheric OA is needed in order to resolve exact sources and chemical processes. This will aid in the development of effective mitigation strategies for OA in order to address potential hazards in a cost-effective manner.

The Aerodyne Aerosol Chemical Speciation Monitor (ACSM) has been successfully used to measure temporal variations in non-refractory (NR)-PM_1 components, including OA, sulfate (SO_4^{2-}), nitrate (NO_3^-), ammonium (NH_4^+), and chloride (Cl^-) (Ng et al., 2010, 2011; Budisulistiorini et al., 2014; Parworth et al., 2015; Petit et al., 2015; Ripoll et al., 2015). In order to resolve sources of OA, positive matrix factorization (PMF) is typically applied to ACSM datasets, which is a bilinear unmixing model (Ulbrich et al., 2009; Zhang et al., 2011; Budisulistiorini et al., 2013). PMF is extremely useful in resolving the complex OA composition into a limited number of meaningful components that can be explained by the observed time and chemical variations in ambient OA (Zhang et al., 2011). However, mathematical deconvolution of an ACSM dataset by PMF may yield non-unique solutions in some cases due to the linear transformations referred as "rotations" of the factors (Ulbrich et al., 2009). Alternatively, multilinear engine (ME-2) was developed to overcome the rotational ambiguity of the solutions by constraining priori information of known profiles (Lanz et al., 2007; Canonaco et al., 2013). However, the constrained factors need to be carefully selected. PMF and ME-2 have been shown to be comparable for identification of the same major sources of OA (Ramadan et al., 2003; Frohlich et al., 2015).

To assign the OA sources (or subtypes) from either PMF or ME-2 analysis, OA factors extracted from factor analysis of ACSM mass spectral data are compared to lumped groups of

molecules that are linked to known tracers by similar sources or processes. PMF factors dominated by distinct ions at *m/z* 43 and 44 are typically associated with semi-volatile oxygenated OA (SV-OOA) and low-volatility OOA (LV-OOA), respectively, with the ion fraction at *m/z* 44 (f_{44}) increasing with age and oxidation state (Ng et al., 2010, 2011). High ion fractions at *m/z* 57 (f_{57}) is usually attributed to hydrocarbon-like organic aerosol (HOA) that represents OA from fossil fuel combustion, which is a type of POA, and is typically well correlated with known primary tracers such as elemental carbon (EC) and carbon monoxide (CO) (Zhang et al., 2005). PMF analysis of ACSM datasets has also resolved a POA subtype resulting from biomass burning emissions, which has been termed biomass burning OA (BBOA) (Aiken et al., 2008; Mohr et al., 2009; Ng et al., 2011; Canagaratna et al., 2015; Frohlich et al., 2015). The BBOA PMF factor has been shown to strongly correlate with molecular tracers of biomass burning, such as levoglucosan (Budisulistiorini et al., 2016). Recent studies have shown that SOA due to the acid-catalyzed multiphase chemistry of isoprene epoxydiols (IEPOX), which are predominant oxidation products of isoprene under low-NO_x conditions (Paulot et al., 2009), yields an abundant ion *m/z* 82 and is termed the IEPOX-OA factor (Lin et al., 2012; Budisulistiorini et al., 2013, 2015). The IEPOX-OA factor has been shown to strongly correlate with molecular tracers of IEPOX-derived SOA (Budisulistiorini et al., 2013, 2015, 2016). Recently, a new factor has been resolved from PMF of ACSM datasets that is associated with SOA produced from the atmospheric oxidation of isoprene under low-NO_x conditions that involves isoprene-derived hydroxyhydroperoxides (Riva et al., 2016). This new PMF factor yields a prominent ion at *m/z* 91 (Budisulistiorini et al., 2013, 2015; Hu et al., 2014) and has been termed the 91Fac (Robinson et al., 2011; Budisulistiorini et al., 2013, 2015). The elemental compositions of OA have also been observed to provide useful constraints on OA sources

(Canagaratna et al., 2015). For example, LV-OOA has been reported to have oxygen-to-carbon atomic ratios (O:C) approaching 1 (DeCarlo et al., 2010), while SV-OOA has been reported to have lower O:C ratios (~0.5) (Canagaratna et al., 2015). POA, such as HOA, tends to have O:C ratios less than 0.2 (Aiken et al., 2008; Ng et al., 2011; Zhang et al., 2011).

At around 600 Tg emitted per year into the atmosphere, isoprene (2-methyl-1,3-butadiene, C_5H_8) is the most abundant volatile non-methane hydrocarbon (Guenther et al., 2012). The abundance of isoprene is particularly high in the southeastern U.S. due to emissions from broadleaf deciduous tree species (Guenther et al., 2006). Research over the last decade has revealed that isoprene, via hydroxyl radical (OH)-initiated oxidation, is a major source of SOA (Claeys et al., 2004; Edney et al., 2005; Kroll et al., 2005 ; Kroll et al., 2006; Surratt et al., 2006; Lin et al., 2012; Lin et al., 2013a). In addition, it is known that SOA formation is enhanced by anthropogenic emissions, namely oxides of nitrogen (NO_x) and sulfur dioxide (SO_2), that are a source of acidic aerosol onto which photochemical oxidation products of isoprene are reactively taken up to yield a variety of SOA products (Edney et al., 2005; Kroll et al., 2006; Surratt et al., 2006; Surratt et al., 2007b; Surratt et al., 2010; Lin et al., 2013b, 2014) .

Previous work has begun to elucidate some of the critical intermediates of isoprene oxidation that lead to SOA formation through acid-catalyzed heterogeneous chemistry (Kroll et al., 2005; Surratt et al., 2006). Under low-NO_x conditions, such as in a pristine environment, multiple isomers of isoprene epoxydiols (IEPOX) have been demonstrated to be critical to the formation of isoprene SOA (Paulot et al., 2009; Bates et al., 2014). On advection of IEPOX to an urban environment and mixing with anthropogenic emissions of acidic sulfate aerosol, SOA formation is enhanced (Surratt et al., 2006; Lin et al., 2012; Lin et al., 2013b). This pathway has been shown to yield 2-methyltetrols as major SOA constituents of ambient $PM_{2.5}$ (Claeys et al,

2004; Surratt et al., 2010; Lin et al., 2012). Further work has revealed a number of additional IEPOX-derived SOA tracers, including C_5-alkene triols (Wang et al., 2005; Lin et al., 2012), *cis*- and *trans*-3-methyltetrahydrofuran-3,4-diols (3-MeTHF-3,4-diols) (Lin et al., 2012; Zhang et al., 2012), IEPOX-derived organosulfates (OSs) (Surratt et al., 2010; Lin et al., 2012), and IEPOX-derived oligomers (Lin et al., 2014). Some of the IEPOX-derived oligomers have been shown to contribute to aerosol components known as brown carbon that absorb light in the near ultraviolet (UV) and visible ranges (Lin et al., 2014). Under high-NO_x conditions, such as encountered in an urban environment, isoprene is oxidized to methacrolein and SOA formation occurs via the further oxidation of methacrolein (MACR) (Kroll et al., 2006; Surratt et al., 2006) to methacryloyl peroxynitrate (MPAN) (Chan et al., 2010; Surratt et al., 2010; Nguyen et al., 2015). It has recently been shown that when MPAN is oxidized by OH it yields at least two SOA precursors, methacrylic acid epoxide (MAE) and hydroxymethyl-methyl-α-lactone (HMML) (Surratt et al., 2006; Surratt et al., 2010; Lin et al., 2013a; Nguyen et al., 2015). Whether SOA precursors are formed under high- or low-NO_x conditions, aerosol acidity is a critical parameter that enhances the reaction kinetics through acid-catalyzed reactive uptake and multiphase chemistry of either IEPOX or MAE/HMML (Surratt et al., 2007b; Surratt et al., 2010; Lin et al., 2013b). In addition to MACR, other key oxidation products of isoprene, including glycolaldehyde, methylglyoxal, and hydroxyacetone, can undergo multiphase chemistry to yield their respective OS derivatives (Olson et al., 2011; Schindelka et al. 2013; Shalamzari et al., 2013; Noziere et al., 2015). However, the contribution of isoprene on the glyoxal-, methylglyoxal-, and hydroxyacetone-derived OS mass concentrations in the atmosphere remains unclear since these SOA tracers can also be formed from a wide variety of biogenic and anthropogenic precursors (Galloway et al., 2009, Liao et al., 2015).

Due to the large emissions of isoprene, an SOA yield of even 1% would contribute significantly to ambient SOA (Carlton et al., 2009; Henze et al., 2009). This conclusion is supported by measurements showing that up to a third of total fine OA mass can be attributed to IEPOX-derived SOA tracers in Atlanta, GA (JST) and Look Rock, TN (LRK) during summer months (Budisulistiorini et al., 2013, 2015, 2016). A field study in Yorkville, GA (YRK), similarly found that IEPOX-derived SOA tracers comprised 12-19% of the fine OA mass (Lin et al., 2013b). Another field site at Centreville, Alabama (CTR) during the Southern Oxidant and Aerosol Study (SOAS) revealed IEPOX-SOA contributed 18% of total OA mass (Xu et al., 2015). The individual ground sites corroborate recent aircraft-based measurements made in the Studies of Emissions and Atmospheric Composition, Clouds, and Climate Coupling by Regional Surveys (SEAC4RS) aircraft campaign, which estimated an IEPOX-SOA contribution of 32% to OA mass in the southeastern U.S. (Hu et al., 2015).

It is clear from the field studies discussed above that particle-phase chemistry of isoprene-derived oxidation products plays a large role in atmospheric SOA formation. However, much remains unknown regarding the exact nature of its formation, limiting the ability of models to accurately account for isoprene SOA (Carlton et al., 2010b; Foley et al., 2010). Currently, traditional air quality models in the southeastern U.S. do not incorporate detailed particle-phase chemistry of isoprene oxidation products (IEPOX or MAE/HMML) and generally under-predict isoprene SOA formation (Carlton et al., 2010a). Recent work demonstrates that incorporating the specific chemistry of isoprene epoxide precursors into models increases the accuracy of isoprene SOA predictions (Pye et al., 2013; Karambelas et al., 2014; McNeilll., 2015), suggesting that understanding the formation mechanisms of biogenic SOA, especially with regard to the effects of anthropogenic emissions, such as NO_x and SO_2, will be key to more accurate models. More

accurate models are needed in order to devise cost-effective control strategies for reducing $PM_{2.5}$ levels. Since isoprene is primarily biogenic in origin, and therefore not controllable, the key to understanding the public health and environmental implications of isoprene SOA lies in resolving the effects of anthropogenic pollutants.

The objectives of this dissertation are to chemically characterize OA constituents and apportion submicron OA in the southeastern U.S. to specific sources. Chapters II and III describe the deployment of the ACSM at a rural site (CTR) and an urban site (JST), respectively, in order to investigate NR-PM_1 in near-real time. ME-2 analysis is applied to the yearlong CTR dataset to resolve the potential sources of OA, whereas PMF and ME-2 are applied to the yearlong and seasonal ACSM datasets at JST in order to clearly resolve the complexity of OA sources in an urban area. The results of Chapters II and III suggest higher IEPOX-OA loadings warmer months, especially in summer, indicating that photochemistry and/or multiphase chemical reactions yield substantial amounts of isoprene-derived SOA. Chapter IV presents results from an intensive field study conducted in summer at the Birmingham, AL (BHM) ground site during the 2013 SOAS campaign in order to investigate the impact of anthropogenic pollution on isoprene-derived SOA. Finally, Chapter V summarizes the conclusions from this dissertation and suggests future work.

CHAPTER II:
SOURCE APPORTIONMENT OF SUBMICRON ORGANIC AEROSOL COLLECTED FROM CENTREVILLE, ALABAMA, DURING 2015-2016 USING THE AEROSOL CHEMICAL SPECIATION MONITOR (ACSM)[1]

2.1 Overview

Over the last 5 years, a number of ACSMs have been deployed for long-term measurements of NR-PM_1 at several locations around the world, including urban areas such as New York City, USA (Ng et al., 2011), Beijing, China (Sun et al., 2012), Santiago, Chile (Carbone et al., 2013), Atlanta, USA (Budisulistiorini et al., 2013, 2016), Helsinki, Finland (Aurela et al., 2015), Paris, France (Petit et al., 2015) and London, England (Reyes-Villegas et al., 2016) as well as continental background sites in South Africa (Tiitta et al., 2014), in the Southern Great Plains, USA (Parworth et al., 2015), in the western Mediterranean Basin (Ripoll et al., 2015), and in the Great Smoky Mountains National Park, USA (i.e., Look Rock) (Budisulistiorini et al., 2015, 2016). The ACSM has the major advantage of providing long-term chemical characterization of NR-PM_1 and resolution of OA sources over the high-resolution aerosol mass spectrometer (HR-AMS), since it is cheaper to operate over longer timescales and does not require continuous attention from site managers (Ng et al., 2011). Thus, the objective of this study was to deploy the ACSM for 1 year in order to continuously chemically characterize submicron OA in a rural area of the Southeastern U.S. (CTR) and to identify sources of OA by seasons.

[1] To be submitted to Atmospheric Environment.

2.2 Experimental Section

2.2.1 Site description

The CTR site (32.90ºN, 87.23ºW) located in Bibb County, AL, is one of the designated rural sites affiliated with the Southeastern Aerosol Research and Characterization (SEARCH) network (Hansen et al., 2003; Solomon et al., 2003; Edgerton et al., 2006). This site is located in a large field and is surrounded by dense forest (Figure 2-1). As a result, the CTR site would likely experience large biogenic volatile organic compound (BVOC) emissions, including isoprene and monoterpenes and their subsequent photochemical oxidation products (Hagerman et al., 2007). Potential anthropogenic emission sources are approximately within 110 km radius of the sampling site, including Montgomery, AL (southeast of CTR), Birmingham, AL (northeast of CTR), and Tuscaloosa, AL (northwest of CTR).

2.2.2 Real-time monitoring by ACSM

The Aerodyne ACSM was deployed at the CTR site to continuously measure NR-PM_1 at a time resolution of 30 minutes for 1 year (March 16, 2015 – March 02, 2016). ACSM sampling methods and operating details have been previously described (Budisulistiorini et al., 2013, 2014, 2016). During the sampling, the diagnostics in the ACSM were routinely checked. The ACSM inlet sampling flow and ionization efficiency (IE) were calibrated every season during the study. Ionizer and electronic offset were tuned depending on the diagnostics to ensure the appropriate conditions. The particle collection efficiency (CE) was determined following the approach described by Middelbrook et al. (2012). Detailed mass calculations of aerosol constituents by the ACSM have been previously described (Ng et al., 2011). All data were reported in local time (Central Standard Time, CST).

2.2.3 ME-2 analysis

ME-2 was applied in this study by adding *a priori* information of well-known profiles into the model (Paatero et al., 2002). The source finder (SoFi, Canonaco et al., 2013) tool version 4.8 for Igor Pro (Wave Metrics Inc., Lake Oswego, OR) was used for ME-2 analysis. *A priori* information of OA source mass spectra was introduced into the model using the *a* value technique in ME-2 (Crippa et al., 2014). The yearlong OA data from the ACSM was analyzed by ME-2 using three factor-constrained scenarios. Scenario 1 constrained HOA, BBOA, IEPOX-OA, and 91Fac with ME-2. This is the intensive constraint because none of the previous studies has done the SOA (IEPOX-OA and 91Fac) constrained with ME-2 (Canonaco et al., 2013; Reyes-Villegas et al., 2016). Scenario 2 constrained HOA, BBOA and IEPOX-OA with ME-2 due to the fact that IEPOX-OA is well-known to relate with isoprene-derived SOA under low-NO_x conditions, which were conditions thought to occur at CTR, and observed at in many areas in southeastern U.S. (Ng et al., 2011; Budisulistiorini et al., 2013, 2014, 2015, 2016; Xu et al., 2015). The last scenario (Scenario 3) constrained only HOA and BBOA, which is consistent with suggestions from previous studies that only POA should be constrained with ME-2 (Canonaco et al., 2013; Reyes-Villegas et al., 2016). Several *a* values (ranging from 0.05 up to 1) were performed to investigate the reasonable deviation of constrained factors from reference mass spectra. Crippa et al. (2014) demonstrated that an *a* value of 0.3 for BBOA yielded reasonable freedom in ME-2 based on the sensitivity analysis of the *a*-value approach with 25 AMS datasets. Mean BBOA mass spectra taken from Ng et al. (2011) were the main reference mass spectra to determine BBOA in this study. Detailed analysis of ME-2 are described elsewhere (Canonaco et al., 2013; Crippa et al., 2014). It is worth noting that SOA components were not

constrained with ME-2 in Sceanrio 3, consistent with prior work (Canonaco et al., 2013, Crippa et al., 2014).

2.2.4 Measurements of SOA tracers

A high-volume aerosol filter sampler was scheduled every third day to collect ambient $PM_{2.5}$ at 1 m^3 min^{-1} for 24 hours on pre-baked Tissuquartz^{TM} filters (8 x 10 in, Pall Life Sciences). Detailed operation of the high-volume $PM_{2.5}$ sampler is described elsewhere (Budisulistiorini et al., 2015; Riva et al., 2015; Rattanavaraha et al., 2016). These filters were extracted and analyzed by gas chromatography/election ionization quadrupole mass spectrometry (GC/EI-MS). Detailed filter extraction protocols and GC/EI-MS operating procedures have been previously described by Rattanavaraha et al. (2016).

Extraction efficiency was determined by analyzing 3 pre-baked filters spiked with 50 ppmv of 2-methyltetrols, 2-methylglyceric acid, levoglucosan, and *cis*- and *trans*-3-MeTHF-3,4-diols. Extraction efficiency was above 95% and used to correct the quantification of samples. Extracted ion chromatograms (EICs) of *m/z* 262, 219, 231 were used to quantify the *cis*-/*trans*-3-MeTHF-3,4-diols, 2-methyltetrols and 2-methylglyceric acid, and C_5-alkene triols, respectively (Surratt et al., 2006). 2-Methyltetrols, 3-MeTHF-3,4-diol isomers, and 2-methylglyceric acid were quantified using authentic standards synthesized in-house; synthetic procedures for these isoprene-derived SOA tracers are described elsewhere (Budisulistiorini et al., 2015; Rattanavaraha et al., 2016; Zhang et al., 2012). Levoglucosan was quantified using 1,6-anhydro-β-D-glucose (99%, Sigma-Aldrich) as an authentic standard. C_5-alkene triols were quantified using the average response factor of the 2-methyltetrols as a surrogate.

2.2.5 Collocated measurements

SEARCH provided a suite of additional instruments at the CTR site that measured meteorological and chemical variables, including temperature, relative humidity (RH), trace gases (i.e., CO, O_3, SO_2, NO_x, and NH_3), and continuous PM monitoring (Budisulistiorini et al., 2013, 2014, 2016; Hu et al., 2015; Xu et al., 2015; Rattanavaraha et al., 2016). Detailed descriptions of the collocated instruments can be found in Hansen et al. (2003) and Edgerton et al. (2006). Unfortunately, measurement of planetary boundary layer (PBL) height was not available at the site during this study. Therefore, only absolute diurnal patterns of constitutes of interest will be shown in Section 2.3 without taking into account the effects of PBL height evolution. O:C was calculated using the methods described by Canagaratna et al. (2015).

During the ACSM deployment at CTR, the Talladega National Forest, Oakmulgee District, reported prescribed burns around the sampling site. These reports of prescribed burns were used in interpreting trends in OA sources resolved by ME-2 analyses.

2.3 Results and discussion

2.3.1 Overview of measurements

The yearlong ACSM measurement period at CTR extended from March 20, 2015 through March 02, 2016, capturing NR-PM_1 component concentrations and OA sources across spring 2015, summer 2015, fall 2015, and winter 2016. Table 2-1 lists the exact dates that ACSM measurements were collected during each season. Temporal variations of meteorological data, trace gases, NR-PM_1 component concentrations, and SOA tracers are illustrated in Figure 2-2. Descriptive statistics of the measurements are summarized in Table 2-2 by season.

Regarding the preliminary collocated data from SEARCH (level 0, unpublished), the average temperature was highest in summer (25.3 $\pm$ 4.3 ºC) and lowest in winter (10.5 $\pm$ 6.9 ºC).

RH varied by seasons with the lowest in winter (68.8 ± 15.3%). Rainfall occurred intermittently on average less than 0.01 inches per day. The average concentrations of CO and NO_x were highest in winter compared to other seasons, suggesting that either higher combustion-related emissions occurs in Centreville during winter or lower PBL heights that would concentrate these primary pollutants. Ozone (O_3) and SO_2 remained fairly constant over all seasons. NR-PM_1 mass concentrations as measured by the ACSM were highest in summer (7.9 ± 3.4 $\mu g\ m^{-3}$ on average) and lowest in spring (2.9 ± 1.8 $\mu g\ m^{-3}$ on average). As shown in Table 2-2, average concentrations of OA were highest in summer (5.9 ± 2.9 $\mu g\ m^{-3}$) and lowest in spring (1.8 ± 1.3 $\mu g\ m^{-3}$). Higher OA loadings in summer suggest that photochemistry and/or multiphase chemical reactions yield substantial amounts of SOA, consistent with the high concentrations of IEPOX-derived SOA tracers (427.5 ± 424.5 ng m^{-3}) during the same period. Meanwhile, high loadings of OA in winter were influenced by some spikes of OA, as shown in Figure 2-2c, associated with the highest concentrations of levoglucosan (226.2 ± 204.5 ng m^{-3}), suggesting some local sources of BBOA emissions. During summer, the average SO_4^{2-} concentration was 1.3 ± 0.6 $\mu g\ m^{-3}$, making it the largest inorganic component during this season. The average NO_3^- was unchanged throughout the year. The average NH_4^+ concentration was highest in summer (0.4± 0.2 $\mu g\ m^{-3}$), meanwhile, with slightly lower levels (0.2±0.1 $\mu g\ m^{-3}$) observed in spring, fall and winter. Cl^- was present at low levels throughout the year.

As shown in Table 2-2, the mean concentrations of IEPOX-derived SOA tracers measured from high-volume aerosol filters were significantly higher (*t-test, p-value < 0.05*) in summer (427.5 ± 424.5 ng m^{-3}) than spring (159.1 ± 209.1 ng m^{-3}) and fall (53.8 ± 55.3 ng m^{-3}). IEPOX-derived SOA tracers was present at low levels (0.9 ± 1.8 ng m^{-3}) in winter. Individual IEPOX-derived SOA tracers measured by GC/EI-MS are summarized in Table 2-3. Levoglucosan was

measured as an OA tracer for fresh biomass burning. The average mass concentrations of levoglucosan during winter (226.2 $\pm$ 204.5 ng m^{-3}) was much higher than other seasons.

2.3.2 OA factors resolved by yearlong ME-2 analysis

ME-2 was applied to the yearlong OA mass spectral dataset collected by the ACSM. Three scenarios of factors constrained were conducted: Scenario 1 had HOA, BBOA, IEPOX-OA and 91Fac constrained; Scenario 2 had HOA, BBOA and IEPOX-OA constrained; and Scenario 3 had only HOA and BBOA constrained. The diagnostics plots of each scenario are shown in Figures 2-3 – 2-5. The Person correlation (R) of ME-2 analysis of yearlong factors derived using these three factor-constrained scenarios with collocated measurement, reference mass spectra and SOA tracers are shown in Table 2-4. The factors resolved from ME-2 show stronger correlations (R = 0.60 - 0.98) with its respective mass spectra in Scenario 1 than in Scenario 2 (R = 0.74 – 0.90) and Scenario 3 (R = 0.69 – 0.96). Scenario 1 and Scenario 3 show the strongest correlations between IEPOX-OA and IEPOX-derived SOA tracers (R = 0.82), whereas moderate correlation between IEPOX-OA and IEPOX-derived SOA tracers (R = 0.46) was observed in Scenario 2. Scenario 1 also has the strongest correlation between BBOA and levoglucosan (R = 0.56) compared to Scenario 2 (R = 0.26) and Scenario 3 (-0.46). Additional comparisons of factor mass spectra resolved from three factor-constrained scenarios were investigated to estimate the uncertainties of ME-2 solutions as shown in Figures 2-6 and 2-7. Similar mass spectra of resolved factors from three scenarios (Figure 2-6) associated with mean values and error bars (Figure 2-7) suggest that these three scenarios eventually resolved near-identical factor profiles. The *a* values of 0.1, 0.2 and 0.3 were selected after trial and error according to previous studies (Lanz et al., 2008; Crippa et al., 2014; Petit et al., 2014; Reyes-Vilegas et al., 2016) to reasonably allow the flexible deviations from the target-profiles. Figure 2-8 shows that *a*-value

of 0.3 yields comparable factor contributions across scenarios. Therefore, Scenario 1, HOA/BBOA/IEPOX-OA/91Fac constrained with ME-2 using an *a*-value of 0.3 was selected as an optimum solution of the yearlong CTR dataset because it provided the best correlations with collocated measurements, reference mass spectra and SOA tracers, while still allowing a near-constant solution across scenarios.

As shown in Figure 2-9, SV-OOA was the dominant a major fraction (28%) of total OA from the yearlong CTR analysis, followed by LV-OOA (21%). The O:C ratios of LV-OOA found at CTR (1.48 on average) was higher than SV-OOA (0.75), consistent with other ambient LV-OOA and SV-OOA reported by Canagaratna et al. (2015). Due to the fact that SV-OOA is a surrogate of fresh OOA, SV-OOA has a tendency to form locally and correlates well with NO_3^- (R = 0.69). IEPOX-OA and 91Fac contributed similar levels (14% and 15%, respectively). The average HOA concentration was 0.29 μg m^{-3} (10% of total OA), which is close to detection limit of ACSM (0.20 μg m^{-3}) (Ng et al., 2010). Due to the fact that HOA might be low (approaching detection limits of the ACSM) in rural areas, PMF was unable to resolve HOA at CTR during a previous study occurring during the 2013 SOAS campaign (Xu et al., 2015) as well as other rural areas including Yorkville, GA (YRK) (Xu et al., 2015) and Look Rock, TN (LRK) (Budisulistiorini et al., 2015; 2016). BBOA had the lowest contribution (7% of total OA) at CTR. The moderate correlation (R = 0.56) between BBOA and levoglucosan suggested that BBOA may not be homogenously present throughout the year. The investigation of BBOA associated with local prescribed burns is discussed in Section 2.3.4.

The diurnal cycle of each factor is shown in Figure 2-10. HOA increased during the night and decreased during the day (Figure 2-10a), suggesting that PBL dynamics played an important role of HOA distribution as well as possible transport from urban areas located in AL. The

median diurnal trend of BBOA is flat (Figure 2-10b), whereas the mean diurnal trends increased around 2 PM. The latter suggests the likely effects of occasional local BBOA sources. The detailed discussion about BBOA and local prescribed burns is provided in Section 2.3.4 below. LV-OOA does not show large variations in its diurnal trend (Figure 2-10C), which suggests a regional origin. SV-OOA (Figure 2-10d) and IEPOX-OA (Figure 2-10e) showed a small peak during 1 – 3 PM, which could be related to the photochemistry and subsequent SOA formation processes occurring in the local area. 91Fac increased at night, suggesting the possible role of PBL dynamics (Figure 2-10f) or other sources besides isoprene-derived SOA through a non-IEPOX route. Previous work by Xu et al. (2015) suggested that this factor could be related to nighttime oxidation chemistry of monoterpenes leading to SOA. The average diurnal profile of 91Fac was similar to SV-OOA, which could be related to fresh OA including local isoprene-derived hydroperoxides condensing into aerosol as recently shown by Krechmer et al. (2015) and Riva et al. (2016) at CTR, AL, and Look Rock, TN sites, respectively, or derived from the night time oxidation chemistry of monoterpenes (Xu et al., 2015).

2.3.3 Seasonal comparison of OA factors

Regarding the yearlong ME-2 analyses of ACSM OA mass spectral data collected at CTR, temporal variations were observed by separating yearlong results to seasonal periods. The exact dates during each season are listed in Table 2-1 and were derived from the Farmer's Almanac. As shown in Table 2-2, HOA is highest in summer (0.41 + 0.30 μg m^{-3}) compared to all other seasons (0.14 – 0.23 μg m^{-3} on average). BBOA is highest in winter (0.39 + 1.10 μg m^{-3}) and is associated with the prescribed burns, as discussed in the in Section 2.3.4. Higher IEPOX-OA, 91Fac and SV-OOA loadings in summer suggest that photochemistry and/or multiphase chemical reactions yield substantial amounts of SOA compared to all other seasons. LV-OOA

was slightly higher in fall (2.16 μg m^{-3}) than summer (2.03 μg m^{-3}), potentially suggesting that some SOA in summer and long-distance SOA from other sites may age and carry over to fall season at CTR. LV-OOA represents a highly-aged (oxidized) OA from various sources. Identifying the exact sources of LV-OOA remains a significant challenge and should continue to be the focus of future work.

2.3.4 Effects of prescribed burns to OA apportionment

Notably, the occurrence of prescribed burning events has been detected by the ACSM, as indicated by dramatic peaks in the OA time series (Figure 2-2c). In order to investigate the effects of prescribed burns on the OA apportionment, the yearlong dataset was separately analyzed by ME-2 in two cases: with and without spike peaks. The results showed that both cases provided similar source apportionment of OA, suggesting that the effect of prescribed burns was not significant relative to the background OA at CTR in 2015. This is likely due to the low frequency of prescribed burning events with the added requirement of the appropriated wind direction needed to carry OA from burning sources to the sampling site.

Seven prescribed burns during 2015-2016 are examined here. Dates, burning locations, wind speeds and wind directions are shown in Figure 2-11. Note that the dates of prescribed burns agree with the dates of spike peaks of OA shown in Figure 2-2c. The ACSM data was divided into two cases: one focusing only on the data of spike peaks denoted as prescribed burn events, the other referred to the rest of data as reference periods. The two cases were separately analyzed by ME-2 with BBOA constrained to observe the source apportionment. The results showed that prescribed burn events contributed higher BBOA (23%) compared to the reference periods (9%) to the total OA as shown in Figure 2-12. The correlation between BBOA and levoglucosan during prescribed burn events ($R = 0.95$, $n = 4$) is much higher than the reference

periods (R = 0.07, n = 60), indicating that the ACSM has the capability to capture fresh BBOA during prescribed events. On the other hand, the reference periods may contain aged BBOA from various sources over a year. The BBOA time series during prescribed burn events is well correlated with CO (R = 0.75, n = 203), confirming the presence of combustion trace gases. Future work is needed to understand how aged biomass burning might contribute to the BBOA loadings resolved from ME-2 analyses during the non-prescribed burning events, especially since BBOA during these times doesn't correlate well with levoglucosan. Recent work has shown that fresh BBOA tracers, like levoglucosan, can easily degrade in the atmosphere due to further oxidation (Kessler et al., 2010).

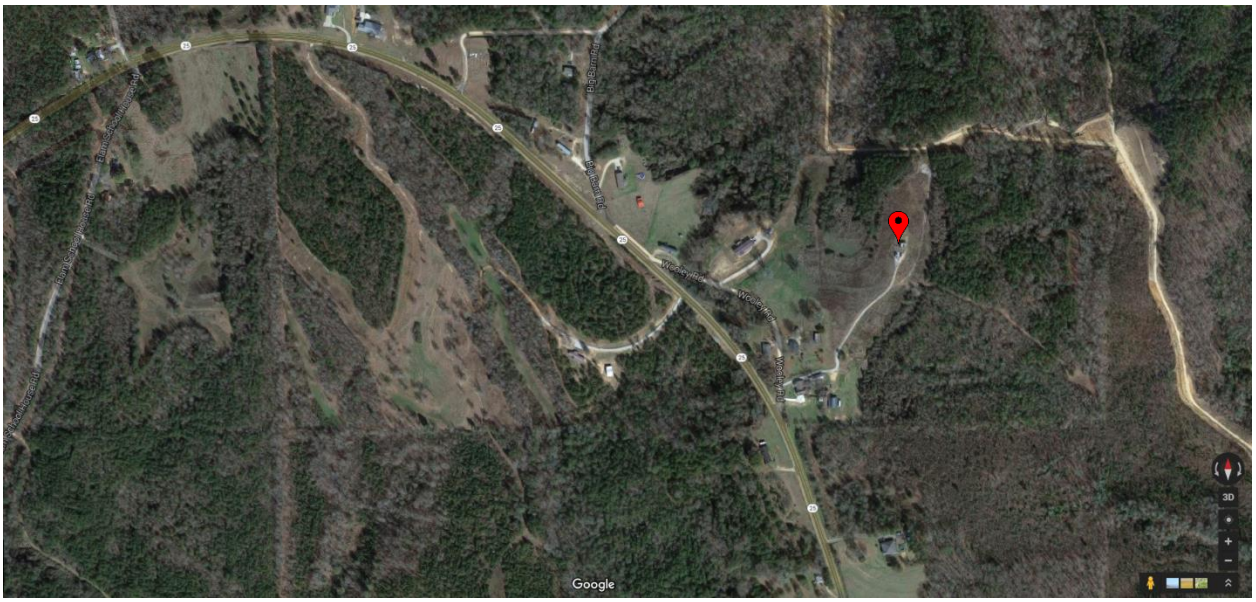

Figure 2-1. Map of the CTR site (red mark) adopted from Google Earth on July 10, 2016.

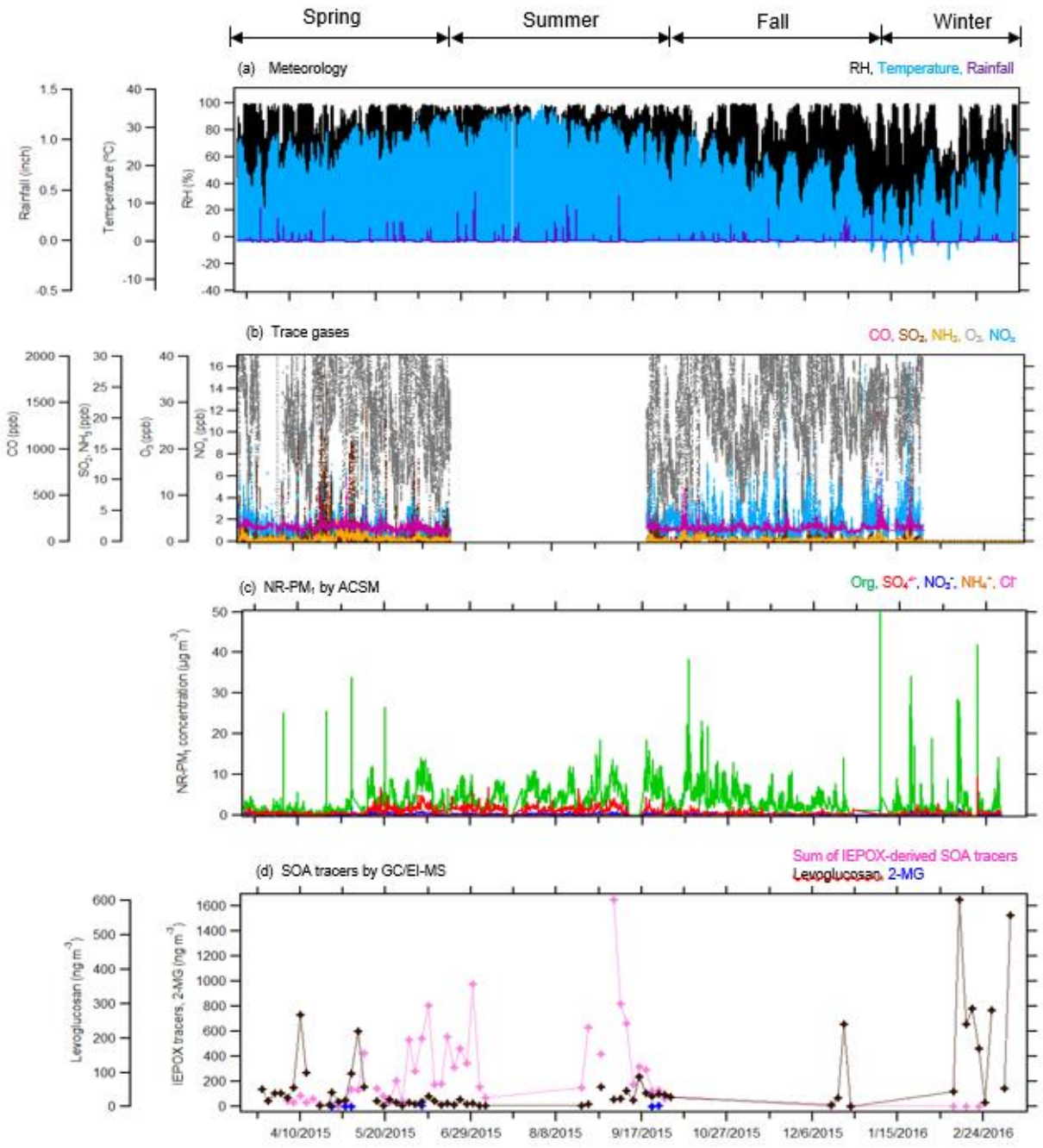

Figure 2-2. Temporal variation of (a) meteorological data, (b) trace gases, (c) NR-PM_1 measured by ACSM and (d) SOA tracers detected from high-volume $PM_{2.5}$ filter samples using GC/EI-MS at the CTR site. Seasonal scales set from using 2015 The Old Farmer's Almanac.

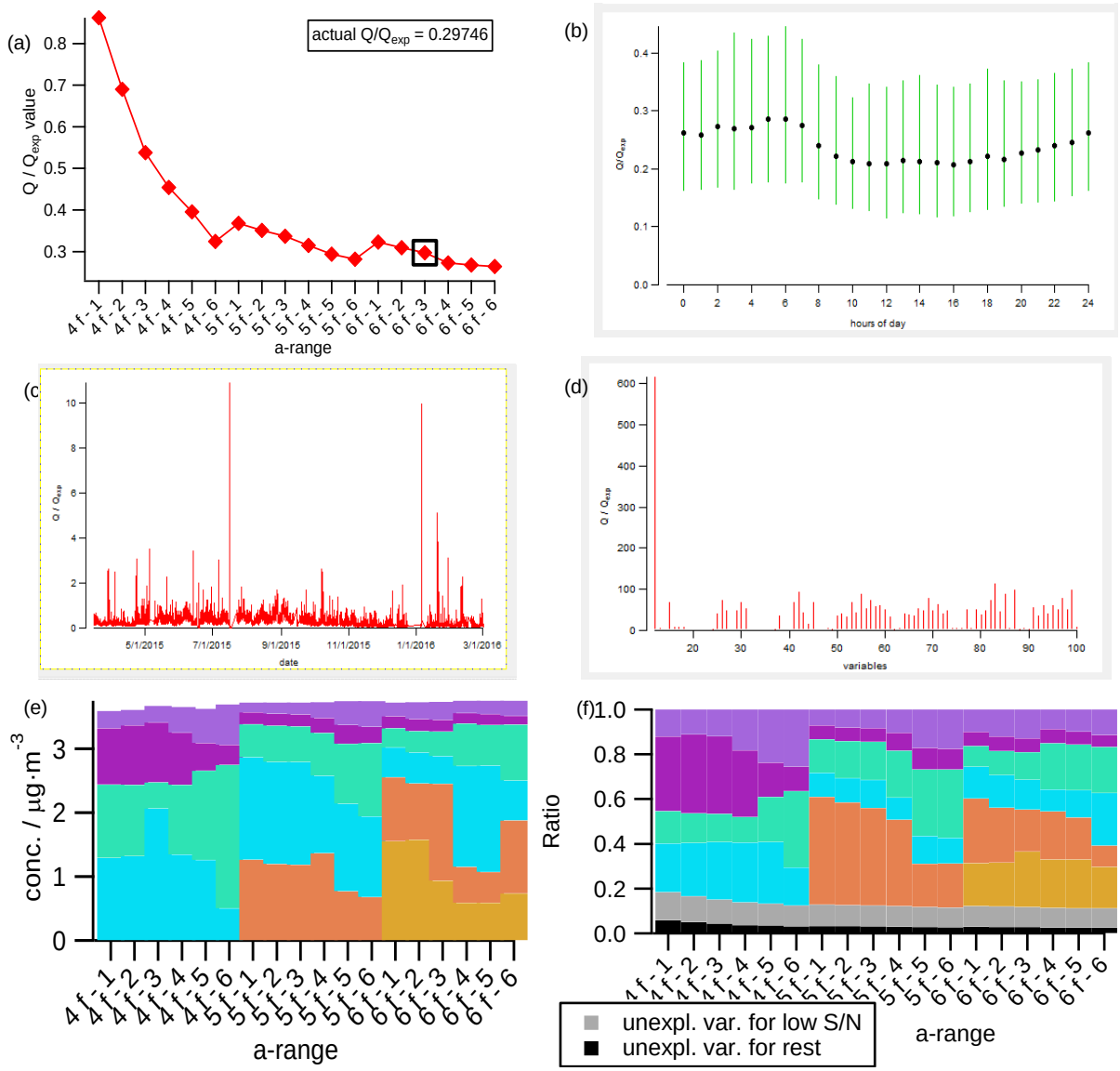

Figure 2-3. Diagnostic plots of yearlong at CTR from ME-2 analysis with HOA, BBOA, IEPOX-OA and 91Fac constrained (*a*-value = 0.3): Q/Q_{exp} as a function of number of factors (p) and *a* values (a), hours of day (b), time series (c) and mass spectra (d). Mass concentration (e) and fractional contribution (f) of OA factors for each number of factor and *a* value.

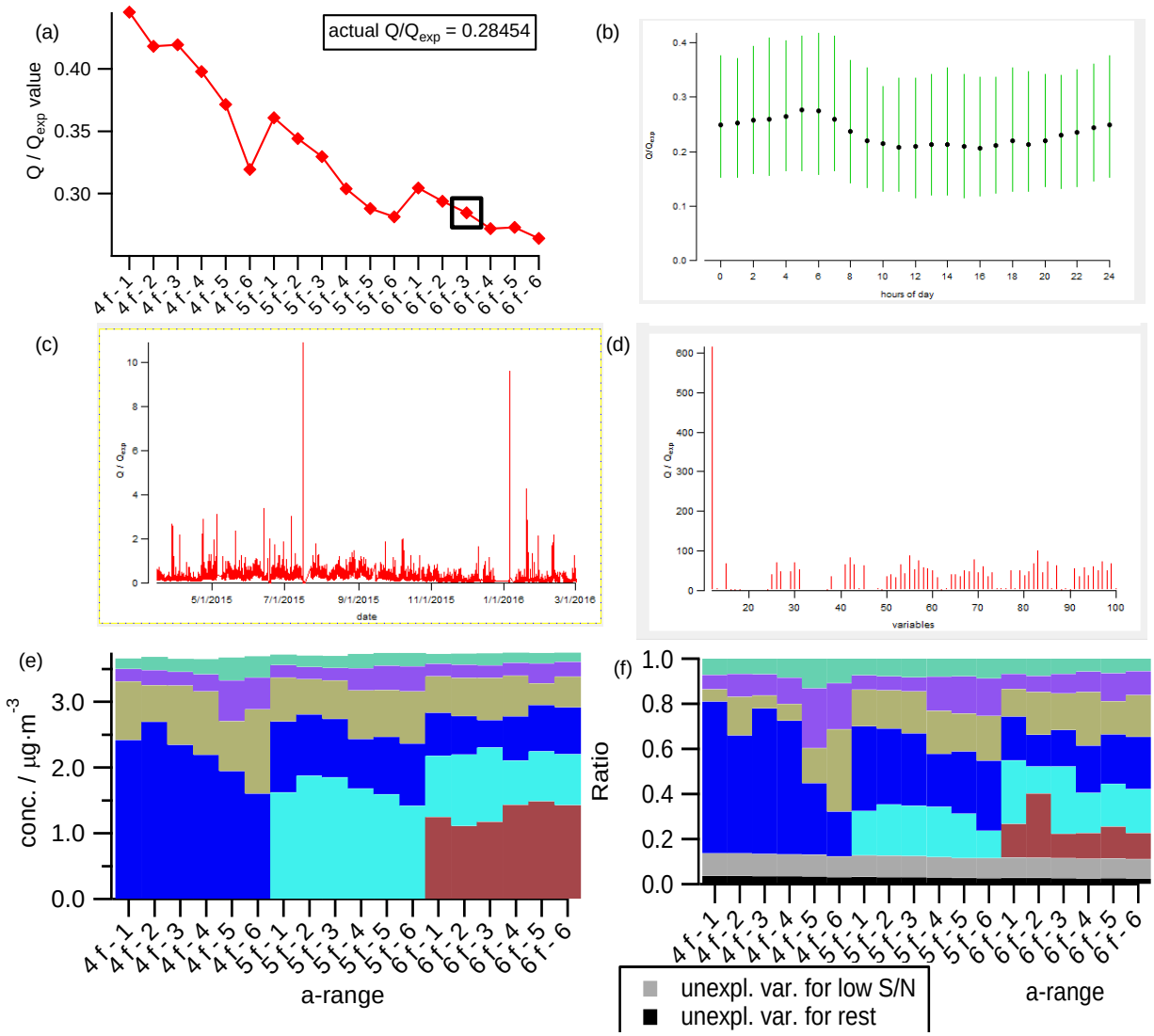

Figure 2-4. Diagnostic plots of yearlong at CTR from ME-2 analysis with HOA, BBOA and IEPOX-OA constrained (*a*-value = 0.3): Q/Q_{exp} as a function of number of factors (p) and *a* values (a), hours of day (b), time series (c) and mass spectra (d). Mass concentration (e) and fractional contribution (f) of OA factors for each number of factor and *a* value.

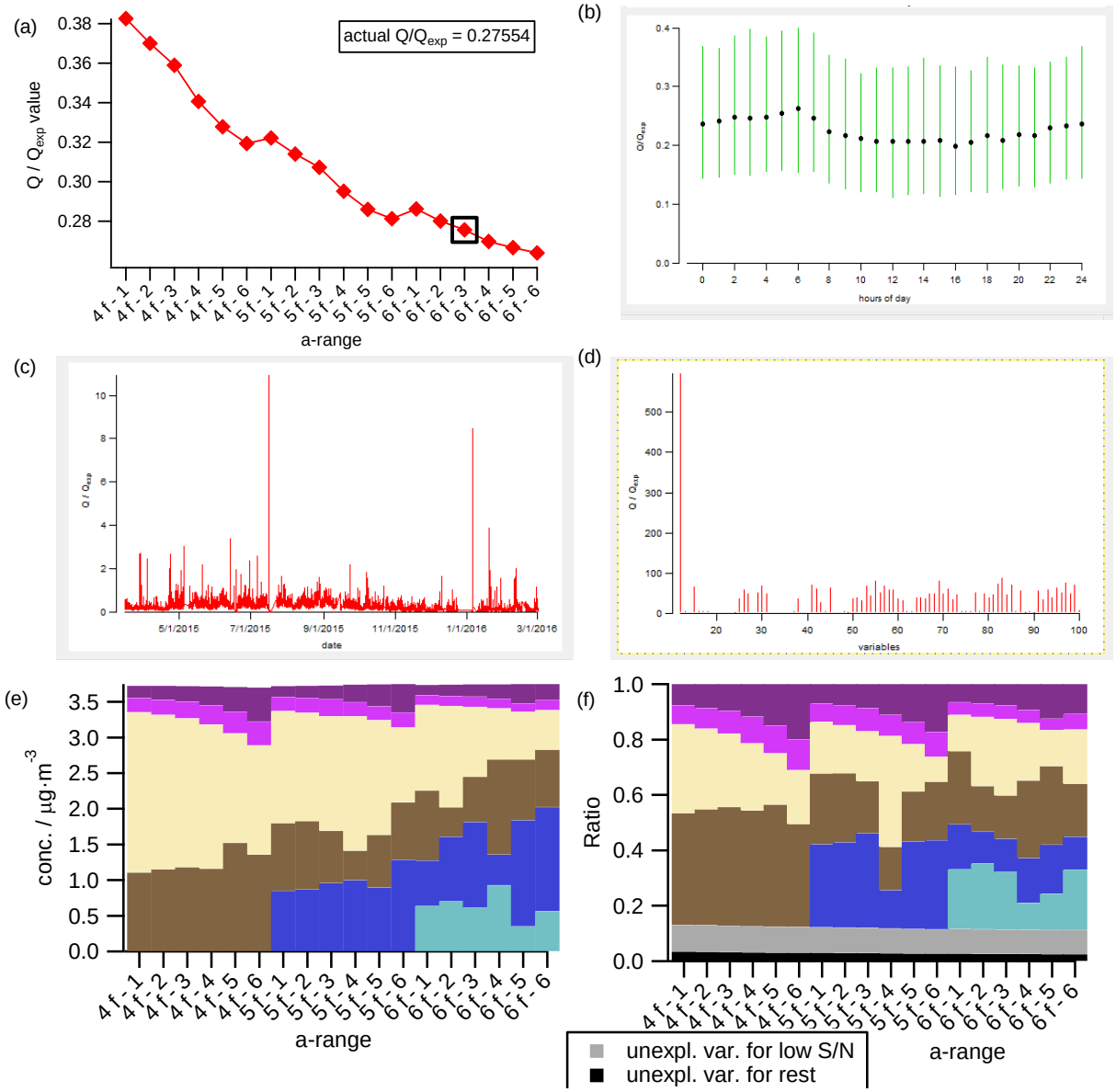

Figure 2-5. Diagnostic plots of yearlong at CTR from ME-2 analysis with HOA and BBOA constrained (*a*-value = 0.3): Q/Q_{exp} as a function of number of factors (p) and *a* values (a), hours of day (b), time series (c) and mass spectra (d). Mass concentration (e) and fractional contribution (f) of OA factors for each number of factor and *a* value.

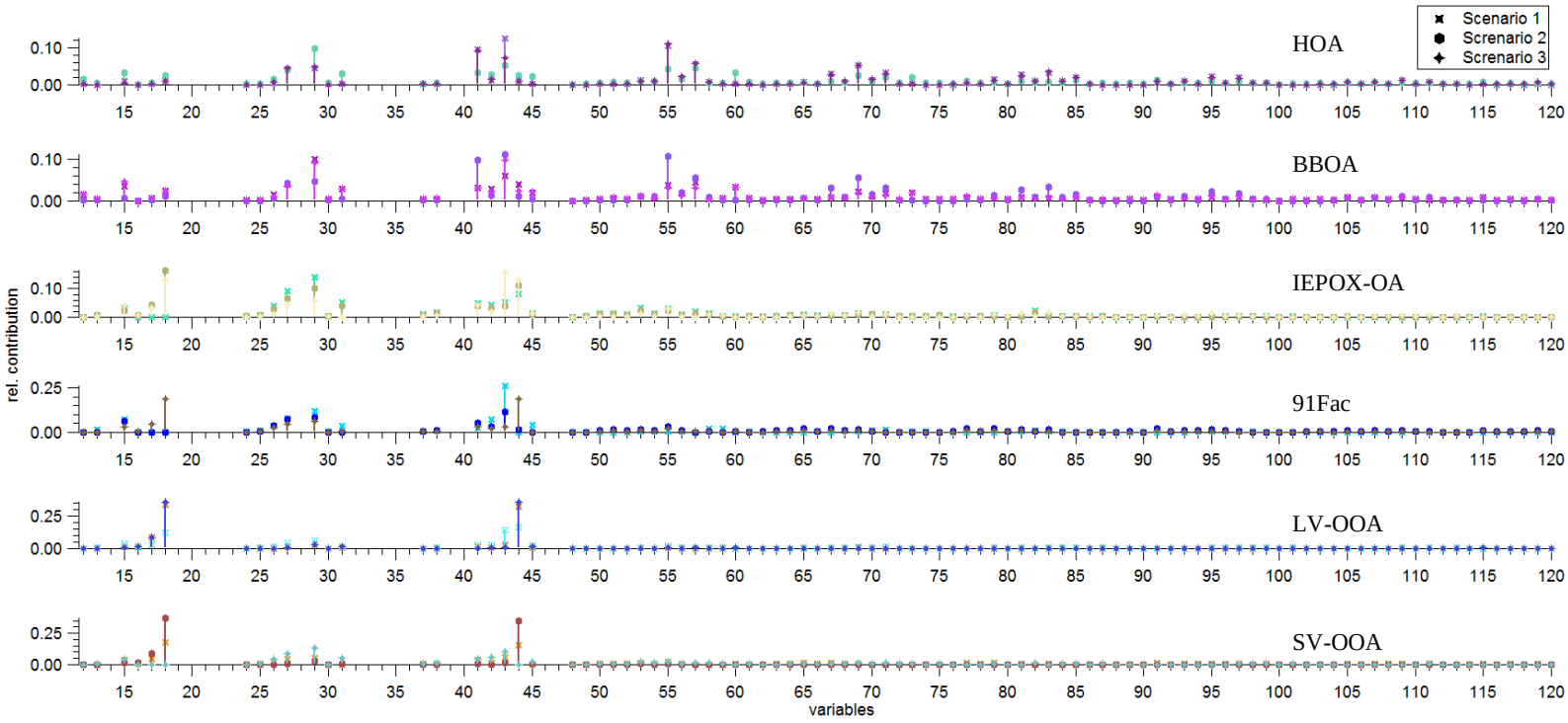

Figure 2-6. The comparison of mass spectra of resolved factors from ME-2 with HOA/BBOA/ IEPOX-OA/91Fac constrained (Scenario 1), HOA/BBOA/IEPOX-OA constrained (Scenario 2), and HOA/BBOA constrained (Scenario 3).

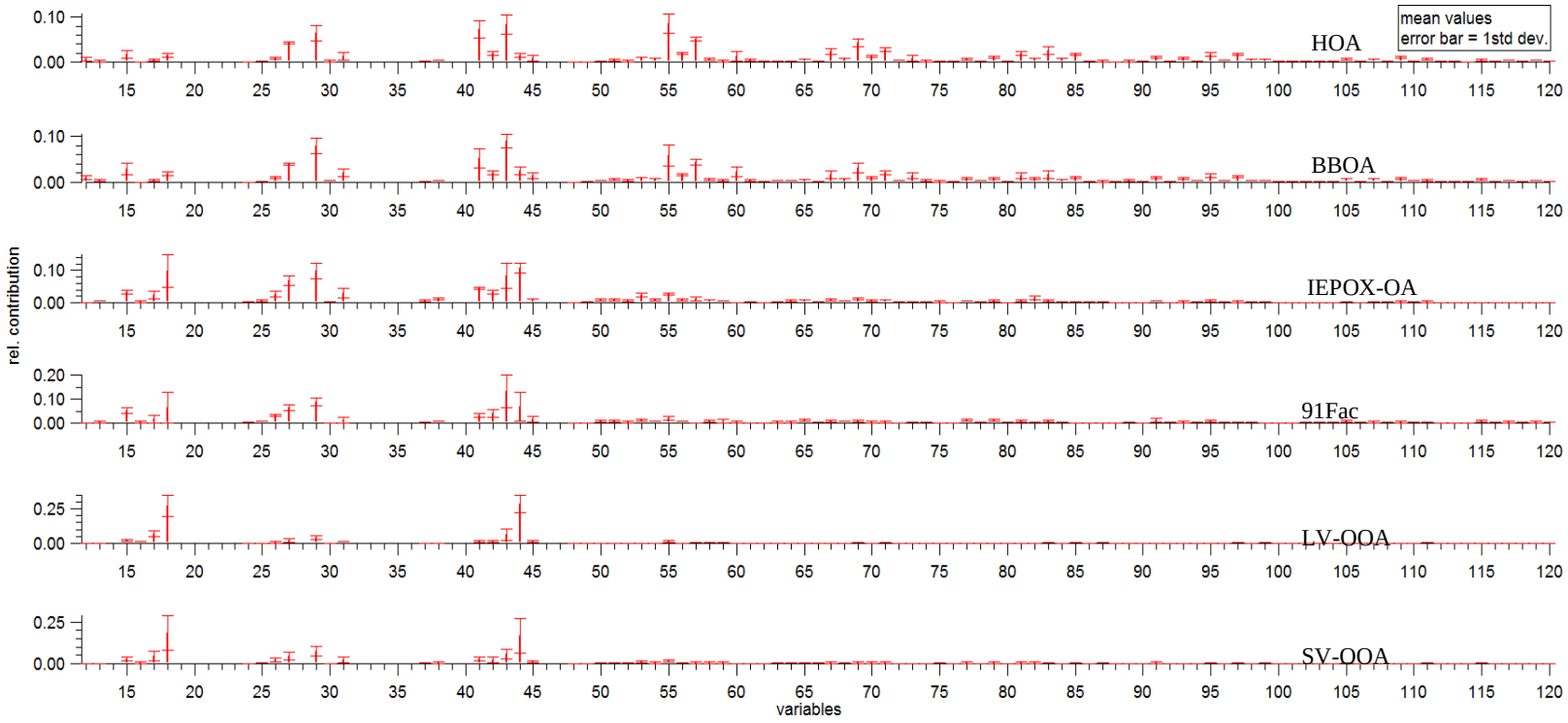

Figure 2-7. Mean values and error bar of mass spectra from three ME-2 with three factor-constrained scenarios.

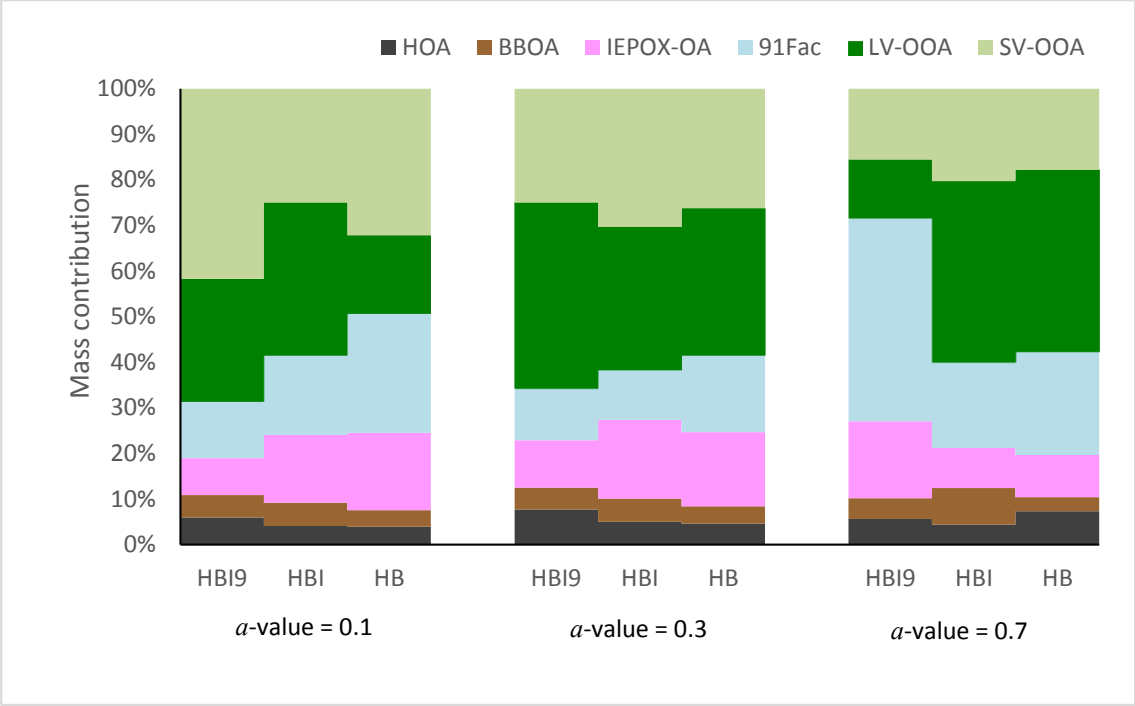

Figure 2-8. Mass contributions of OA factors resolved from ME-2 analysis as a function of *a*-values at the three factor-constrained scenarios.

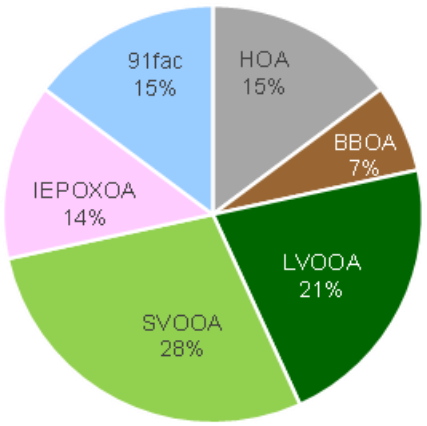

Average mass concentration (μg m^{-3})	
LV-OOA	1.52
SV-OOA	0.93
91Fac	0.43
IEPOX-OA	0.39
HOA	0.29
BBOA	0.18

Figure 2-9. Mass contribution of factors resolved from Scenario 1 (ME-2 with all HOA/BBOA/ IEPOX-OA/91Fac constrained).

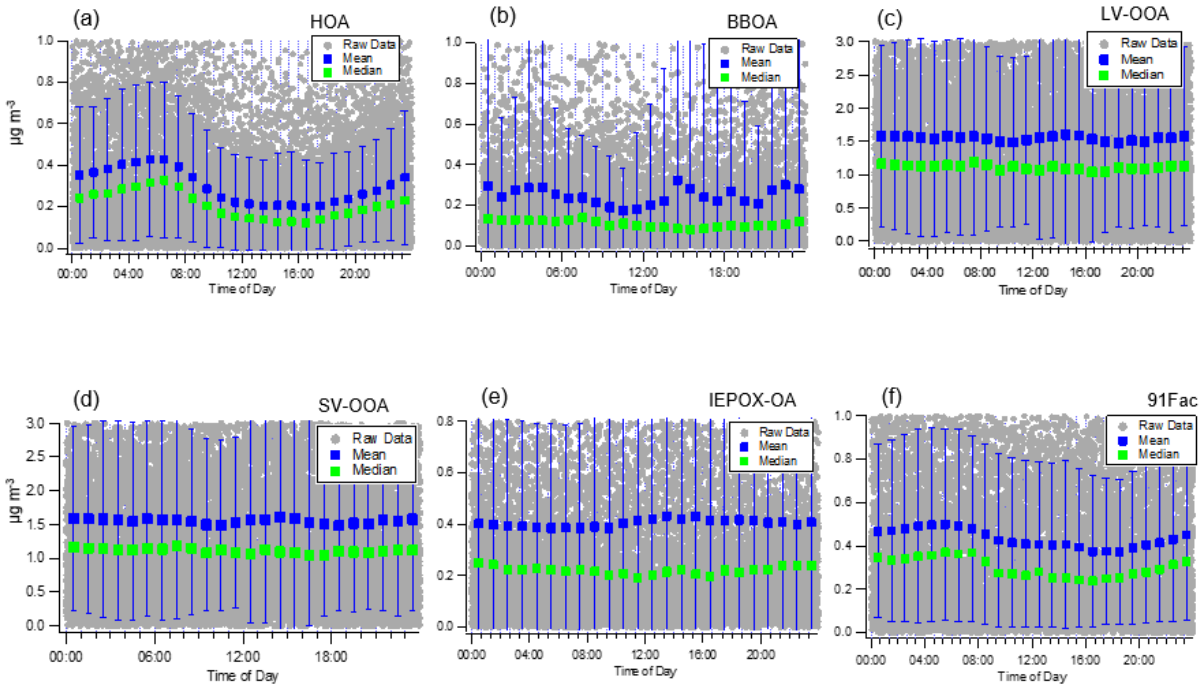

Figure 2-10. Diurnal cycles of factors resolved from yearlong ME-2 with HOA/BBOA/ IEPOX-OA/91Fac constrained (*a*-value = 0.3).

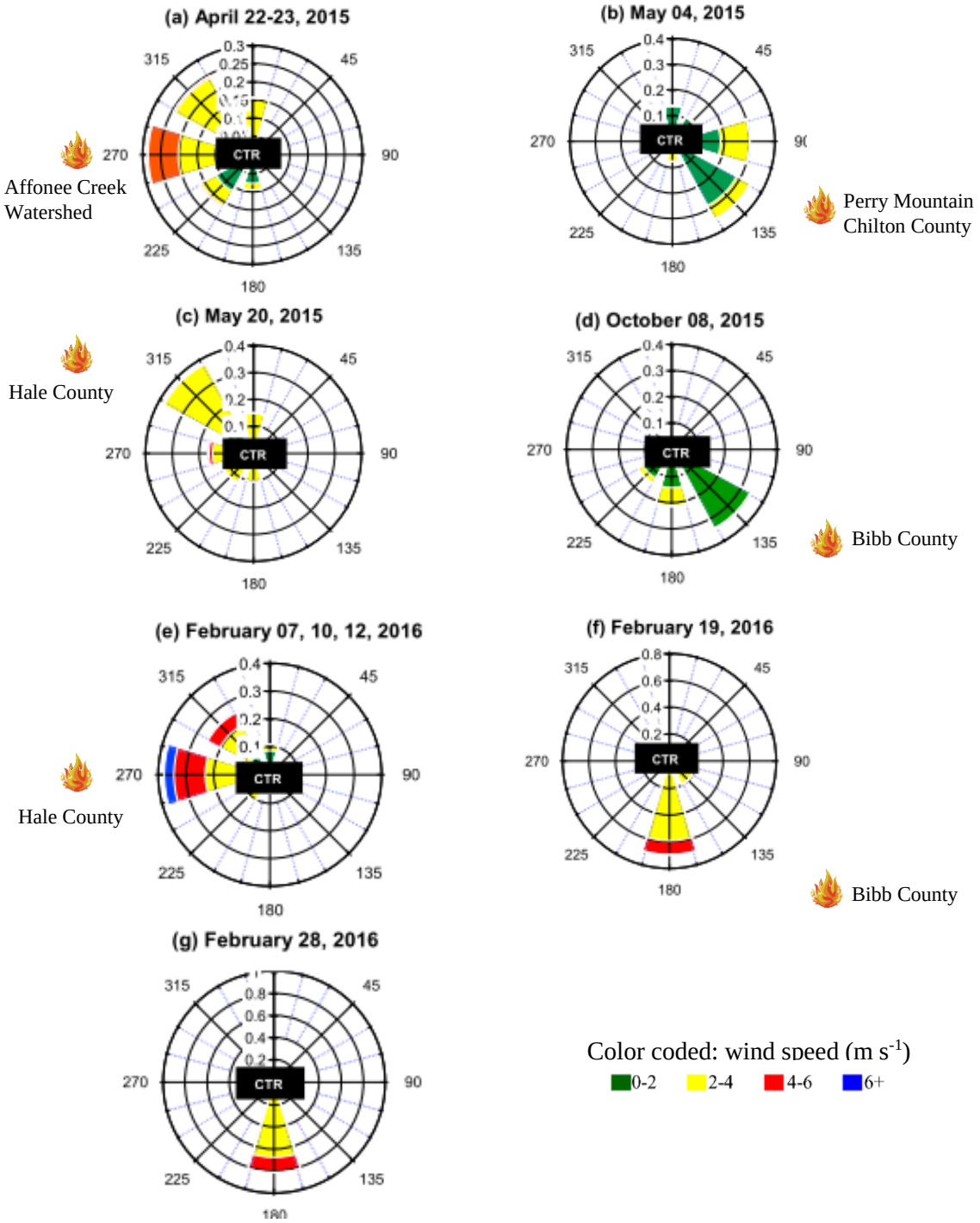

Figure 2-11. Dates, locations of prescribed burns, wind speeds and directions at CTR.

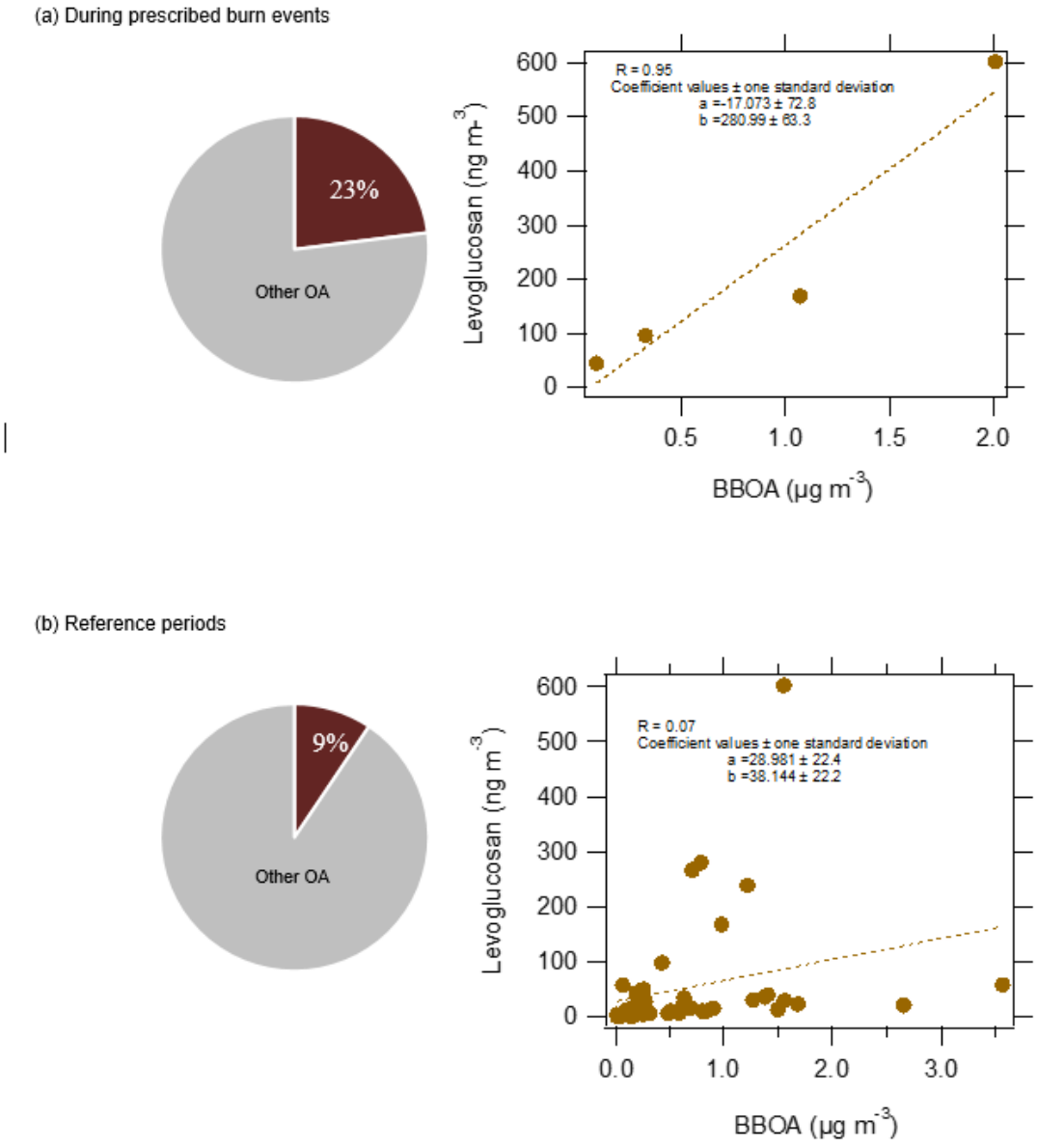

Figure 2-12. Mass contributions of BBOA (dark brown fraction in pie charts) and correlations between BBOA and levoglucosan during (a) prescribed burn events and (b) reference periods (non-prescribed burning events).

Table 2-1. Sampling periods classified as spring, summer, fall and winter by following the 2015/2016 The Old Farmer's Almanac.

Season	Dates
Spring	March 20 – June 20, 2015
Summer	June 21 – September 21, 2015
Fall	September 22 – December 20, 2015
Winter	December 21, 2015 – March 02, 2016*

*last day of deployment

Table 2-2. Summary of collocated measurements of meteorological variables, gaseous species, PM_1 constituents and SOA tracers.

Category	Condition	Spring (March 20 – June 20, 2015)				Summer (June 21 – Sept 20, 2015)				Fall (Sept 21 – Dec 21, 2015)				Winter (Dec 21, 2015 – Mar 02, 2016)			
		Avg	SD	Min	Max	Avg	SD	Min	Max	Avg	SD	Min	Max	Avg	SD	Min	Max
Meteorology *	BP (mbar)	1000	3.86	986.4	1010	998.9	2.6	991.2	1008	1001	6.0	989.6	1017	1001	6.2	977.4	1015
	SR (W m^{-2})	221.7	307.5	0.0	1148.3	242.9	320.1	0.6	1144.2	129.1	211.4	0.2	994.6	136.7	231.5	0.2	1080.3
	RH (%)	74.8	20.2	20.9	99.8	76.6	17.5	23.7	99.6	74.1	20.6	16.9	99.9	68.8	23.3	16.8	99.8
	Temp (°C)	20.7	5.4	1.0	33.4	25.3	4.3	11.5	36.3	16.5	6.1	-1.6	30.2	10.5	6.9	-6.0	25.9
	Rainfall (inch)	0.00	0.01	0.00	0.33	0.00	0.01	0.00	0.50	0.00	0.01	0.00	0.23	0.00	0.01	0.00	0.34
Trace gases (ppbv)*	CO	151.4	34.8	23.8	691.2	145.6	42.4	15.4	540.6	143.6	29.6	3.7	572.2	155.1	54.3	15.4	2746
	NO_x	1.0	1.2	0.0	13.3	1.0	1.2	0.0	13.8	1.6	1.6	0.0	17.4	1.6	1.9	0.0	16.4
	O_3	33.3	15.0	0.0	100.5	34.4	14.0	2.4	111.5	30.0	12.0	1.1	65.6	33.7	10.0	3.9	70.1
	NH_3	0.5	0.5	0.0	6.5	0.4	0.3	0.0	4.2	0.2	0.2	0.0	3.8	0.3	0.3	0.0	11.1
	SO_2	1.0	2.8	0.0	31.8	0.5	1.0	0.0	31.1	0.3	0.8	0.0	14.8	0.3	0.7	0.0	47.4
PM_1 ($\mu g\ m^{-3}$)	NR-PM_1	2.9	1.8	0.1	20.6	7.9	3.4	0.4	20.9	4.8	3.5	0.1	39.9	3.2	2.8	0.1	34.5
	Org	1.8	1.3	0.0	16.2	5.9	2.9	0.2	19.1	4.0	3.2	0.0	38.1	2.2	2.6	0.0	31.6
	SO_4^{2-}	0.7	0.4	0.0	3.1	1.3	0.6	0.1	5.8	0.4	0.3	0.0	3.6	0.5	0.4	0.0	2.9
	NO_3^-	0.2	0.1	0.0	1.0	0.3	0.1	0.0	0.9	0.2	0.1	0.0	1.3	0.3	0.3	0.0	2.6
	NH_4^+	0.2	0.1	0.0	0.8	0.4	0.2	0.0	1.0	0.2	0.1	0.0	1.5	0.2	0.1	0.0	1.2
	Cl^-	0.0	0.0	0.0	0.1	0.0	0.0	0.0	0.1	0.0	0.0	0.0	0.0	0.0	0.0	0.0	0.1
SOA tracers (ng m^{-3})	IEPOX tracers	159.1	209.1	0.0	806.1	427.5	424.5	0.0	1650.4	53.8	55.3	0.0	132.0	0.9	1.8	0.0	6.2
	2-MG	0.42	1.3	0.0	6.47	0.17	0.7	0.0	2.85	1.26	2.8	0.0	6.28	0.00	0.0	0.0	0.00
	Levoglucosan	42.1	61.6	0.0	267.5	26.1	24.0	0.0	87.8	26.6	12.9	0.0	37.3	226.2	204.5	0.0	602.5
OA factors ($\mu g\ m^{-3}$)	HOA	0.23	0.29	0.00	3.40	0.41	0.30	0.00	2.40	0.36	0.30	0.00	2.78	0.14	0.20	0.00	2.54
	BBOA	0.18	0.72	0.00	16.40	0.21	0.24	0.00	3.38	0.23	0.51	0.00	8.53	0.39	1.10	0.00	23.34
	IEPOX-OA	0.43	0.44	0.00	2.57	0.81	0.50	0.00	3.32	0.18	0.14	0.00	0.95	0.11	0.08	0.00	1.48
	91Fac	0.37	0.40	0.00	2.34	0.70	0.39	0.00	2.36	0.45	0.34	0.00	2.44	0.13	0.14	0.00	2.87
	LV-OOA	0.88	0.84	0.00	6.30	2.03	1.40	0.00	10.34	2.16	1.74	0.00	22.08	0.92	0.83	0.00	15.62
	SV-OOA	1.00	1.04	0.00	16.68	1.23	0.67	0.00	5.16	0.87	0.68	0.00	6.37	0.57	1.08	0.00	28.01

*Preliminary data (level 0) from SEARCH

Table 2-3. Summary of SOA tracers measured by GC/EI-MS.

SOA tracers	*m/z*	Frequency of detection (%)	Average concentration (ng m^{-3})	Max concentration (ng m^{-3})
Spring (n = 31)				
IEPOX SOA tracers*				
(1) 2-methylerythritol	219	81	45.38	187.53
(2) 2-methylthreitol	219	77	15.47	63.58
(3) (E)-2-methylbut-3-ene-1,2,4-triol	231	77	65.26	367.10
(4) (Z)-2-methylbut-3-ene-1,2,4-triol	231	77	21.70	122.29
(5) 2-methylbut-3-ene-1,2,3-triol	231	71	11.03	63.79
(6) *cis*-3-MeTHF-3,4-diol	262	3	0.03	0.90
(7) *trans*-3-MeTHF-3,4-diol	262	10	0.19	2.39
2-MG	219	13	0.42	6.47
Levoglucosan	204	94	42.07	267.52
Summer (n = 17)				
IEPOX SOA tracers*				
(1) 2-methylerythritol	219	88	115.96	412.15
(2) 2-methylthreitol	219	88	38.27	124.64
(3) (E)-2-methylbut-3-ene-1,2,4-triol	231	88	177.30	701.88
(4) (Z)-2-methylbut-3-ene-1,2,4-triol	231	88	63.44	273.66
(5) 2-methylbut-3-ene-1,2,3-triol	231	88	31.50	128.30
(6) *cis*-3-MeTHF-3,4-diol	262	6	0.20	3.47
(7) *trans*-3-MeTHF-3,4-diol	262	24	0.86	6.30
2-MG	219	6	0.17	2.85
Levoglucosan	204	88	26.11	87.84
Fall (n = 5)*				
IEPOX SOA tracers				
(1) 2-methylerythritol	219	60	19.68	42.20
(2) 2-methylthreitol	219	60	7.10	13.96
(3) (E)-2-methylbut-3-ene-1,2,4-triol	231	80	18.48	52.49
(4) (Z)-2-methylbut-3-ene-1,2,4-triol	231	60	5.61	15.45

(5) 2-methylbut-3-ene-1,2,3-triol	231	60	2.82	8.01
(6) *cis*-3-MeTHF-3,4-diol	262	0	n/a	n/a
(7) *trans*-3-MeTHF-3,4-diol	262	20	0.14	0.70
2-MG	219	20	1.26	6.28
Levoglucosan	204	100	26.63	37.28
Winter (n = 12)				
IEPOX SOA tracers*				
(1) 2-methylerythritol	219	17	0.37	2.81
(2) 2-methylthreitol	219	8	0.13	1.57
(3) (E)-2-methylbut-3-ene-1,2,4-triol	231	25	0.42	2.17
(4) (Z)-2-methylbut-3-ene-1,2,4-triol	231	0	n/a	n/a
(5) 2-methylbut-3-ene-1,2,3-triol	231	0	n/a	n/a
(6) *cis*-3-MeTHF-3,4-diol	262	0	n/a	n/a
(7) *trans*-3-MeTHF-3,4-diol	262	0	n/a	n/a
2-MG	219	0	n/a	n/a
Levoglucosan	204	92	226.17	602.48

*IEPOX tracers = summation of (1) to (7)

Table 2-4. The Person correlation (R) of ME-2 analysis of yearlong factors derived from three factor-constrained scenarios (cases) with collocated measurements, reference mass spectra and SOA tracers.

Correlations	Case 1: HOA, BBOA, IEPOX-OA and 91Fac constrained						Case 2: HOA, BBOA and IEPOX-OA constrained						Case 3: HOA and BBOA constrained					
	HOA	**BBOA**	**IEPOX-OA**	**91fac**	LV-OOA	SV-OOA	**HOA**	**BBOA**	**IEPOX-OA**	91fac	LV-OOA	SV-OOA	**HOA**	**BBOA**	IEPOX-OA	91Fac	LV-OOA	SV-OOA
R_{TS}																		
CO	0.40	0.72	0.20	0.25	0.29	0.64	0.72	0.46	0.66	0.19	0.44	0.25	0.46	0.75	0.29	0.69	0.33	0.22
HNO_3	0.23	0.20	0.39	0.32	0.33	0.29	0.21	0.21	0.24	0.38	0.28	0.33	0.25	0.20	0.26	0.28	0.32	0.41
NH_3	0.09	0.41	0.20	0.09	0.14	0.27	0.42	0.10	0.28	0.19	0.18	0.11	0.23	0.49	0.03	0.34	0.15	0.20
NO_x	0.27	0.08	0.12	0.02	0.08	0.20	0.08	0.38	0.20	0.12	0.18	0.02	0.28	0.09	0.15	0.16	0.08	0.14
NO_y	0.31	0.18	0.01	0.08	0.13	0.28	0.18	0.39	0.29	0.01	0.21	0.09	0.39	0.19	0.18	0.27	0.15	0.01
NO	0.09	0.00	0.01	0.02	0.01	0.06	0.00	0.10	0.06	0.01	0.02	0.02	0.11	0.00	0.04	0.05	0.00	0.01
NO_2	0.29	0.09	0.11	0.03	0.09	0.21	0.09	0.39	0.22	0.11	0.19	0.03	0.29	0.10	0.17	0.17	0.09	0.13
O_3	0.02	0.01	0.01	0.02	0.02	0.02	0.01	0.01	0.01	0.02	0.02	0.02	0.01	0.00	0.02	0.01	0.02	0.02
SO_2	0.05	0.03	0.03	0.01	0.03	0.07	0.03	0.06	0.08	0.03	0.01	0.01	0.07	0.06	0.00	0.08	0.03	0.01
SO_4	0.37	0.01	0.77	0.62	0.39	0.40	0.06	0.14	0.34	0.77	0.17	0.60	0.22	0.00	0.47	0.34	0.33	0.76
NO_3	0.65	0.47	0.42	0.54	0.51	0.69	0.49	0.62	0.66	0.42	0.54	0.54	0.62	0.49	0.57	0.63	0.48	0.46
R_{MS}																		
Ref_HOA	0.98	0.67	0.47	0.54	0.09	0.29	0.79	0.98	0.64	0.32	0.05	0.46	0.96	0.69	0.55	0.21	0.05	0.53
Ref_BBOA	0.76	0.96	0.80	0.75	0.33	0.57	0.95	0.75	0.83	0.67	0.30	0.71	0.72	0.96	0.79	0.49	0.30	0.71
Ref_91fac	0.87	0.79	0.77	0.60	0.45	0.74	0.83	0.87	0.81	0.77	0.41	0.75	0.86	0.77	0.69	0.64	0.40	0.82
Ref_SV-OOA	0.67	0.73	0.69	0.55	0.69	0.86	0.72	0.67	0.67	0.86	0.67	0.90	0.64	0.71	0.58	0.81	0.66	0.92
Ref_LV-OOA	0.28	0.59	0.61	0.36	0.88	0.96	0.49	0.28	0.44	0.95	0.87	0.90	0.27	0.52	0.41	0.96	0.87	0.87
Ref_IEPOX-OA	0.52	0.81	0.95	0.61	0.64	0.86	0.64	0.53	0.74	0.97	0.62	0.84	0.50	0.75	0.76	0.82	0.61	0.83
$R_{Tracers}$																		
IEPOX_SOA	0.65	0.44	0.82	0.74	0.62	0.51	0.54	0.43	0.46	0.81	0.38	0.73	0.38	0.82	0.64	0.40	0.64	0.82
Levoglucosan	0.08	0.56	0.24	0.15	0.01	0.00	0.55	0.26	0.02	0.24	0.12	0.12	0.35	-0.46	-0.11	0.01	0.03	0.18
O:C ratio	0.12	0.26	0.43	0.08	1.48	0.75	0.18	0.12	0.16	0.55	1.59	0.79	0.12	0.19	0.08	0.89	1.62	0.65
Mass conc (ug m^{-3})	0.29	0.18	0.39	0.43	1.52	0.93	0.19	0.19	0.65	0.41	1.17	1.13	0.17	0.14	0.61	0.64	1.20	0.98
Mass fraction	13%	6%	12%	13%	19%	25%	7%	9%	16%	16%	11%	30%	8%	5%	21%	16%	12%	28%

CHAPTER III:
SOURCE APPORTIONMENT OF SUBMICRON ORGANIC AEROSOL COLLECTED FROM ATLANTA, GEORGIA, DURING 2014-2015 USING THE AEROSOL CHEMICAL SPECIATION MONITOR (ACSM)[2]

3.1 Overview

Although the ACSM was previously deployed at the Jefferson Street (JST) site in downtown Atlanta, Georgia (GA), during 2011-2012 by Budisulistiorini et al. (2013, 2014, 2016), the main research objective in this study is to revisit the same site during 2014-2015 in order to evaluate if year-to-year changes occur in the amounts and types of OA or if they remain fairly consistent from year-to-year. Submicron OA is seasonally analyzed during this new sampling period by PMF in order to apportion OA subtypes, and thus, resolve potential sources and chemical processes. In addition, ME-2 is applied when a unique solution could not be resolved by PMF. A suite of real-time collocated measurements from the Southeastern Aerosol Research and Characterization (SEARCH) network will be correlated with the ACSM data in order to interpret OA subtypes resolved from factor analysis. SOA molecular tracers measured offline from high-volume $PM_{2.5}$ filter samples by using gas chromatography interfaced to electron ionization quadrupole mass spectrometry (GC/EI-MS) are compared to PMF/ME-2 factor solutions in order to aid in the identification of OA subtypes (sources).

[2] To be submitted to Atmospheric Environment.

3.2 Experimental Section

3.2.1 Site description

The JST site (33.7775ºN, 84.4166ºW) is one of the designated urban sites that are affiliated with the SEARCH network. This site has been a part of this air quality observation and monitoring program since 1998 (Hansen et al., 2003; Solomon et al., 2003; Edgerton et al., 2006). As shown in Fig. S1, the JST site is located in a mixed commercial-residential area that is approximately 4 km northwest of downtown Atlanta, GA.

3.2.2 Real-time monitoring by ACSM

The Aerodyne ACSM was deployed at the JST site to continuously measure NR-PM_1 using a time resolution of 30 minutes for 1 year (March 20, 2014 – February 08th, 2015). ACSM sampling methods and operating details have been previously described (Budisulistiorini et al. 2013, 2014). Briefly, the ACSM uses an aerodynamic lens to sample and focus submicron particles (75 - 650 nm) into a narrow beam (Liu et al., 2007), with a flow of approximately 85 cm^3 min^{-1}. The aerosol beam is transmitted into the chambers, where it is flash vaporized on a high-temperature vaporizer operated at 600 ºC, ionized by hard electron impact ionization (70 eV) and subsequently detected by a quadrupole mass spectrometer. During the sampling for this study, the diagnostics in the ACSM were routinely checked. Ionizer and electronic offset were tuned depending on the diagnostics to ensure the appropriate conditions. Details of mass calculations of aerosol constituents by the ACSM have been described (Ng et al., 2011). The particle collection efficiency (CE) was determined following the approach described by Middelbrook et al. (2012) and applied in the same manner as previously described (Budisulistiorini et al., 2013). The application of CE = 0.5 in this study was consistent with the previous studies by Budisulistiorini et al. (2013, 2014, 2015, 2016). For a given species,

concentration was calculated based on the addition of the ion signals at each fragments and the ionization efficiency (IE). The ACSM was directly calibrated with ammonium nitrate ($(NH_4)NO_3$) and ammonium sulfate ($(NH_4)_2SO_4$) in order to determine the response factor (RF) of NO_3^- and the relative ionization efficiencies (RIE) of SO_4^{2-}, and NH_4^+; this aided in more accurate quantification of these inorganic components (Ng et al., 2011; Budisulistiorini et al., 2014). The ACSM inlet sampling flow and IE were calibrated every season during the study. The calibration parameters are shown in Table S1. The RIE values for NH_4^+ and SO_4^{2-} derived from calibration experiments performed each season were applied to respective season, while the default RIE values of 1.1, 1.3, and 1.4 for NO_3^-, Cl^- and organics, respectively, were used for each season (Allan et al., 2003; Jimenez et al., 2003; Ng et al., 2010, 2011; Budisulistiorini et al., 2013, 2014, 2015, 2016). All data are reported in local time, taking into account daylight savings. By excluding abnormal events (i.e., power outages, calibrations, etc.), the ACSM measured ~ 93% of the 1-year sampling period.

3.2.3 PMF analysis

The sources of OA were determined with the PMF Evaluation Tool panel (PET v2.04) interfaced with IGOR (WaveMetrics, Inc., Portland, Oregon) using the methods described by Ulbrich et al. (2009) and Zhang et al. (2011). Ions at *m/z* 12 through 120 were utilized for PMF analysis in order to avoid potential interferences from the internal calibration standard (naphthalene) with ion signal at *m/z* 128. PMF analysis was initially conducted by season as established by the Farmer's Almanac for 2014-2015 (Table 1). Spring and fall datasets were separated into finer periods during PMF analysis in order to capture transitional periods that contained changing sources. This will be discussed in more detail in Section 3.3.

For each dataset, the number of factors was selected based on the Q/Q_{exp}, as previously outlined by Ulbrich et al. (2009). However, a significant decrease in Q/Q_{exp} as the number of factors increase is not sufficient to determine the correct number of factors (Ulbrich et al., 2009). As a result, the optimal solution in this study was determined after examining the residuals of PMF fits, interpretability of a factor's diurnal trend, correlation of factors with external tracers, and characteristic ion signatures of each factor's mass spectrum. The error matrix was calculated by the aforementioned customized software, which downweights the *m/z* masses calculated from the *m/z* 44 ion signal. *M/z* values with signal-to-noise (S/N) ratios below 0.2 were downweighted by a factor of 10, and those with S/N ratios between 0.2 and 1 were downweighted by a factor of 2 (Budisulistiorini et al., 2013, 2014). The rotational ambiguity of solutions was examined by changing the parameter FPEAK and the robustness of solutions were evaluated by starting PMF with different initial conditions (parameter SEED, varying from 0 to 100 in steps of 5). The uncertainties of PMF factors were determined by 100 bootstrapping repetitions (Ulbrich et al., 2009). The reference mass spectra used in this study were obtained from the AMS spectral database at http://cires.colorado.edu/jimenez-group/AMSsd/. As recommended by Ng et al. (2010), HOA was identified when a factor had prominent ions at *m/z* 29, 43, 57, 71, 85, 99 ($C_nH_{2n+1}^+$ ion series) and *m/z* 27, 41, 55, 69, 83, 97 ($C_nH_{2n-1}^+$ ion series). HOA derived from primary sources has been previously reported to have good correlation (R ranging from 0.77 to 0.91) with known combustion tracer species, including CO, NO_x, polycyclic aromatic hydrocarbons (PAH), and black or elemental carbon (BC/EC) (Zhang et al., 2005a, 2005b; Sun et al., 2011, 2015; Huang et al., 2013). BBOA was identified when a factor had significant ion signals in the mass spectrum at *m/z* 60 and 73, which are associated with anhydrous sugars, such as levoglucosan, emitted from "fresh" wood burning (Schneider et al., 2006; Alfarra et al., 2007;

Lanz et al., 2007; Mohr et al., 2009; Minguillón et al., 2011;). OOA factors were differentiated based on the ratio of *m/z* 44 to total ion signal (f_{44}), where the factor with greater f_{44} was identified as LV-OOA (more aged or low-volatility OA) and the factor with smaller f_{44} as SV-OOA (less aged or semi-volatility OA). The ion signal at *m/z* 44 has been observed to originate from the thermal decomposition of carboxylic acids on the vaporizer, resulting in a significant CO_2^+ ion peak. The ion signal at *m/z* 43 mainly derives from the fragmentation of hydrocarbon chains and carbonyls that form $C_3H_7^+$ and $C_2H_3O^+$ ions, respectively (Alfarra et al., 2004). The IEPOX-OA factor was identified by known characteristic ions at *m/z* 82 ($C_5H_6O^+$) and 75 ($C_3H_7O_2^+$) in its mass spectrum (Robinson et al., 2011; Slowik et al., 2011; Budisulistiorini et al., 2013, 2016). The 91Fac was assigned to a factor when its respective mass spectrum contained a characteristic ion at *m/z* 91 ($C_7H_7^+$). 91Fac has been recently reported in isoprene-influenced areas that have low-NO_x levels (Robinson et al., 2011; Budisulistiorini et al., 2015, 2016); however, the source of this factor is unknown. Recent work by Boyd et al. (2015) has demonstrated that this factor can be derived from β-pinene + NO_x system and Riva et al. (2016) has recently demonstrated that this factor can also be derived from isoprene-derived hydroxyhydroperoxides at the Look Rock, TN (LRK) field site in the southeastern U.S..

Additional evidence to support the identification of each factor included time series correlation with tracer species and diurnal trends in mass concentrations. Since the main goal of this study was to investigate the seasonal variations of OA sources, the PMF datasets were organized by season. It should be noted that PMF and ME-2 (described in the next section) was initially applied to the yearlong ACSM dataset. The initial analysis revealed the need to conduct OA source apportionment by season in order to better resolve minor OA types.

3.2.4 ME-2 analysis

In addition to PMF analyses, ME-2 was applied in this study to reduce rotational ambiguity of factors by adding a priori information of well-known profiles into the model (Paatero et al., 2002), especially in cases where PMF was unable to provide a unique solution. The source finder (SoFi, Canonaco et al., 2013) tool version 4.8 for Igor Pro (Wave Metrics Inc., Lake Oswego, OR) was used for ME-2 analysis. A priori information of OA source spectra was introduced into the model using the α value technique in ME-2 (Crippa et al., 2014). Several α values (ranging from 0.05 up to 1) were performed to investigate the reasonable deviation of constrained factors from reference mass spectra. Crippa et al. (2014) demonstrated that an α value range of 0.05-0.2 for HOA and 0.3 for BBOA yielded reasonable freedom in ME-2 based on the sensitivity analysis of α value approach with 25 AMS datasets. Mean HOA and BBOA mass spectra taken from Ng et al. (2011) were the main reference mass spectra to determine HOA and BBOA in this study. Detailed analysis of ME-2 are described elsewhere (Canonaco et al., 2013; Crippa et al., 2014). The SOA components were not constrained with ME-2 in previous studies (Canonaco et al., 2013, Crippa et al., 2014, Reyes-Villegas et al., 2016). Regarding the presence of IEPOX-OA at JST in 2012 (Budisulistiorini et al., 2016), the present study also constrained the IEPOX-OA factor in the yearlong dataset in ME-2 analysis.

3.2.5 Measurements of SOA tracers

A high-volume aerosol filter sampler was run every third day to collect ambient $PM_{2.5}$ at 1 m^3 min^{-1} for 24 hours on pre-baked Tissuquartz™ filters (8 x 10 in, Pall Life Sciences). Detailed operating conditions of the high-volume sampler are described elsewhere (Budisulistiorini et al., 2015; Riva et al., 2015; Rattanavaraha et al., 2016). Field blank filters were collected every month in order to identify any potential contamination in aerosol filter samples. All filters were

stored in the dark at -20 ºC until extraction and analysis. SOA was extracted from the quartz filters and quantified by GC/EI-MS as described in detail by Rattanavaraha et al (2016). Briefly, a 37-mm diameter circular punch form each filter was sonicated with 20 mL of high-purity methanol (LC/MS CHROMASOLV-Grade, Sigma-Aldrich) for 45 minutes and then filtered through a polytetrafluorethylene (PTFE) syringe filter to remove insoluble particles and residual quartz filter fibers. The filtrate was blown dry with a gentle stream of nitrogen (N_2) and immediately trimethylsilylated by reaction with 100 μL of BSTFA + TMCS (99:1 *v/v*, Supelco) and 50 μL of pyridine (anhydrous, 99.8 %, Sigma-Aldrich) at 70 °C for 1 hour. Derivatized samples were analyzed by a Hewlett-Packard (HP) 5890 Series II Gas Chromatograph coupled to a HP 5971A Mass Selective Detector within 24 hours after trimethylsilylation.

Extraction efficiency was determined by analyzing 3 pre-baked filters spiked with 50 ppmv of 2-methyltetrols, 2-methylglyceric acid, levoglucosan, and *cis*- and *trans*-3-MeTHF-3,4-diols. Extraction efficiency was above 95% and used to correct the quantification of samples. Extracted ion chromatograms (EICs) of *m/z* 262, 219, 231 were used for quantification of the *cis*-/*trans*-3-MeTHF-3,4-diols, 2-methyltetrols and 2-methylglyceric acid, and C_5-alkene triols, respectively (Surratt et al., 2006). 2-Methyltetrols, 3-MeTHF-3,4-diol isomers, and 2-methylglyceric acid were quantified using authentic standards as described elsewhere (Budisulistiorini et al., 2015; Rattanavaraha et al., 2016; Zhang et al., 2012). Levoglucosan was quantified using 1,6-anhydro-β-D-glucose (99%, Sigma-Aldrich) as an authentic standard. C_5-alkene triols were quantified using the average response factor of the 2-methyltetrols as a surrogate.

3.2.6 Collocated measurements

SEARCH provided a suite of additional instruments at the JST site that measured meteorological and chemical variables, including temperature, relative humidity (RH), trace

gases (i.e., CO, O_3, SO_2, NO_x, and NH_3), and monitored PM continuously (Budisulistiorini et al., 2013, 2014, 2016; Hu et al., 2015; Xu et al., 2015; Rattanavaraha et al., 2016). Detailed descriptions of the collocated instruments can be found in Hansen et al. (2003) and Edgerton et al. (2006). Unfortunately, the measurement of planetary boundary layer (PBL) height was not made at the site during this study. Therefore, only absolute diurnal patterns of constitutes of interest will be shown in Section 3.3 without consideration of the effects of PBL height evolution.

3.2.7 Estimation of aerosol properties

O:C was calculated by equation 1 below, which is the recently updated parameterization for calculating ambient O:C values from unit-mass resolution data such as from the ACSM (Canagaratna et al., 2015).

$$\mathrm{O{:}C} = 0.079 + 4.31(f_{44}) \quad (1)$$

In equation 1, f_{44} is fractional ion intensity at *m/z* 44 from unit-mass resolution measured by the ACSM.

Liquid water content (LWC) and aerosol pH were estimated using the ISORROPIA-II (Nenes et al., 1998; Fountoukis and Nenes, 2007) thermodynamic equilibrium model operated in the forward mode. In this paper, LWC was estimated based on the composition and phase state of an NH_4-SO_4-O_3-Cl-Na-Ca-K-Mg-water inorganic aerosol in thermodynamic equilibrium with gas-phase precursors, such as NH_3 SO_4^{2-}, NO_3^-, and NH_4^+ ion concentrations measured by the ACSM and the RH, temperature, Na^+, K^+, Ca^{2+}, Mg^{2+}, and gas-phase ammonia (NH_3) measured by SEARCH were used as input into the model. The ISORROPIA-II model estimates particle-phase hydronium ion concentration per unit volume of air (H^+, μg m^{-3}), aerosol liquid water

content (LWC, μg m^{-3}), and aqueous aerosol mass concentration (μg m^{-3}), as previously described by Budisulistiorini et al. (2015).

3.3 Results and discussion

3.3.1 Overview of measurements

The yearlong ACSM measurement period at JST extended from March 20, 2014 through February 8, 2015, capturing NR-PM_1 component concentrations and OA sources across spring 2014, summer 2014, fall 2014, and winter 2015. Table 3-1 lists the exact dates that ACSM measurements were collected during each season. Temporal variations of meteorological data, trace gases, NR-PM_1 component concentrations, and SOA tracers are illustrated in Figure 3-1. Descriptive statistics of the measurements are summarized in Table 3-2 by season.

The average temperature was highest in summer (25 $\pm$ 3.4 ºC) and lowest in winter (4.7 $\pm$ 3.7 ºC). RH varied by season with the highest in winter (85.9 $\pm$ 15.3%). Rainfall occurred intermittently averaging 0.1 inches per day. The average concentrations of CO and NO_x were highest in winter, suggesting either higher emissions of primary pollutants in Atlanta during winter or lower PBL heights that would concentrate these primary pollutants. The average concentrations of CO and NO_x are consistent with Budisulistiorini et al. (2016). Ozone (O_3) was highest in warmer months and decreased in colder months (Figure 3-1b). SO_2 concentrations remained constant throughout the year, ranging 0.5 – 0.7 ppbv. NR-PM_1 mass concentrations as measured by the ACSM were highest in summer (16.7 $\pm$ 8.4 μg m^{-3} on average) and lowest in winter (8.0 $\pm$ 5.7μg m^{-3} on average), which differs from the 2012 measurement period when the fall season had the highest NR-PM_1 mass concentration (Budisulistiorini et al., 2016). Organic species (or OA) dominated total NR-PM_1 mass (55.5 – 73.6%), especially during the warm seasons. As shown in Table 3-2, average concentration of organic component was highest in

summer (11.4 ± 5.5 μg m^{-3}) and lowest in winter (4.4 ± 3.2 μg m^{-3}). Higher OA loadings in summer suggest that photochemistry and/or multiphase chemical reactions yield substantial amounts of SOA, consistent with previous findings at the JST site (Budisulistiorini et al., 2013, 2016). During summer, the average SO_4^{2-} concentration was 3.5 ± 1.9 μg m^{-3}, making it the largest inorganic component during this season. SO_4^{2-} had its lowest average concentration (1.2 ± 0.7 μg m^{-3}) during winter. Conversely, NO_3^- was highest in winter (1.8 ± 1.4 μg m^{-3}) and lowest in summer (0.8 ± 0.4 μg m^{-3}). These seasonal variations of inorganic species are consistent with prior studies at JST (Budisulistiorini et al., 2013, 2016). The average NH_4^+ concentration was highest in summer (1.0 ± 0.5 μg m^{-3}) and lowest in winter (0.5 ± 0.4 μg m^{-3}). By contrast, seasonal variation of NH_4^+ is inconsistent with ACSM measurements reported at JST in 2012 by Budisulistiorini et al. (2016), who observed the highest concentration, 1.1 ± 0.6 μg m^{-3}, in fall and the lowest concentration, 0.4 ± 0.2 μg m^{-3}, in spring. This discrepancy could be explained by meteorological data between different years. Cl^- was present at low levels and will not be further discussed in this study.

As shown in Table 3-2, the mean concentrations of IEPOX-derived SOA tracers measured from high-volume aerosol filters were significantly higher (*t-test, p-value < 0.05*) in summer (391.7 ± 240.7 ng m^{-3}) than fall (5.4 ± 6.1 ng m^{-3}) and winter (1.1 ± 0.9 ng m^{-3}). It should be noted that the IEPOX-derived SOA tracers were not measured during spring due to unavailable high-volume aerosol filter samples. Individual IEPOX-derived SOA tracers measured by GC/EI-MS are summarized in Table 3-3. The most abundant IEPOX-derived SOA tracers included (E)-2-methylbut-3-ene-1,2,4-triol (154.3 ng m^{-3} on average), 2-methylerythritol (107.9 ng m^{-3} on average), and 2-methylthreitol (29.8 ng m^{-3} on average). Levoglucosan was measured as an OA tracer for fresh biomass burning. The average mass concentrations of levoglucosan during fall

(221.9 $\pm$ 175.9 ng m^{-3}) and winter (197.8 $\pm$ 123.0 ng m^{-3}) seasons were much higher than in summer (19.9 $\pm$ 14.4 ng m^{-3}).

The wind rose plots (Figure S3-2) show that westerly winds dominated in spring and summer seasons, while the fall and winter seasons were characterized by high frequencies of northwesterly and easterly winds. Prevailing winds with the highest speeds were more frequent in winter than in any other season.

Aerosol LWC and pH were estimated by ISORROPIA-II. A weak negative correlation (R = -0.35, n = 91) between aerosol LWC and pH was observed over the yearlong sampling, suggesting pH decreases with increasing LWC of aerosol. On average, aerosol LWC was higher in summer (8.4 μg m^{-3}) than in winter (1.7 μg m^{-3}), which is consistent with recent work (Guo et al., 2015). However, total aerosol LWCs estimated in the present study are lower than reported by Guo et al. (2015), which is likely due to the fact that only aerosol LWC contributions from inorganic species were available as inputs in the ISORROPIA-II model. Even though Guo et al. (2015) considered the water fraction from organic species, they found that it had a small contribution to total aerosol LWC and could be neglected if measurement techniques were not available at a particular site to estimate it. Aerosol pH was estimated to remain acidic year round (pH = 1.61, on average), consistent with prior studies reporting aerosol pHs ranging between 0 and 2 throughout the southeastern US region (Budisulistiorini et al., 2013, 2015, 2016; Guo et al., 2015; Rattanavaraha et al., 2016; Xu et al., 2015). As shown in Table 3-2, aerosol was most acidic (pH = 1.4, on average) at JST in summertime, which is consistent with a recent study by Budisulistiorini et al. (2016).

3.3.2 OA factors resolved by yearlong PMF and ME-2 analysis

Initially, we applied PMF and ME-2 to the yearlong OA mass spectral dataset collected by the ACSM. PMF analysis resolved a 6-factor solution, for which the OA mass spectra and time series associated with each PMF factor are shown in Figures S3-3a and S4a, respectively. By constraining HOA, BBOA, and IEPOX-OA at an *a*-value of 0.2, ME-2 resolved 6-factor solution as PMF (Figures S3-3b and S3-4b). The correlation of factors resolved from yearlong PMF and ME-2 with collocated measurement and reference mass spectra are shown in Table S3-2. The correlations of each factor with its respective reference mass spectra and tracers are stronger in ME-2 analysis than PMF. For example, the constrained IEPOX-OA factor has a stronger correlation (R = 0.99) with IEPOX reference mass spectra from ME-2 analysis than PMF (R = 0.87). As a result, the correlation between IEPOX-OA and IEPOX tracers (R = 0.94) is stronger in ME-2 than PMF analysis (R = 0.79), indicating an appropriate constraint of IEPOX-OA with ME-2 in the yearlong dataset. The *a*-value of 0.2 was chosen for the optimum ME-2 solution using the diagnostics shown in Figure S3-5. The residuals (i.e., unexplained variable for low signal-to-noise ratio and unexplained variable for rest) of 4-, 5- and 6-factor solutions are similar suggesting the stability of solutions. The analysis of OA types as a function of number of factors and *a* values indicated that an *a*-value of 0.2 (6f-3) was a reasonable choice for a 6-factor solution because it allowed flexibility in the solution, while still providing a near-constant mass contribution of each OA type across various *a* values and showing the best correlations with reference mass spectra and collocated measurements. As shown in Figure S3-b and S4b, the time series of each factor resolved from both PMF and ME-2 analysis have similar temporal trends. HOA was observed all year, while BBOA was highest during colder periods. Yearlong ME-2 analysis provided an average day-of-week pattern of each factor at JST (Figure S3-6). No day-

of-week variation of LV-OOA, IEPOX-OA and 91Fac was observed, suggesting that these factors are likely influenced by long-range transport and atmospheric oxidation. However, SV-OOA increases during the weekends and early during the weekdays, and then decreases during the late weekday, suggesting that local SOA formation influenced its formation. On average, HOA decreases during weekends, which is likely due to the less traffic-related activities compared to weekdays, whereas BBOA increases during weekends, possibly caused by increased residential burning when Atlanta residents are home from work. As shown in Table S3-2, HOA strongly correlated with primary emissions such as CO (R = 0.75 - 0.78) and NO_x (R = 0.74 – 0.76). BBOA has a strong correlation (R = 0.81 – 0.98) with reference mass spectra of BBOA (Ng et al., 2010) and with levoglucosan (R = 0.72 – 0.89). LV-OOA was moderately correlated with SO_4^{2-} (R = 0.56 – 0.75), whereas SV-OOA has a weak correlation with NO_3^- (R = 0.12 – 0.14). Yearlong PMF and ME-2 analysis suggested similar trends of IEPOX-OA with the maximum contribution in summer (Figure S3-4). IEPOX-OA correlated well (R = 0.82 – 0.99) with IEPOX-OA mass spectra (Budisulistiorini et al., 2016) and with IEPOX-derived SOA tracers (R = 0.79 – 0.95). However, the yearlong PMF and ME-2 analysis suggested the presence of IEPOX-OA in wintertime, which is inconsistent with the seasonal analysis presented by previous studies (Xu et al., 2015; Budisulistiorini et al., 2016). Regarding yearlong ME-2 analysis, IEPOX-OA contributed ~ 12% of total OA in winter, despite the fact that the sum of IEPOX-derived SOA concentrations over the entire winter period discussed in Section 3.3.1 was very low (1.1 + 0.9 ng m^{-3}). It is worth noting that PMF and ME-2 analyses assume constant profiles over the period of the dataset (Paatero et al., 1994; Canonaco et al., 2013; Reyes-Villegas et al., 2016), which may not be necessarily true throughout the year at JST where meteorological conditions and emissions vary greatly. As a result, seasonal analysis was

conducted in order to more clearly resolve certain OA sources and reasonably estimate mass contributions of each factor.

3.3.3 OA factors resolved by seasonal PMF and ME-2 analysis

Some seasons (spring and fall) were further segregated into finer periods in order to capture heterogeneity in certain emissions, such as biogenic VOC emissions. The periods of seasonal PMF and ME-2 analysis are summarized in Table 3-1. The finer periods within spring and fall seasons were classified as subspring-1, subspring-2, subfall-1, and subfall-2 to capture finer changes of potential sources. By applying PMF and ME-2 analysis to resolve OA sources, 3 to 6 factors were identified depending on the specific season. As described in the following sections, the statistical diagnostics by PMF and ME-2 aided in determining potential sources of OA during each season or sub-seasonal period. Rotational forcing parameter (FPEAK) between -1 to 1 for each dataset was investigated and neither significant rotation nor improved correlations of factor profile and time series (less than 10%) were observed. As a result, the default rotational ambiguity (FPEAK = 0) was used for the analysis presented in this study.

3.3.3.1 Subspring-1 period

As shown in Table S3-3, the application of PMF to the ACSM dataset indicated that 3 factors was an optimum solution to determine the number of OA sources. The Q/Q_{exp} value decreased less than 10% when increasing from a 3-factor to 5-factor solution, suggesting that the 4^{th} and 5^{th} factor are not necessary in the PMF solution. $R_{TS\&MS}$ values indicated that factor splitting occurred when applying 4- and 5-factor solutions, as some of factors had similar time series and mass spectra ($R_{TS\&MS} > 0.8$). SEED analysis within PMF clearly suggested that 3 factors was the best solution because the analysis provided identical contributions for each factor regardless of the starting SEED. However, in the 3-factor PMF solution, the mass spectrum of

the BBOA factor was well correlated with both the reference BBOA (R = 0.82) and IEPOX-OA (R = 0.84) mass spectra (Table S3-4). To confirm the 3-factor PMF solution, ME-2 was performed separately by constraining both HOA and BBOA. As a comparison of the PMF and ME-2 results, the 3- and 4-factor ME-2 solutions and the 3-factor PMF solution are shown in Table S3-5. Strongest correlations are observed between the 3 factors resolved from ME-2 with collocated measurements and reference mass spectra, suggesting that 3 factors is the optimum solution for the source apportionment of OA. Regarding the 3-factor ME-2 solution, LV-OOA (65%) was the most abundant OA type, whereas HOA and BBOA contributed 20% and 15%, respectively. HOA was well correlated with known primary emissions, including both CO (R = 0.81) and NO_x (R = 0.69). The HOA and BBOA factors resolved in the 3-factor ME-2 solution were more strongly correlated ($R \geq 0.97$) with their respective reference mass spectra than the BBOA (R = 0.82) and HOA (0.94) resolved in the 3-factor PMF solution (Table S3-5). The BBOA factor resolved from both PMF and ME-2 analysis, was moderately correlated with combustion tracers CO ($R \geq 0.61$) and NO_x ($R \geq 0.41$). The 3-factor PMF and ME-2 solutions both contained the LV-OOA factor, which had a strong correlation (R = 0.97) with the reference mass spectrum. LV-OOA resolved from PMF and ME-2 had the highest O:C ratio (0.86) of all factors, suggesting an aged aerosol consistent with prior work (DeCarlo et al., 2010; Canagaratna et al., 2015). LV-OOA from both analyses yielded a weak correlation (R = 0.26) with SO_4^{2-} during this subspring-1 period.

3.3.3.2 Subspring-2 period

Application of PMF to this period yielded 6 factors, including HOA, BBOA, LV-OOA, SV-OOA, IEPOX-OA, and 91Fac. The PMF diagnostics were analyzed as described above in Section 3.3.3.1. Results of SEED analysis are presented in Table S3-6, which indicate that 6

factors is an optimum solution. LV-OOA, IEPOX-OA, SV-OOA, 91Fac, HOA and BBOA contributed 35, 25, 12, 10, 10, and 9%, respectively, to the total OA mass (Table S3-7). HOA was well correlated with CO (R = 0.68) and moderately correlated with NO_x (R = 0.51). Similar to the subspring-1 period, the LV-OOA mass spectrum had a strong correlation (R = 0.93) with its reference mass spectrum (Table S3-7) and had the highest O:C ratio (1.14). LV-OOA was moderately correlated (R = 0.63) with SO_4^{2-} (Table S3-7), possibly indicating similar sources or chemistry. SV-OOA had a lower O:C ratio (0.35) than LV-OOA, consistent with previous work (Canagaratna et al., 2015; Xu et al., 2015). IEPOX-OA strongly correlated with its reference mass spectrum (R = 0.93, Table S3-7) and SO_4^{2-} (R = 0.82, Table S3-7), consistent with recent studies (Budisulistiorini et al., 2013, 2016; Xu et al., 2015). During subspring-2, isoprene SOA chemistry begins to contribute substantially to the OA mass. Furthermore, PMF resolved the 91Fac mass spectrum, which is associated with isoprene SOA formation through a non-IEPOX route (Krechmer et al., 2015; Riva et al., 2016), and was also well correlated (R = 0.87, Table S3-7) with its reference mass spectrum. IEPOX-OA was approximately twice as large as the OA mass fraction of 91Fac, which is consistent with recent studies at LRK (Budisulistiorini et al., 2015, 2016).

3.3.3.3 Summer

As shown in Table S3-8, the starting Q/Q_{exp} of 1.09 (close to 1) suggested a close fit of the residuals on the order of the input error matrix for the data (Ng et al., 2011). The plot of Q/Q_{exp} values versus the number of factors indicated that at least two factors were necessary to explain the dataset, especially due to the steep declining trend in the Q/Q_{exp} value shown when adding the second factor. SEED diagnostics suggested as much as 4 or 5 factors might provide a better PMF solution due to an identical mass contribution of each factor was invariant with

starting point. As shown in Table S3-9, the 5-factor solution appeared to yield the best PMF result based on showing the strongest correlations (R~ 0.91 – 0.95) with external tracers and/or reference mass spectra. However, the 6-factor solution from ME-2 with HOA and BBOA constrained (*a* value = 0.3) yielded strong correlations (R~ 0.91 – 0.95) of the resolved factors with collocated measurements and reference mass spectra, as shown in Table 3-10. The 5-factor solution from PMF was unable to resolve BBOA, whereas the 6-factor solution from ME-2 resolved a low-mass contribution of BBOA (2%), consistent with low levoglucosan mass concentrations measured by the GC/EI-MS in summer (19.9 $\pm$ 14.4 ng m^{-3} on average). As a result, the 6-factor solution from ME-2 was selected as the optimum solution. ME-2 resolved LV-OOA (27%), SV-OOA (26%), IEPOX-OA (29%), 91Fac (11%), HOA (5%) and BBOA (2%). As expected, HOA was moderately correlated with CO (R = 0.55) and NO_x (R = 0.40). LV-OOA was weakly correlated with SO_4^{2-} (R= 0.16), and yielded the highest O:C ratio (1.12). The IEPOX-OA factor was strongly correlated with IEPOX-derived SOA tracers measured by GC/EI-MS (R = 0.92), consistent with prior work (Budisulistiorini et al., 2013, 2016). A weaker correlation (R = 0.23) found between IEPOX-OA and SO_4^{2-} in this study, than reported at other locations throughout the southeastern US region (Budisulistiorini et al., 2013, 2015, 2016; Xu et al., 2015). Similar to the subspring-2 period, 91Fac accounted for approximately half of the IEPOX-OA mass fraction.

3.3.3.4 Subfall-1 period

As shown in Table S3-10, SEED analysis of the PMF solutions strongly suggested that a 4-factor solution was better than 5- or 6- factor solutions. The potential factors resolved were HOA, LV-OOA, SV-OOA, and 91Fac. The correlations of factors resolved from PMF with collocated measurements, reference mass spectra and SOA tracers are shown in Table 3-12.

However, the GC/EI-MS analysis for SOA tracers suggested high levoglucosan mass concentratios during the fall period (221.9 + 175.9 ng m^{-3} on average), although PMF did not resolve the BBOA factor. Thus, ME-2 analysis was also conducted with HOA and BBOA being constrained. The correlation between the resolved factors from PMF and ME-2 with collocated measurement and reference mass spectra are shown in Table S3-13. All 5 factors resolved by ME-2 analysis strongly correlated with reference mass spectra (Table S3-13). HOA was weakly correlated with CO (R = 0.22) and NO_x (R = 0.26), which were weaker than correlations observed in the other seasons. LV-OOA was moderately correlated with SO_4^{2-} (R = 0.51) and had a higher O:C ratio (0.92) than SV-OOA (0.35). IEPOX-OA was not resolved during the subfall-1 period, consistent with low concentrations (5.4 ng m^{-3} on average) of the IEPOX-derived SOA tracers as shown in Tables 3-2 and 3-3. 91Fac was highly correlated with the reference mass spectra (R = 0.94) and with IEPOX-derived SOA tracers (R = 0.98), suggesting that 91Fac was at least partially influenced by isoprene oxidation chemistry. 91Fac was observed to contribute 24% of the total OA mass during this period and was likely influenced in part by monoterpene oxidation chemistry as described by Xu et al. (2015). The most abundant OA was LV-OOA (37%). SV-OOA, HOA and BBOA contributed 17, 14 and 8%, respectively, to the total OA mass (Table 3-13).

3.3.3.5 Subfall-2 period

A 4-factor solution was selected based on the PMF diagnostics and the best correlations with collocated measurements as shown in Tables S3-14 and S3-15, respectively. SEED analysis demonstrated invariant factor contributions of the 4-factor solution. Correlation with reference mass spectra as well as time series of trace gases, confirmed that the 4-factor solution produced the best correlation. The 4-factor solution from PMF resolved LV-OOA (32%), SV-OOA (26%),

HOA (22%), and BBOA (20%). As observed in several other seasons from this study, HOA was strongly correlated with CO (R = 0.88) and NO_x (R = 0.76), LV-OOA had a weak correlation with SO_4^{2-} (R = 0.35), but had an O:C ratio (1.05) that was higher than SV-OOA (0.43). BBOA was strongly correlated (R = 0.88) with levoglucosan measured by GC/EI-MS from high-volume aerosol filters.

3.3.3.6 Winter

PMF analysis suggested that 4 factors provided an optimum solution (Tables S3-16 and S17), which was also indicated by ME-2 analysis (Table S3-18). ME-2 analysis of the winter data was of particular interest to determine whether 91Fac could be resolved since prior work hypothesized that 91Fac is derived from the atmospheric oxidation of monoterpenes emitted from conferous trees (Boyd et al., 2015; Budisulistiorini et al., 2015); however, 91Fac was not resolved from ME-2 analysis. Nevertheless, results from ME-2 analysis were used for winter because it provided the strongest correlations with collocated data sets and with reference mass spectra. ME-2 analysis resolved the HOA, BBOA, LV-OOA and SV-OOA factors. The largest mass fraction of OA was LV-OOA (63%), whereas HOA and BBOA contributed 17 and 14%, respectively, with SV-OOA contributing only 6% to the total OA mass. As expected, HOA was well correlated with CO (R = 0.73) and NO_x (R = 0.77). The largest average mass concentration of levoglucosan (197.8 μg m^{-3}) over the entire sampling year was measured from high-volume aerosol filter samples collected at JST during this time period by GC/EI-MS. As a result, BBOA was tightly constrained during ME-2 analysis with an *a* value of 0.05. The BBOA resolved from ME-2 was strongly correlated (R = 0.87) with levoglucosan. Similar to all other seasons, LV-OOA had a higher O:C ratio (0.98) than SV-OOA (0.64). SV-OOA weakly correlated with NO_3^- (R = 0.29).

3.3.4 Seasonal comparison of OA sources

Figure 3-2 shows the seasonal variations of all OA subtypes during the 1-year sampling period at JST and the seasonal comparison of average mass concentrations contributed by each OA source. Seasonal mass spectra of OA subtypes are compared in Figures S3-7 – S3-12. ME-2 analysis provided results similar to PMF in subspring-1, subfall-2 and winter, whereas ME-2 resolved more factors in summer and subfall-1, suggesting that PMF is adequate to explain source apportionment of OA in colder seasons where primary emissions play an important role. By contrast, the performance of ME-2 is superior in the warmer seasons where SOA may vary greatly due to oxidation processes. It should be noted that only subspring-2 and subsfall-2 used the OA matrix (mass spectral profile and time series) derived from PMF analysis, as described above in Sections 3.3.2.2 and 3.3.3.5, respectively. HOA was found in all seasons and had similar mass spectra across seasons (Figure S3-7). HOA had prominent ions at *m/z* 27, 29, 41, 44, 55, 57, 71, 85, and 99, consistent with previous studies (Budisulistiorini et al., 2015; Ng et al., 2010; Zhang et al., 2005a). The spectral similarity of HOA across seasons (Figure S3-7) suggests that HOA likely has the same primary emission sources year round. The diurnal trends of HOA during different seasons, compared in Figure 3-8a, were similar across all seasons, with peaks in HOA from 8-10 am (local time) and after 8 pm (local time) as shown in Figure 3-4a. The diurnal profiles are consistent with traffic rush hours in downtown Atlanta and agree with previous studies (Sun et al., 2011; Budisulistiorini et al., 2013, 2016). Yearlong ME-2 analysis of HOA provided an average day-of-week pattern in HOA at JST (Figure S3-6) which revealed that HOA decreased during weekends presumably concomitant with decreased traffic-related activity compared to weekdays.

BBOA was observed in all seasons, with the highest mass contributions observed during colder seasons which may result from residential heating or biomass burning. BBOA contains the fragment ion at *m/z* 60, which corresponds mostly to the $C_2H_4O_2^+$ ion and has been previously shown to serve as a good tracer for fresh biomass burning (Alfarra et al., 2007; Aiken et al., 2009; DeCarlo et al., 2010). Other characteristic BBOA ions at *m/z* 29 (CHO^+) and 73 ($C_3H_5O_2^+$) have been demonstrated to result from the fragmentation of anhydrosugars, such as the levoglucosan marker, during biomass combustion (Alfarra et al., 2007; Aiken et al., 2009). Average diurnal trends in BBOA were similar in colder seasons, suggesting similar sources of biomass burning with an increased during the night and decreased during the day (Figure 3-4b) likely related to residential wood burning as well as PBL dynamics. In addition, day-of-the-week patterns resolved from of yearlong ME-2 analysis of BBOA (Figure S3-6) indicated that BBOA increases during weekends, possibly as a result of increased residential burning when Atlanta residents are home from work. However, the diurnal cycle of BBOA varied less during the summer and subfall-1 periods than during colder seasons, suggesting that BBOA during the summer and subfall-1 periods was likely aged and/or transported from long distances.

LV-OOA contained a prominent ion at *m/z* 44 (Figure S3-9) and had the highest O:C ratio across all seasons, indicating a more aged OA type. Various levels of correlation were found between LV-OOA and SO_4^{2-} across seasons (R ranging 0.28 to 0.66), suggesting varying degrees of oxidation within the urban OA consistent with previous studies (Sun et al., 2011; Budisulistiorini et al., 2016). This observation could explain different average diurnal trends across each season were observed (Figure 3-4c).

SV-OOA contained a higher 43-to-44 ion ratio (Figure S3-10) compared to that of LV-OOA in all seasons, which thus appears to be a key differentiating characteristic between these

two profiles (Ng et al., 2010). Due to the fact that SV-OOA is a surrogate for fresh OOA, variations in the average diurnal profiles of SV-OOA were observed across each season (Figure 3-3d), likely resulting from different meteorological conditions, sources, and photochemical distributions.

IEPOX-OA was only observed in subspring-2 and summer and is associated with high isoprene emissions during warmer periods (Guenther et al., 2006). Average diurnal profiles of IEPOX-OA were fairly flat (Figure 3-4e); however, there is a small increase (0.2 μg m^{-3}) during the summer season between 12-2 PM local time, consistent with previous observations at JST (Budisulistiorini et al., 2013). However, the flat diurnal profiles of IEPOX-OA during both seasons suggests at regional source (Budisulistiorini et al., 2015, 2016). 91Fac resolved during subspring-2, summer and subfall-1 periods have similar mass spectra (Figure S3-12). During those periods, the average diurnal profile 91Fac showed a peak at night, suggesting the role of PBL dynamics (Figure 3-4f); however, during summer there was a small peak in 91Fac between 9 - 11 AM local time, which could be related to isoprene-derived hydroperoxides condensing into aerosol as recently shown by Krechmer et al. (2015) and Riva et al. (2016) at Centerville, Alabama, and Look Rock, Tennessee sites, respectively.

Temporal variations in the relative contributions of OA sources at JST from each season are depicted in Figure 3-2. The sum of LV-OOA and SV-OOA dominated the mass fraction of OA in all seasons at JST (46 – 70%), in agreement with data from other urban locations (Zhang et al., 2007; Jimenez et al., 2009). Wind speed and direction (as well as other meteorological parameters) could likely explain the different concentrations of LV-OOA across seasons. As shown in Figure 3-2b, average LV-OOA concentration was highest in subspring-1 (5.70 μg m^{-3}) and significantly higher (t test, *p-value* < 0.05) than subfall-2 (2.70 μg m^{-3}). LV-OOA represents

a highly-aged (oxidized) OA from various sources, identification of which remains a significant challenge and should be the focus of future work.

SV-OOA was highest in summer (2.96 μg m^{-3} on average, Figure 3-2b), suggesting that photooxidation may play a role in local SV-OOA formation. The traffic (HOA) contribution represented 5 – 22% of total OA (Figure 3-2a) mass year-round. Near-identical mass concentrations of HOA observed across all seasons (Figure 3-2b), suggests similar sources. As shown in Figures 3-2a and 3-2b, the contribution of BBOA to total OA was comparable in colder seasons (14 – 20%) and low contribution in summer (2%). IEPOX-OA contributed 25 – 29% of total OA mass (Figure 3-2a) in warmer seasons, consistent with prior studies (Budisulistiorini et al., 2013, 2015, 2016; Hu et al., 2015; Xu et al., 2015). In this study, IEPOX-OA was higher in summer (3.31 μg m^{-3} on average) than subspring-2 (2.23 μg m^{-3} on average), most reasonably explained by increased leaf surface area, solar radiation, and ambient temperature (Guenther, 2006). Notably, during subspring-2 and summer seasons, IEPOX-OA was nearly as abundant as LV-OOA, and thus an important OA source. 91Fac contributed 10, 11, and 24% during subspring-2, summer, and subfall-1 periods, respectively, to the total OA mass. Although an association of 91Fac with biogenic emissions has been hypothesized (Robinson et al., 2011; Slowik et al., 2011), recent studies have demonstrated that this factor is most likely derived from organic hydroxyhydroperoxides of isoprene (Krechmer et al., 2015; Riva et al., 2016) or from nighttime oxidation chemistry of monoterpenes (Xu et al., 2015).

Correlations of aerosol LWC and pH with OA type are shown in Tables S3-19 and S20. OA types resolved from yearlong factor analysis yielded weak correlations with LWC (R between -0.05 to -0.30, n = 91). However, stronger correlations between OA type and LWC were observed when applying seasonal factor analysis. For example, IEPOX-OA from subspring-2

showed a moderate negative correlation with LWC (R = 0.54), whereas IEPOX-OA resolved from summer was not well correlated with LWC. In addition, BBOA was negatively and moderately correlated with LWC (R = -0.65) during the subspring-1 period. These observations suggest that LWC may play a role in either enhancing or suppressing the formation of certain OA types, but this needs to be further explored in future work.

From yearlong factor analysis, weak negative correlation (R= -0.27, n = 91) was observed between LV-OOA and aerosol pH, whereas no correlation (R= 0, n = 91) was observed between IEPOX-OA and aerosol pH. These findings are consistent with recent studies (Budisulistiorini et al., 2013, 2015, 2016; Xu et al. 2015). By applying seasonal factor analysis, stronger (negative) correlations of IEPOX-OA with aerosol pH were observed, especially during the subspring-2 (R= -0.67, n=9) and summer (R= -0.42, n = 25) periods. To our knowledge, this is the first time that such a correlation has been resolved from field measurements (Budisulistiorini et al., 2013, 2015, 2016; Lin et al., 2013; Xu et al., 2015; Rattanavaraha et al.. 2016). Negative correlations between IEPOX-OA and aerosol pH are consistent with laboratory and chamber studies demonstrating that acidic and wet sulfate aerosol enhances IEPOX-derived SOA formation (Surratt et al., 2007, 2010; Lin et al., 2012, 2014; Gaston et al., 2014; Nguyen et al., 2014; Riedel et al., 2015, 2016). The moderate negative correlation of IEPOX-OA with aerosol pH (R= -0.67 in subspring-2 and -0.42 in summer) indicates that the aerosols are likely acidic enough to promote IEPOX-derived SOA formation even though the aerosol pH does not vary much in the southeastern US, consistent with recent work (Guo et al., 2015; Xu et al., 2015). When IEPOX-SOA tracers are at their highest levels during summer, stronger correlations observed between IEPOX-OA with SO_4^{2-} (R= 0.72) than with LWC (R= -0.07) indicates that SO_4^{2-} levels are the

most important parameter in forming IEPOX-OA (Gaston et al, 2014, Riedel et al., 2015, 2016; Xu et al., 2015).

3.3.5 Year-to-year comparison of OA subtypes at JST

Table 3-4 compares chemical characterization of NR-PM_1 collected at JST during 2011, 2012, and 2013 (Budisulistiorini et al., 2013, 2016; Xu et al., 2015) with that during 2014 (this study). In all years, the average mass concentration of NR-PM_1 was consistently highest in summer. The average NR-PM_1 mass (16.7 μg m^{-3}) in summer 2014 was quite similar to that observed during summer 2011 (16.8 μg m^{-3}, Budisulistiorini et al., 2013). However, the NR-PM_1 mass during summers of 2011 and 2014 were almost double that of summer 2012 (8.8 μg m^{-3}, Budisulistiorini et al., 2016). Table 3-4 rules out a difference in average rainfall to explain the discrepancy; however, other meteorological variables, such as differences in air masses arriving to the sampling site, could be responsible. Further investigation is required, but Table 3-4 establishes that year-to-year changes in NR-PM_1 mass during summer can occur. Average NR-PM_1 mass during spring 2014 (12.5 μg m^{-3}, the average of subspring-1 and -2 periods) was higher than 2012 (6.2 μg m^{-3}), whereas fall 2014 (9.5 μg m^{-3}, average of subfall-1 and -2 periods) was lower than falls 2011 (13.7 μg m^{-3}) and 2012 (12.5 μg m^{-3}). In addition, average NR-PM_1 mass during winter 2014/2015 (8.0 μg m^{-3}) was lower than winter 2012 (10.5 μg m^{-3}). In all years, NR-PM_1 mass during warmer seasons was dominated by organics and sulfate with relative contributions having a range of 65 – 76% and 10 – 20%, respectively. NO_3^- contributed more towards the total NR-PM_1 mass during winter 2014 (22.3%) than during winter 2012 (9.3%). Average temperature during winter 2014 (8.8 ºC) was colder than during 2012 (12.3 ºC), which provides a possible explanation for the higher mass fraction of nitrate in NR-PM_1 (Lanz et al., 2007).

Year-to-year comparisons show that HOA contributed to OA across all seasons (9 – 30%), but was typically higher in colder seasons. BBOA was most commonly observed in colder seasons. LV-OOA contributed the largest OA mass fraction during spring of 2012 and 2014. This was due to the fact that during summer each year isoprene-derived SOA sources (IEPOX-OA and 91Fac) became more significant and added to the OA mass fraction, whereas during winter seasons POA sources like HOA and BBOA became more dominant. During all years, IEPOX-OA consistently appeared during the warmer periods, especially during summers with mass fraction ranging from 16 – 38% of total OA. 91Fac was only resolved during 2014 at JST, with contributions 10% in spring and 11% in summer and 24% in fall. However, we note that ME-2 with HOA and BBOA constrained is applied in 2014, whereas analysis by PMF alone has been applied to data collected in 2012 and 2013. Coupling OA source apportionment derived from ACSM measurements in southeastern US with regional air quality models will likely improve the predictions of POA and SOA components (e.g., Karambelas et al., 2014), thus leading to the development of effective control strategies.

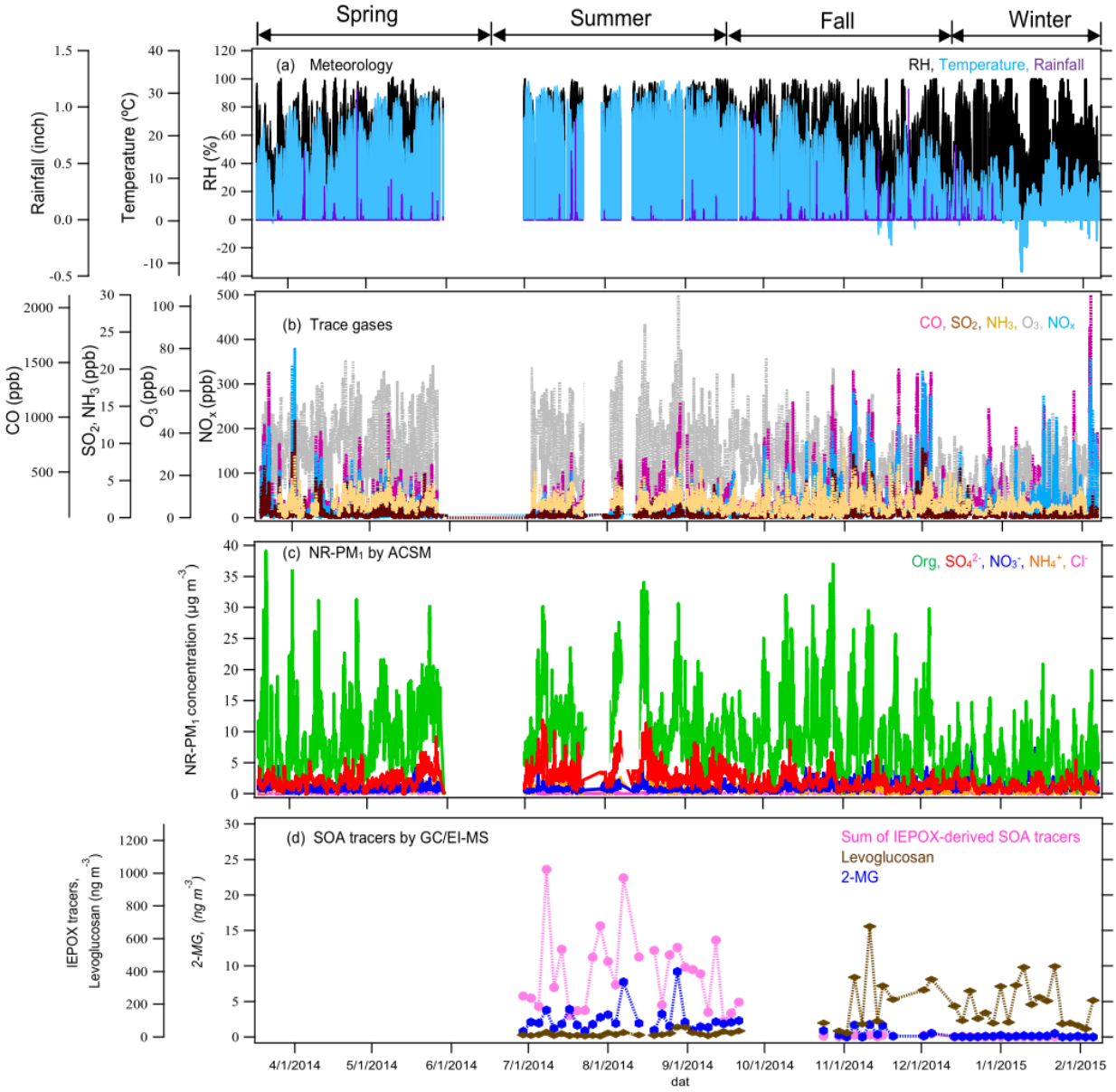

Figure 3-1. Temporal variation of (a) meteorological data, (b) trace gases, (c) NR-PM_1 measured by ACSM and (d) SOA tracers detected from high-volume aerosol filter samples by GC/EI-MS at the JST site. Seasonal scales set from using 2014 Farmer's Almanac.

(a)

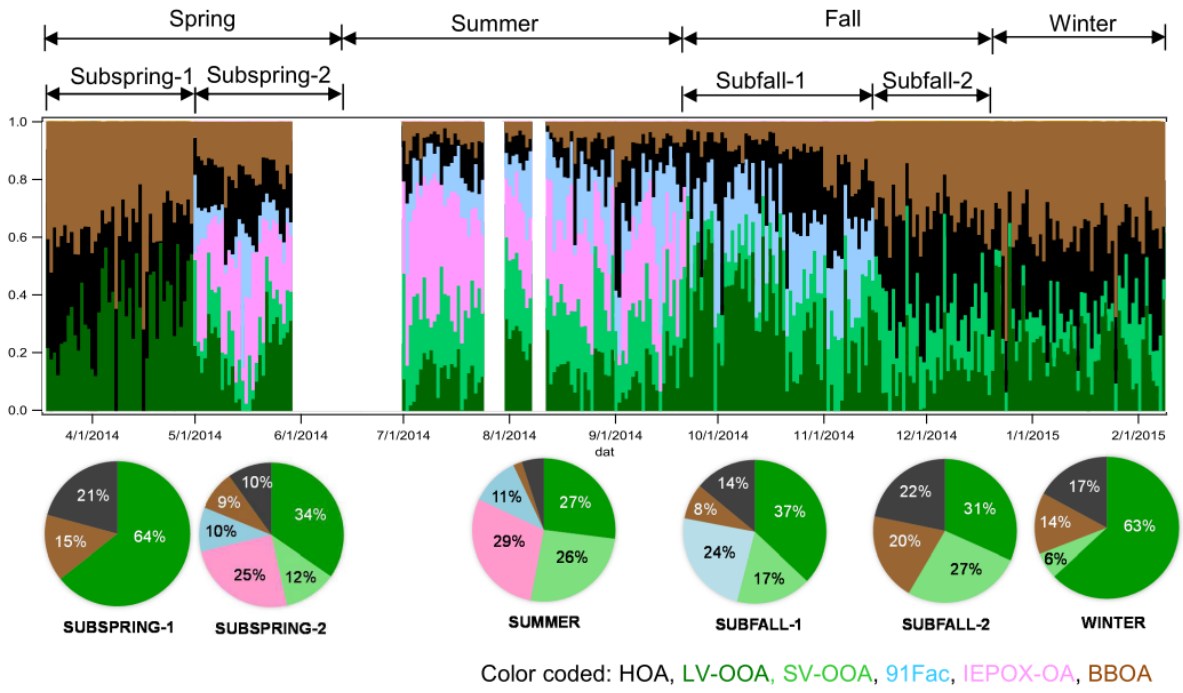

(b)

Conc (μg m^{-3})	Subspring-1	Subspring-2	Summer	Subfall-1	Subfall-2	Winter
HOA	1.87	0.89	0.57	1.22	1.91	0.75
BBOA	1.34	0.80	0.23	0.70	1.74	0.62
IEPOXOA	n/a	2.23	3.31	n/a	n/a	n/a
91Fac	n/a	0.89	1.25	2.09	n/a	n/a
LV-OOA	5.70	3.03	3.08	3.22	2.70	2.77
SV-OOA	n/a	1.07	2.96	1.48	2.35	0.26

Figure 3-2. (a) Temporal variation of the relative contributions of OA sources. (b) Average mass fraction of OA sources during each season and sub season shown as pie charts.

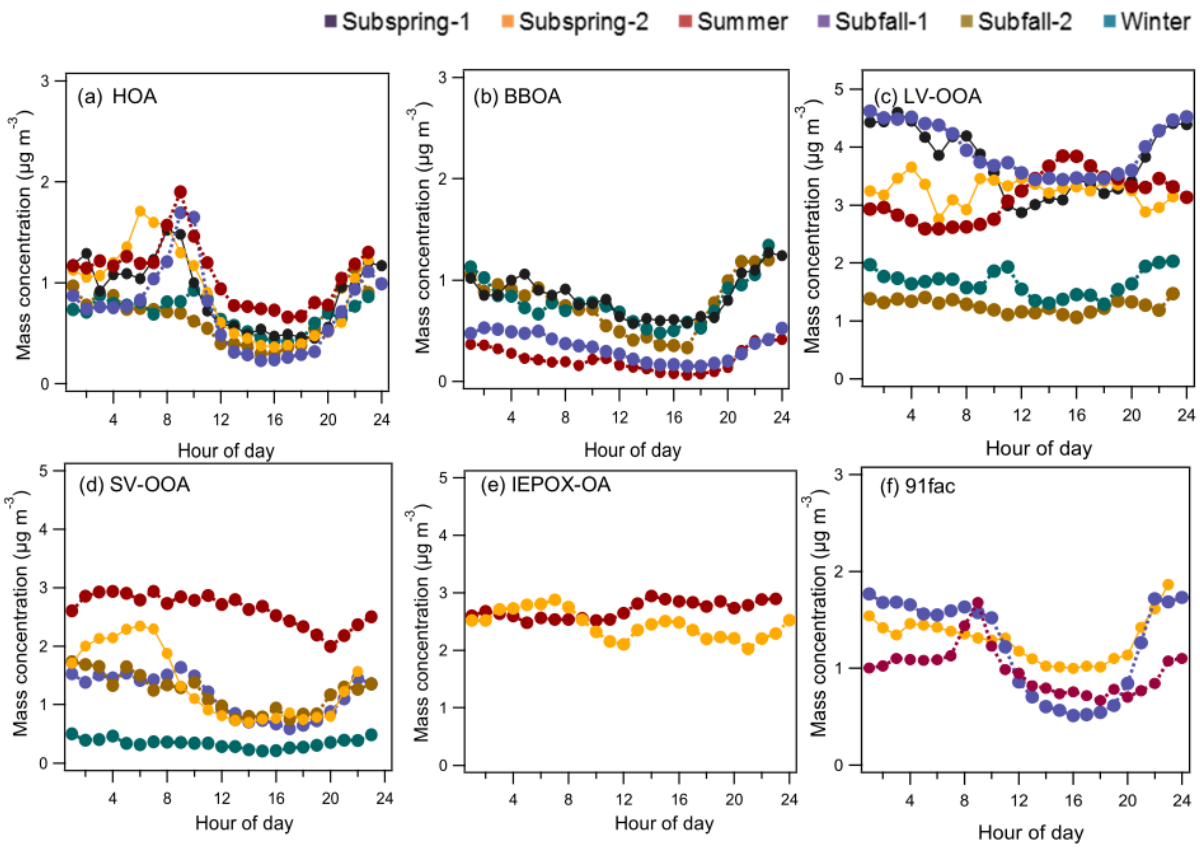

Figure 3-3. Average diurnal cycle of OA sources during different seasons.

Table 3-1. Sampling periods classified as spring, summer, fall and winter by following the 2014 Farmer's Almanac. Finer time periods within spring (subspring-1 and subspring-2) and fall (subfall-1 and subfall-2) were used to improve PMF/ME-2 results by increasing correlations with collocated data sets (trace gases or OA tracers) and reference mass spectra.

Season	Dates
Spring • Subspring-1 • Subspring-2	March 20 – June 20, 2014 • March 20 – April 30, 2014 • May 1 – June 20, 2014
Summer	June 21 – September 21, 2014
Fall • Subfall-1 • Subfall-2	September 22 – December 2014 • September 22 – November 15, 2014 • November 16 – December 20, 2014
Winter	December 21, 2014 – February 8, 2015*

*last day of deployment

Table 3-2. Summary of collocated measurements of meteorological variables, gaseous species, and $PM_{2.5}$ constituents.

Category	Condition	Spring				Summer				Fall				Winter			
		Avg	SD	Min	Max	Avg	SD	Min	Max	Avg	SD	Min	Max	Avg	SD	Min	Max
Meteorology	BP (mbar)	982.8	4.1	969.5	994.9	982.8	2.3	976.0	989.4	985.0	4.6	970.6	996.8	985.5	6.4	970.2	997.2
	SR (W m^{-2})	239.4	314.9	0.0	1083.6	236.8	303.5	0.0	1099.2	153.3	234.5	0.0	905.7	76.2	152.8	0.3	649.4
	RH (%)	65.5	21.6	9.2	102.4	73.9	16.8	27.4	100.3	67.2	20.5	11.2	100.0	85.9	15.3	37.5	99.8
	Temp (°C)	19.4	6.4	-0.8	32.7	25.0	3.4	14.7	33.7	13.1	7.3	-5.9	29.1	4.7	3.7	-12.2	16.0
	Rainfall (inch)	0.2	1.1	0.0	29.5	0.1	1.3	0.0	33.1	0.1	0.7	0.0	14.4	0.3	1.1	0.0	8.3
Trace gas (ppbv)	CO	220.5	121.4	85.6	1347.3	207.7	106.3	82.5	1060.2	278.0	210.9	87.5	1388.8	295.4	200.0	122.2	1196.0
	NO_x	15.5	20.3	0.7	243.1	12.5	13.7	0.5	143.7	28.2	38.1	1.0	274.5	26.1	37.5	1.5	257.9
	O_3	32.3	17.4	1.1	89.5	28.7	18.5	1.2	104.9	19.8	13.7	0.8	73.8	12.0	8.0	1.0	29.2
	NH_3	1.9	0.9	0.0	7.3	1.9	0.8	0.1	8.6	1.7	1.2	0.0	11.2	1.0	0.6	0.3	3.1
	SO_2	0.6	0.7	0.0	9.0	0.4	0.5	0.0	7.5	0.7	1.0	0.0	8.5	0.5	0.9	0.0	6.0
PM_1 ($\mu g\ m^{-3}$)	NR-PM_1	12.8	8.0	0.0	55.6	16.7	8.4	1.5	52.6	12.3	8.7	0.3	54.8	8.0	5.7	0.0	38.9
	Org	8.9	5.7	0.0	39.1	11.4	5.5	1.1	34.0	8.7	6.2	0.2	37.0	4.4	3.2	0.0	20.8
	SO_4^{2-}	2.1	1.2	0.0	9.2	3.5	1.9	0.3	11.8	1.7	1.1	0.0	8.6	1.2	0.7	0.0	5.5
	NO_3^-	0.9	0.6	0.0	4.7	0.8	0.4	0.1	3.5	1.3	0.9	0.1	6.3	1.8	1.4	0.0	7.6
	NH_4^+	0.8	0.4	0.0	2.4	1.0	0.5	0.0	3.1	0.6	0.4	0.0	2.7	0.5	0.4	0.0	4.8
	Cl^-	0.0	0.0	0.0	0.2	0.0	0.0	0.0	0.1	0.0	0.0	0.0	0.2	0.0	0.0	0.0	0.2
	LWC	3.3	2.2	0.6	8.8	8.4	4.8	1.9	22.4	3.2	2.3	.3	9.1	1.7	0.9	0.5	3.4
	Aerosol pH	1.6	0.6	-0.6	2.3	1.4	0.7	0.0	2.3	2.0	1.0	0.1	3.7	1.6	0.8	0.1	3.1
SOA tracers (ng m^{-3})	IEPOX tracers	n/a	n/a	n/a	n/a	391.7	240.7	95.3	1022.5	5.4	6.1	0.0	20.0	1.1	0.9	0.1	3.2
	2-MG	n/a	n/a	n/a	n/a	2.5	1.9	0.8	9.2	0.5	0.7	0.0	1.8	0.1	0.1	0.0	0.5
	Levoglucosan	n/a	n/a	n/a	n/a	19.9	14.4	5.3	61.0	221.9	175.9	23.9	674.6	197.8	123.0	50.0	430.6

Table 3-3. Summary of SOA tracers measured by GC/EI-MS.

SOA tracers	*m/z*	Frequency of detection (%)	Average concentration (ng m^{-3})	Max concentration (ng m^{-3})
Summer (n = 27)				
IEPOX SOA tracers*				
(1) 2-methylerythritol	219	100	107.9	246.2
(2) 2-methylthreitol	219	100	29.8	72.2
(3) (E)-2-methylbut-3-ene-1,2,4-triol	231	100	154.3	468.7
(4) (Z)-2-methylbut-3-ene-1,2,4-triol	231	100	56.4	166.0
(5) 2-methylbut-3-ene-1,2,3-triol	231	100	26.6	80.1
(6) *cis*-3-MeTHF-3,4-diol	262	37	0.9	2.5
(7) *trans*-3-MeTHF-3,4-diol	262	70	<0.01	<0.01
2-MG	219	100	2.4	9.2
Levoglucosan	204	100	19.9	61
Fall (n = 13)*				
IEPOX SOA tracers				
(1) 2-methylerythritol	219	100	2.0	5.8
(2) 2-methylthreitol	219	85	0.9	2.3
(3) (E)-2-methylbut-3-ene-1,2,4-triol	231	85	1.4	6.4
(4) (Z)-2-methylbut-3-ene-1,2,4-triol	231	62	0.5	2.0
(5) 2-methylbut-3-ene-1,2,3-triol	231	38	0.3	1.1
(6) *cis*-3-MeTHF-3,4-diol	262	31	0.9	1.9
(7) *trans*-3-MeTHF-3,4-diol	262	0	0	0
2-MG	219	77	0.6	1.8
Levoglucosan	204	100	221.9	674.6
Winter (n = 17)				
IEPOX SOA tracers*				
(1) 2-methylerythritol	219	65	0.5	1.3
(2) 2-methylthreitol	219	41	0.3	0.8
(3) (E)-2-methylbut-3-ene-1,2,4-triol	231	53	0.5	0.9
(4) (Z)-2-methylbut-3-ene-1,2,4-triol	231	6	0.2	0.2
(5) 2-methylbut-3-ene-1,2,3-triol	231	6	0.0	0.0
(6) *cis*-3-MeTHF-3,4-diol	262	12	0.2	0.2
(7) *trans*-3-MeTHF-3,4-diol	262	0	0	0
2-MG	219	71	0.1	0.5
Levoglucosan	204	100	197.8	430.6

*IEPOX tracers = summation of (1) to (7)

Table 3-4. Yearly variation of average mass concentrations of NR-PM_1 and percent contribution of sources.

Category	Condition	Spring				Summer			Fall				Winter	
		2012[a]	2013 (May)[b]	2014 subspring-1	2014 subspring-2	2011[b]	2012[a]	2014	2011[b]	2012[a]	2014 subfall-1	2014 subfall-2	2012[b]	2014
Meteorology	Solar radiation (W m^{-2})	329.9	n/a	214.2	260.1	239.0	294.0	236.8	131.0	216.4	170.8	125.8	184.6	76.2
	RH (%)	65.2	n/a	59.2	70.7	68.5	69.1	73.9	67.1	67.6	69.2	64.2	66.0	85.9
	Temperature (ºC)	21.3	n/a	15.5	22.6	26.0	26.0	25.0	12.6	14.5	16.0	8.6	12.3	8.8
	Precipitation (mm)	216.9	n/a	203.2	139.7	174.1	80.8	109.6	83.1	76.5	86.1	117.6	84.0	83.2
PM_1	NR-PM_1 ($\mu g\ m^{-3}$)	6.2	9.1	10.7	14.3	16.8	8.8	16.7	13.7	12.5	9.6	9.3	10.5	8.0
	Org (%)	75.9	n/a	65.9	67.2	69.4	70.0	68.0	74.4	65.9	73.6	69.0	69.0	55.5
	SO_4^{2-} (%)	12.0	n/a	19.2	19.9	19.0	17.4	21.0	10.2	15.8	13.2	15.7	13.4	15.4
	NO_3^- (%)	5.6	n/a	7.7	6.9	3.6	4.5	5.0	8.4	9.3	8.1	10.2	9.3	22.3
	NH_4^+ (%)	6.3	n/a	7.2	5.9	8.4	7.9	5.9	6.5	8.6	5.1	5.1	7.9	6.6
	Cl^- (%)	0.2	n/a	0.1	0.0	0.1	0.1	0.1	0.3	0.3	0.0	0.0	0.3	0.2
OA speciation	HOA (%)	20	9	21	10	18	18	5	30	20	14	22	24	17
	BBOA (%)	n/a	9	15	9	n/a	n/a	2	n/a	15	8	20	19	14
	LV-OOA (%)	43	26	64	34	23	44	27	22	37	37	37	30	63
	SV-OOA (%)	n/a	22	n/a	12	26	n/a	26	47	28	17	17	26	6
	IEPOX-OA (%)	37	21	n/a	25	33	38	29	n/a	n/a	n/a	n/a	n/a	n/a
	91Fac (%)	n/a	n/a	n/a	10	n/a	n/a	11	n/a	n/a	24	n/a	n/a	n/a

References: (a) Budisulistiorini et al. (2016); (b) Xu et al. (2015); (c) Budisulistiorini et al. (2013).
n/a = not available or not resolved from factor analysis.

3.4 Supporting Information

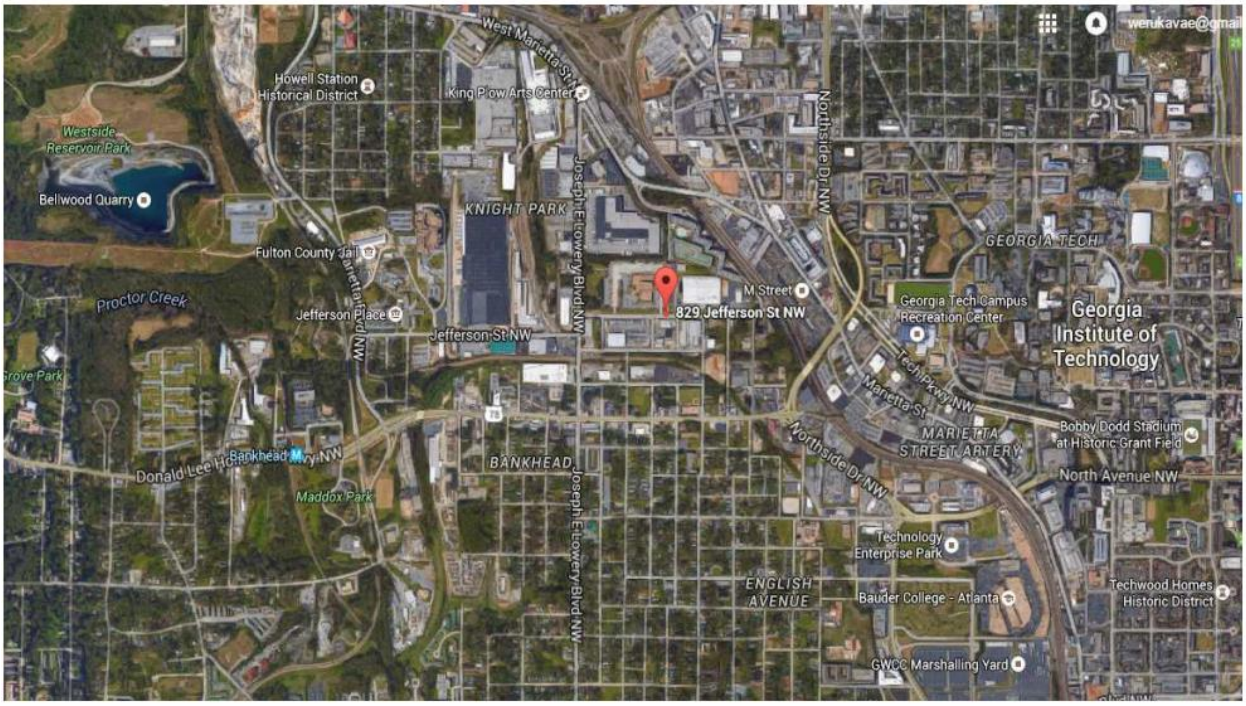

Figure S3-1. Map of the JST site adopted from Google Earth on February, 16, 2016 to depict the surrounding locations. The red mark represents the location of the JST site.

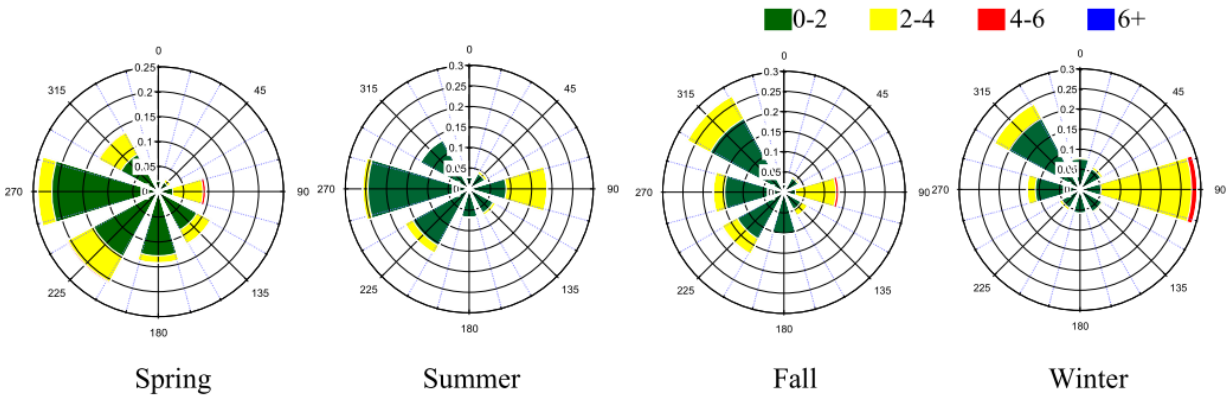

Figure S3-2. Wind roses plotted by season.

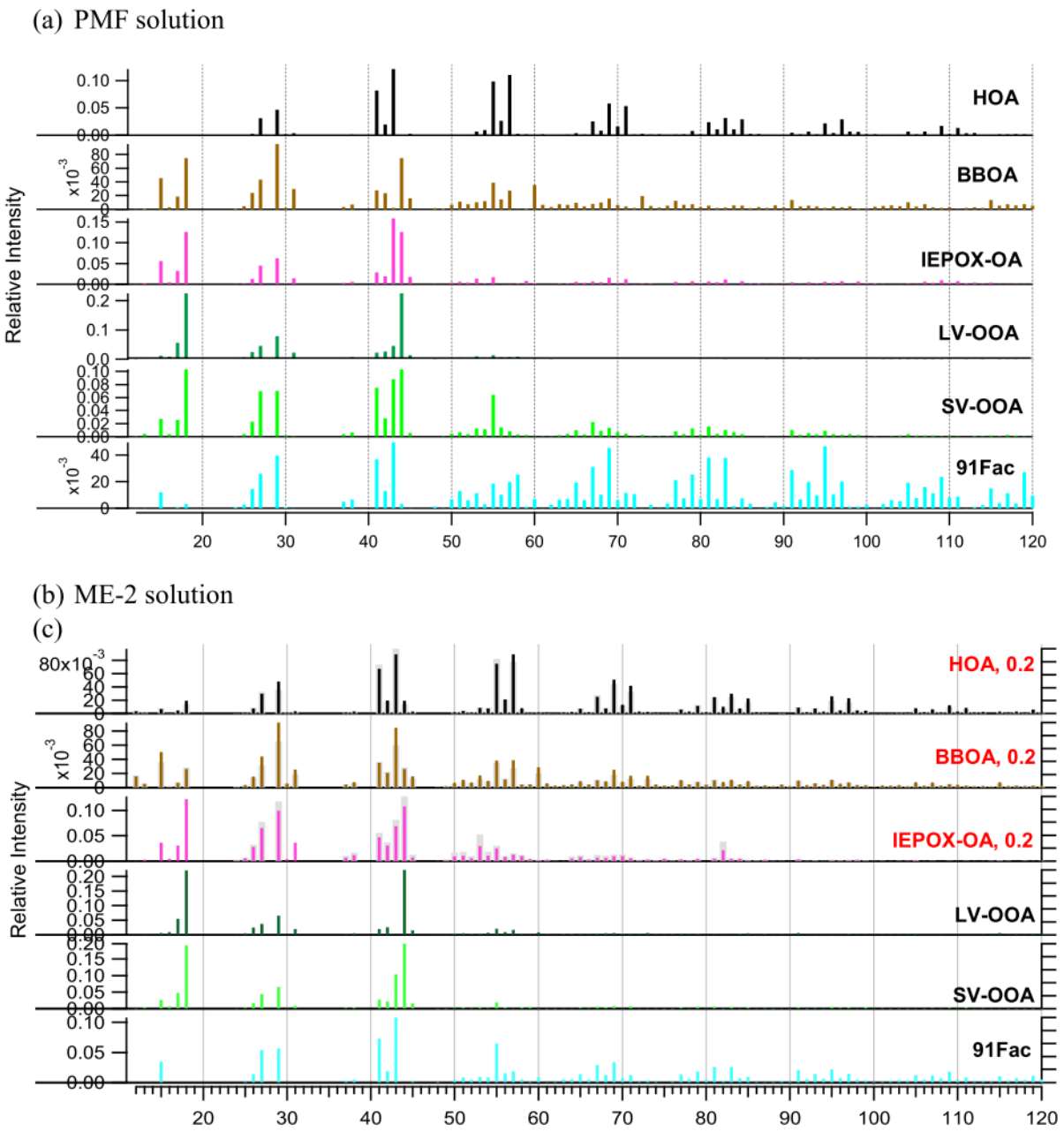

Figure S3-3. Mass spectral profiles (sources) resolved from (a) PMF and (b) ME-2 (*a*-value of 0.2) analyses of the 2014-2015 JST ACSM dataset.

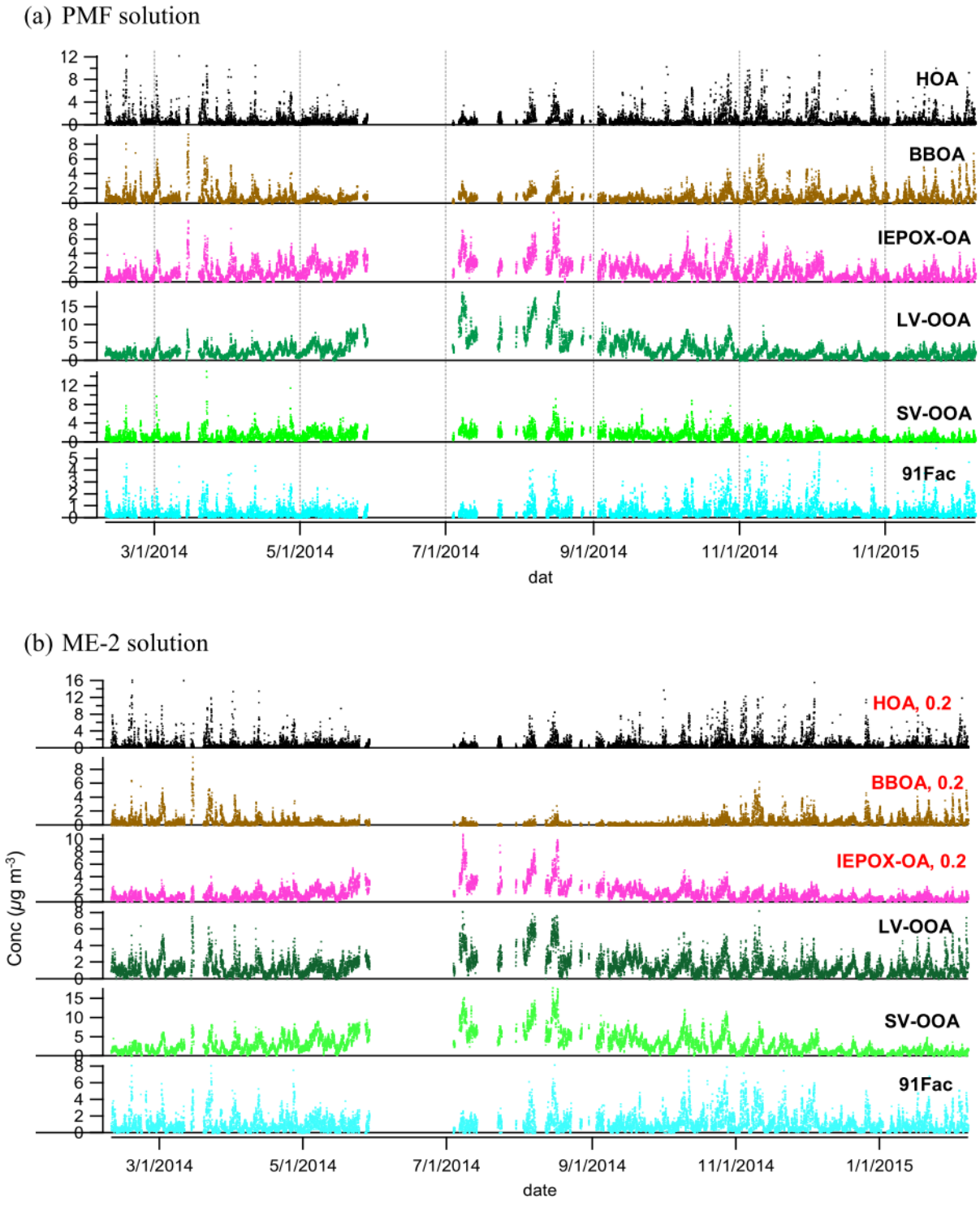

Figure S3-4. Time series of each factor resolved from (a) PMF and (b) ME-2 (a-value of 0.2) analyses of the 2014-2015 JST ACSM dataset.

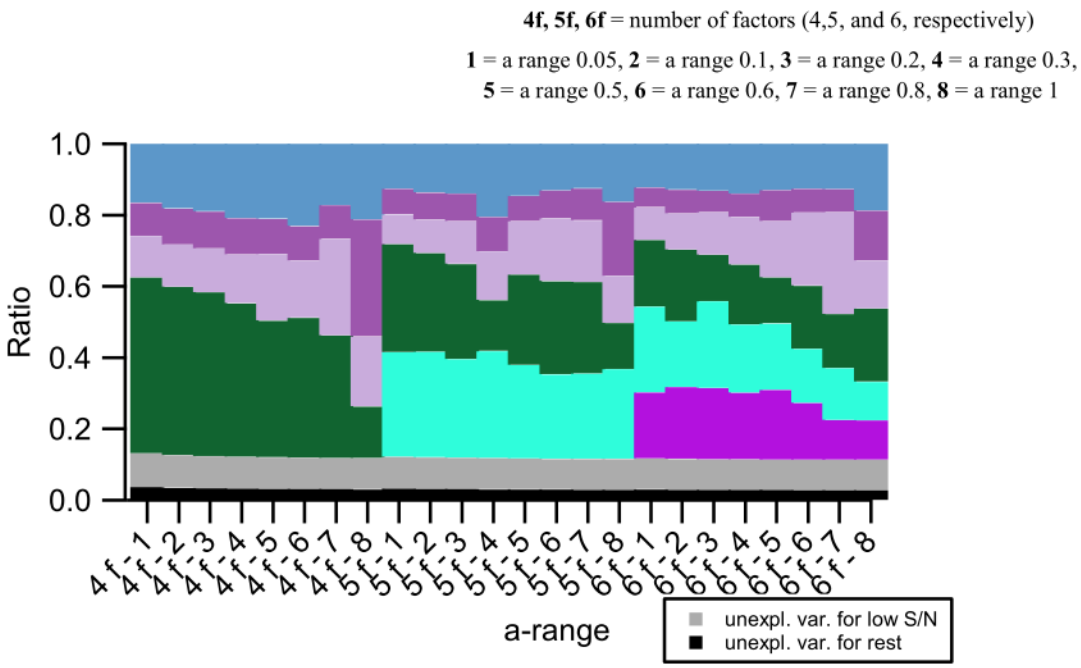

Figure S3-5. Average factor profiles resolved by yearlong analysis by ME-2 depicted as the OA factor changes as a function of the number of factors and regularization parameter (*a* value).

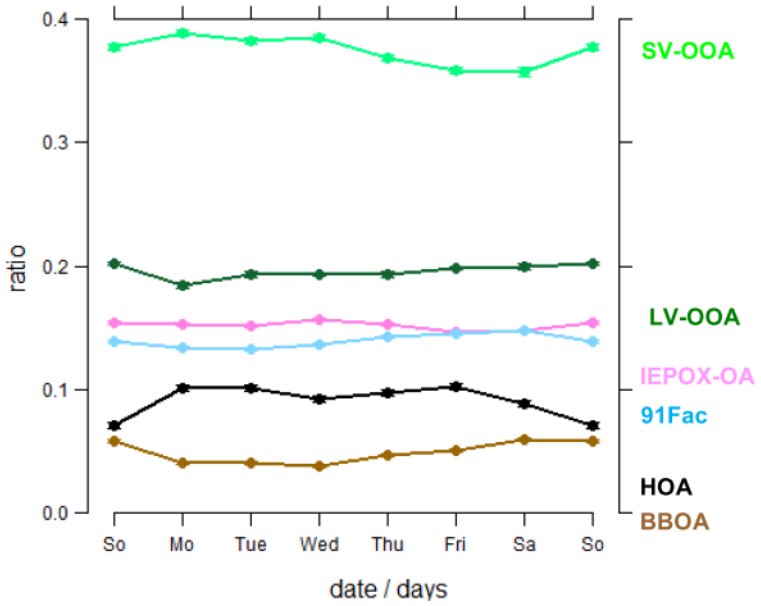

Figure S3-6. Day-of-week variations of factors resolved by yearlong analysis by ME-2 (*a* value = 0.2).

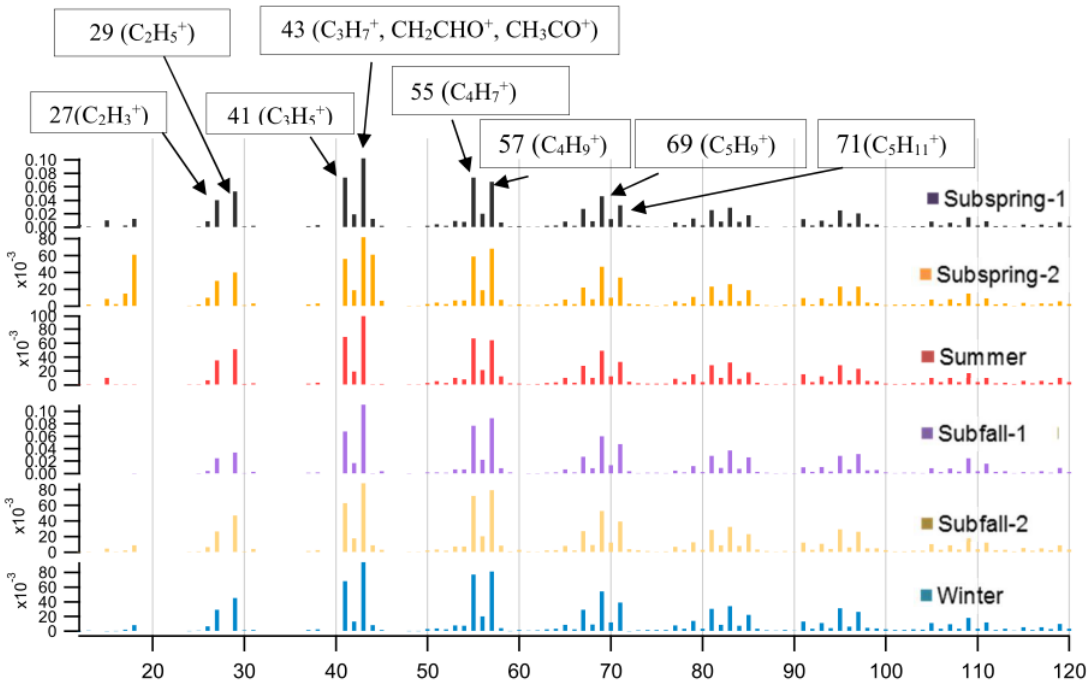

Figure S3-7. HOA mass spectra extracted by ME-2 for subspring-1 and by PMF for other seasons.

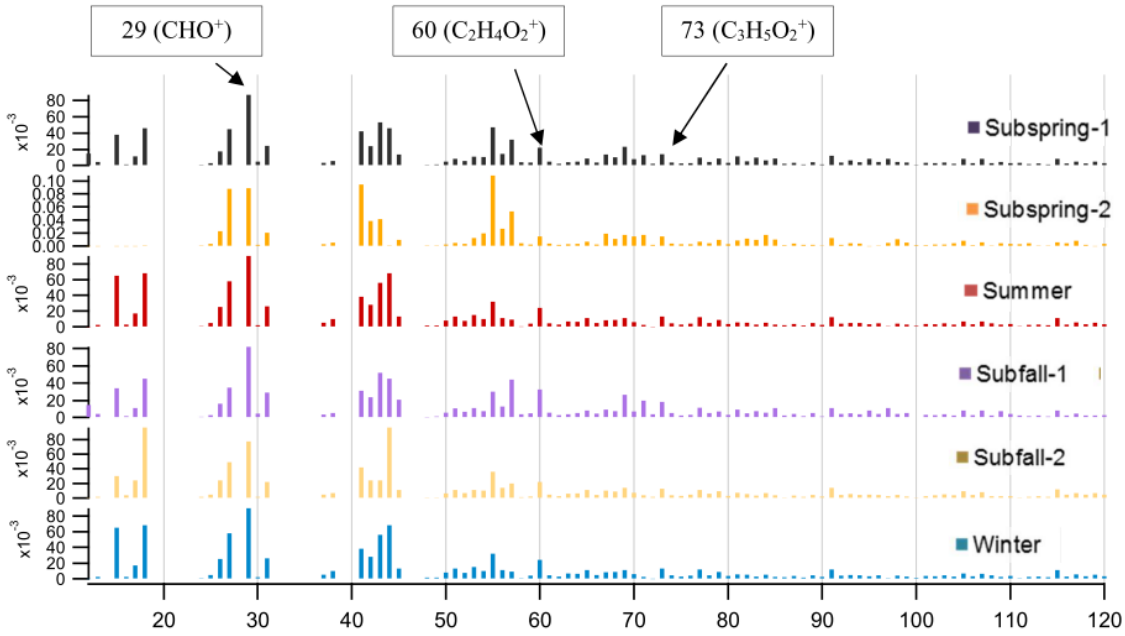

Figure S3-8. BBOA mass spectra extracted by ME-2 for subspring-1 and by PMF for other seasons.

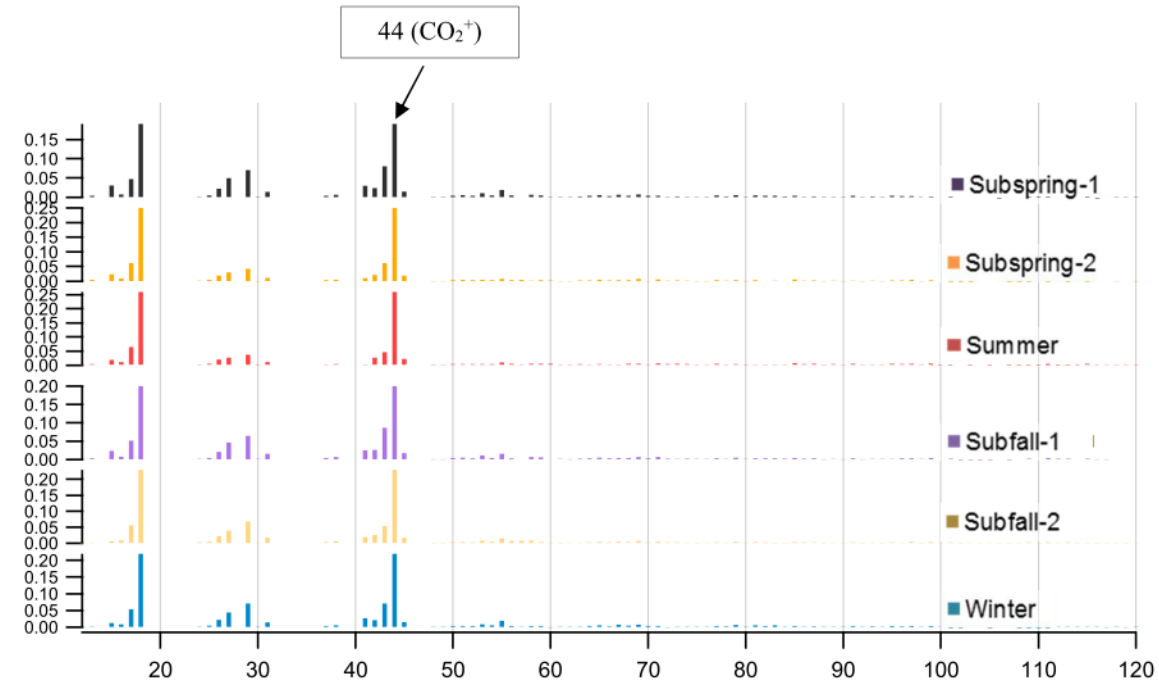

Figure S3-9. LV-OOA mass spectra extracted by ME-2 for subspring-1 and by PMF for other seasons.

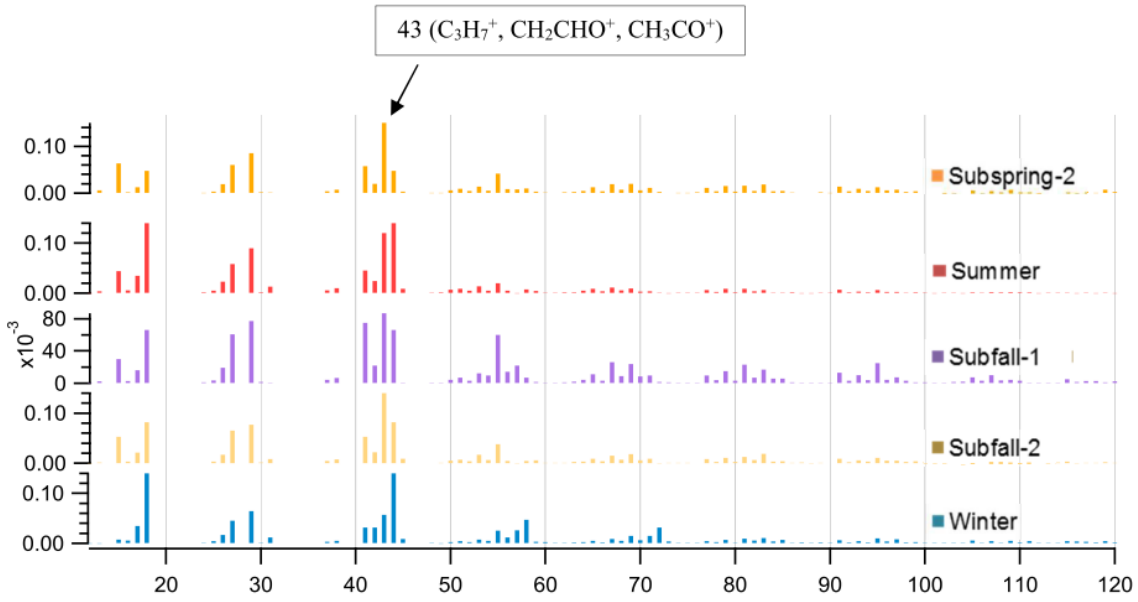

Figure S3-10. SV-OOA mass spectra extracted by PMF.

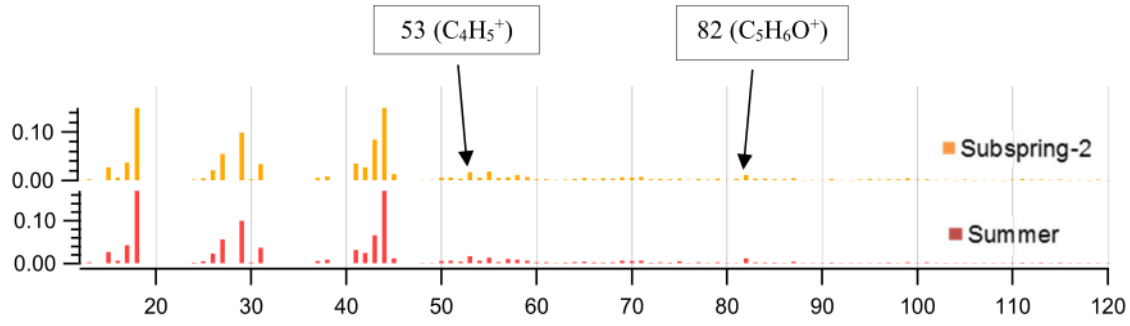

Figure S3-11. IEPOX-OA mass spectra extracted by PMF.

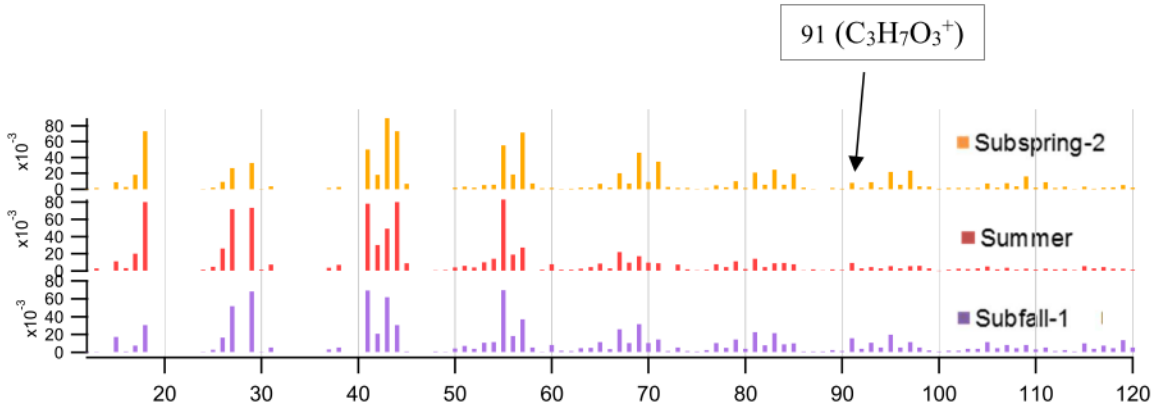

Figure S3-12. 91Fac mass spectra extracted by PMF.

Table S3-1. The calibration values for each season at JST.

Season	Flow rate coefficient values		Ionization efficiency coefficient values		
	Intercept (a)	Slope (b)	NO_3^- RF	NH_4^+ RIE	SO_4^{2-} RIE
Spring	-0.59741 ± 0.0244	1.3507 ± 0.0166	2.88e-11	5.92	0.58
Summer	-0.59558 ± 0.0335	1.3977 ± 0.0230	3.70e-11	6.29	0.54
Fall	-0.58925 ± 0.0373	1.4356 ± 0.0255	2.89e-11	7.16	0.80
Winter	-0.54494 ± 0.0237	1.4143 ± 0.0163	1.01e-11	5.95	0.69

Table S3-2. Person correlation (R) of PMF and ME-2 analysis of yearlong factors with collocated measurement and reference mass spectra.

Correlation	PMF						ME-2					
	HOA	BBOA	IEPOX-OA	LV-OOA	SV-OOA	91Fac	HOA	BBOA	IEPOX-OA	LV-OOA	SV-OOA	91Fac
R_{TS}												
CO	0.78	0.61	0.24	0.05	0.49	0.76	0.75	0.50	0.13	0.31	0.08	0.74
NH_3	0.31	0.22	0.22	0.20	0.29	0.30	0.28	0.13	0.19	0.25	0.21	0.29
NO_x	0.76	0.47	0.16	-0.04	0.36	0.73	0.74	0.41	0.03	0.17	0.00	0.65
NO_y	0.75	0.47	0.16	-0.03	0.36	0.72	0.74	0.40	0.03	0.17	0.00	0.64
NO	0.71	0.42	0.12	-0.05	0.27	0.68	0.71	0.36	0.01	0.13	0.02	0.56
NO_2	0.57	0.42	0.18	0.01	0.43	0.57	0.54	0.36	0.10	0.18	0.04	0.59
O_3	-0.41	-0.17	0.01	0.19	-0.23	-0.47	-0.41	-0.20	0.04	-0.12	0.15	0.44
SO_2	0.57	0.39	0.16	0.03	0.27	0.52	0.56	0.32	0.07	0.18	0.05	0.46
SO_4	0.07	0.12	0.52	0.75	0.30	0.07	0.02	0.06	0.69	0.56	0.66	0.07
NO_3	0.24	0.30	0.13	0.09	0.14	0.29	0.23	0.25	0.13	0.22	0.12	0.30
R_{MS}												
HOA	0.90	0.32	0.43	0.15	0.65	0.63	0.99	0.72	0.44	0.13	0.32	0.87
BBOA	0.34	0.81	0.69	0.56	0.76	0.33	0.76	0.98	0.78	0.42	0.59	0.81
91Fac	0.77	0.66	0.76	0.61	0.95	0.59	0.83	0.82	0.83	0.54	0.71	0.86
SV-OOA	0.55	0.74	0.89	0.80	0.98	0.42	0.66	0.74	0.91	0.74	0.87	0.65
LV-OOA	0.17	0.80	0.86	0.96	0.89	0.13	0.31	0.55	0.94	0.92	0.96	0.29
IEPOX-OA	0.43	0.80	0.82	0.83	0.90	0.36	0.52	0.79	0.99	0.75	0.85	0.58
R_{tracer}												
Levoglucosan	0.56	0.72	0.10	-0.36	0.09	0.61	0.61	0.89	-0.38	0.01	-0.35	-0.61
IEPOX tracers	0.04	0.13	0.79	0.93	0.71	0.01	0.07	-0.24	0.95	0.75	0.89	0.05
O:C ratio	0.08	0.40	0.62	1.05	0.52	0.09	0.16	0.19	0.54	1.03	0.93	0.08

Table S3-3. Diagnostic plots for PMF analysis of subspring-1, 2014.

# of factors	3 factors	4 factors	5 factors
Q/Qexp	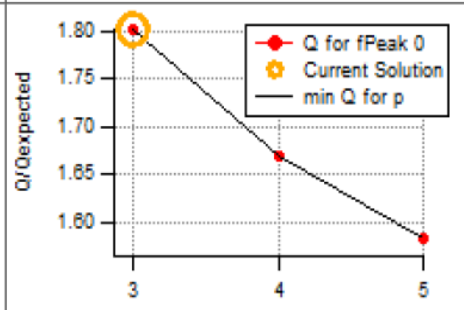	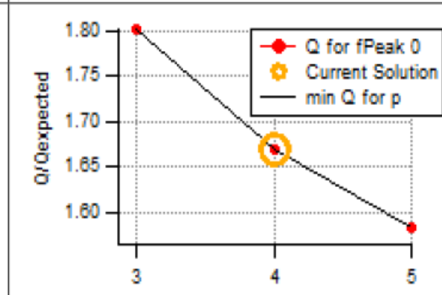	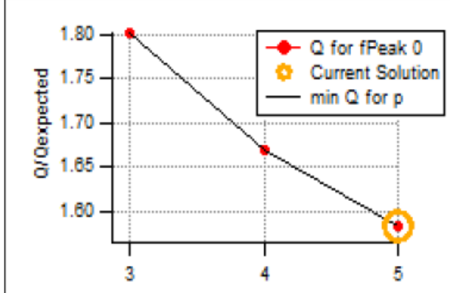
R TS&MS	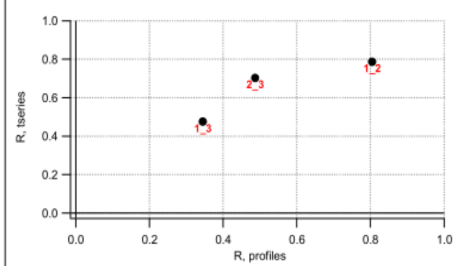	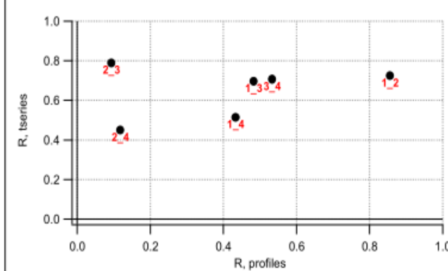	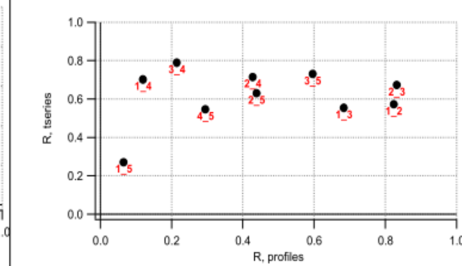
SEED	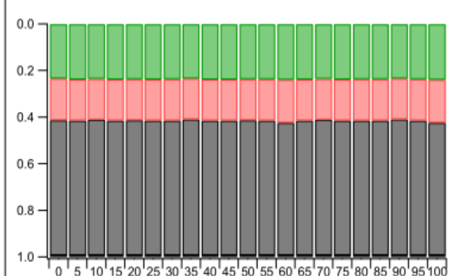	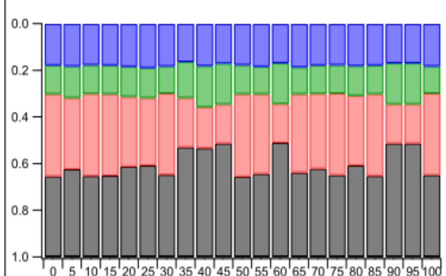	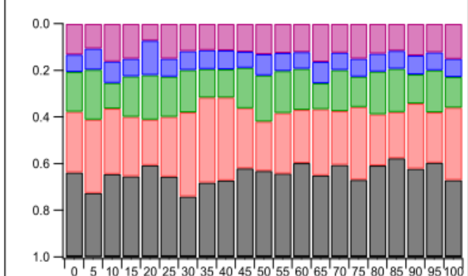

Table S3-4. Person correlation (R) of PMF analysis of subspring-1, 2014 factors with collocated measurement and reference mass spectra.

# of factors	3 factors			4 factors				5 factors				
Assigned factor	LV-OOA	BBOA	HOA	SV-OOA	LV-OOA	BBOA	HOA	LV-OOA	SV-OOA	91fac	BBOA	HOA
R_{TS}												
CO	0.42	0.67	0.83	0.42	0.46	0.68	0.83	0.30	0.60	0.70	0.57	0.80
HNO_3	0.41	0.30	0.07	0.32	0.43	0.27	0.06	0.46	0.25	0.29	0.26	0.04
NO_x	0.27	0.47	0.69	0.28	0.30	0.48	0.70	0.18	0.41	0.46	0.45	0.70
NO_y	0.27	0.48	0.69	0.28	0.31	0.49	0.69	0.20	0.41	0.47	0.45	0.69
NO	0.16	0.35	0.59	0.16	0.22	0.36	0.60	0.12	0.28	0.34	0.33	0.61
NO_2	0.39	0.57	0.68	0.41	0.36	0.58	0.68	0.26	0.53	0.56	0.53	0.66
O_3	-0.21	-0.31	-0.54	-0.31	-0.09	-0.33	-0.54	-0.02	-0.43	-0.29	-0.34	-0.53
SO_2	0.26	0.49	0.64	0.23	0.37	0.49	0.65	0.25	0.34	0.47	0.46	0.65
$ACSM\_SO_4$	0.28	0.08	-0.02	0.19	0.35	0.04	-0.04	0.42	0.10	0.08	0.03	-0.03
$ACSM\_NO_3$	0.42	0.49	0.46	0.38	0.44	0.49	0.46	0.40	0.40	0.45	0.51	0.45
R_{MS}												
HOA	0.26	0.43	0.94	0.42	0.13	0.54	0.94	0.13	0.54	0.59	0.34	0.92
LV-OOA	0.97	0.81	0.34	0.95	0.93	0.34	0.20	0.94	0.92	0.79	0.30	0.17
SV-OOA	0.87	0.81	0.71	0.94	0.78	0.50	0.60	0.79	0.96	0.85	0.41	0.56
IEPOX-OA	0.88	0.84	0.58	0.93	0.78	0.69	0.49	0.80	0.92	0.77	0.63	0.44
BBOA	0.64	0.82	0.50	0.73	0.51	0.79	0.40	0.53	0.77	0.65	0.70	0.36
COA	0.35	0.57	0.89	0.50	0.20	0.69	0.87	0.20	0.62	0.71	0.41	0.83
91fac	0.72	0.77	0.88	0.83	0.58	0.70	0.82	0.58	0.89	0.85	0.53	0.79
O:C ratio	0.14	0.38	0.89	0.68	1.09	0.08	0.08	1.11	0.57	0.44	0.08	0.08
Mass fraction	0.58	0.18	0.23	0.36	0.33	0.13	0.18	0.15	0.08	0.14	0.27	0.36

Table S3-5. The comparison of PMF and ME-2 factor solutions for subspring-1, 2014.

	PMF			ME-2						
	3-factor solution			3-factor solution			4-factor solution			
Assigned factor	HOA	BBOA	LV-OOA	HOA	BBOA	LV-OOA	HOA	BBOA	SV-OOA	LV-OOA
Constrained				*a = 0.3*	*a = 0.3*		*a = 0.3*	*a = 0.3*		
R_{TS}										
CO	0.83	0.67	0.42	0.81	0.61	0.50	0.80	0.63	0.27	0.52
NOx	0.69	0.47	0.27	0.69	0.41	0.34	0.69	0.43	0.15	0.36
NOy	0.69	0.48	0.27	0.68	0.42	0.34	0.69	0.44	0.15	0.37
O_3	-0.54	-0.31	-0.21	-0.53	-0.28	-0.27	-0.53	-0.33	-0.18	-0.12
SO_4	-0.02	0.08	0.28	-0.02	0.05	0.26	-0.03	0.00	0.30	0.29
NO_3	0.46	0.49	0.42	0.44	0.46	0.45	0.43	0.46	0.33	0.45
R_{MS}										
HOA	0.94	0.43	0.26	0.99	0.69	0.29	0.98	0.75	0.39	0.15
BBOA	0.50	0.82	0.64	0.80	0.97	0.59	0.81	0.97	0.68	0.42
LV-OOA	0.34	0.81	0.97	0.31	0.73	0.97	0.32	0.54	0.97	0.92
SV-OOA	0.71	0.81	0.87	0.68	0.85	0.86	0.69	0.76	0.92	0.75
IEPOX-OA	0.58	0.84	0.88	0.56	0.86	0.88	0.57	0.79	0.92	0.75
91fac	0.88	0.77	0.72	0.87	0.89	0.71	0.87	0.88	0.79	0.54
O:C ratio	0.14	0.38	0.89	0.14	0.24	0.86	0.13	0.18	0.76	1.08
Mass fraction of OA	0.23	0.18	0.58	0.20	0.15	0.65	0.19	0.16	0.39	0.26

Table S3-6. Diagnostic plots for PMF analysis of subspring-2, 2014.

# of factors	4 factors	5 factors	6 factors
Q/Qexp	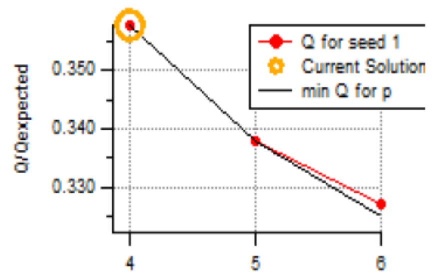	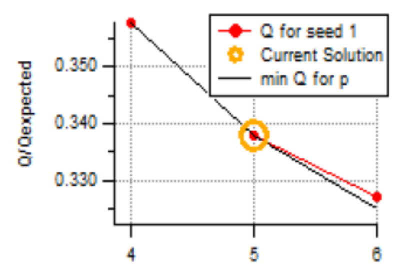	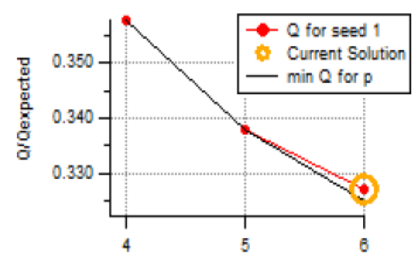
R TS&MS	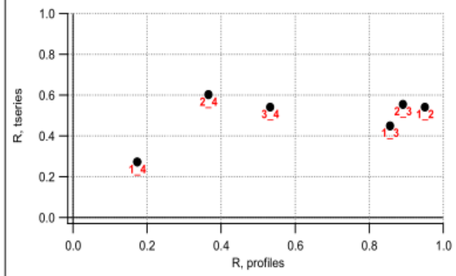	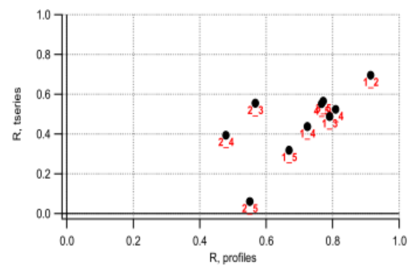	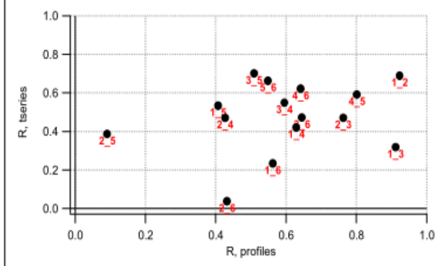
SEED	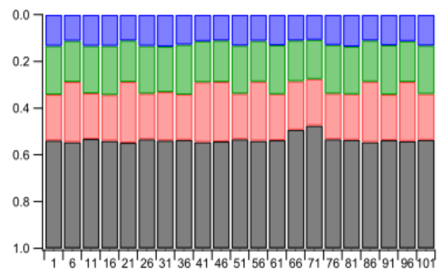	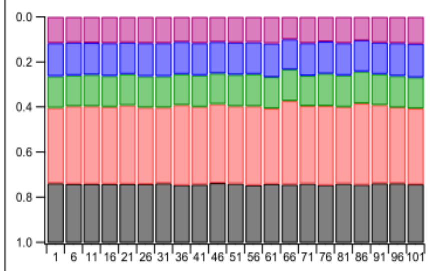	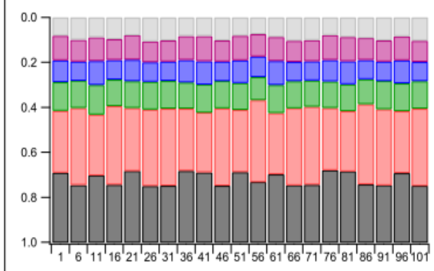

Table S3-7. Person correlation (R) of PMF analysis of subspring-2, 2014 factors with collocated measurement and reference mass spectra.

										Optimum solution					
# of factors	4 factors				5 factors					**6 factors**					
Assigned factor	LV-OOA	SV-OOA	91Fac	HOA	IEPOX-OA	LV-OOA	91Fac	SV-OOA	HOA	**IEPOX-OA**	**LV-OOA**	**SV-OOA**	**BBOA**	**HOA**	**91Fac**
R_{TS}															
CO	0.19	0.48	0.57	0.71	0.27	0.06	0.51	0.59	0.71	**0.22**	**0.11**	**0.55**	**0.52**	**0.68**	**0.68**
HNO_3	0.41	0.18	-0.05	-0.13	0.29	0.50	0.13	-0.07	-0.15	**0.30**	**0.48**	**0.05**	**0.14**	**-0.14**	**-0.14**
NO_x	0.03	0.19	0.52	0.54	0.12	-0.08	0.22	0.52	0.55	**0.09**	**-0.07**	**0.47**	**0.23**	**0.51**	**0.55**
NO_y	0.05	0.21	0.49	0.55	0.13	-0.06	0.23	0.50	0.56	**0.10**	**-0.05**	**0.45**	**0.24**	**0.50**	**0.56**
NO	-0.01	0.05	0.36	0.45	0.07	-0.12	0.07	0.36	0.46	**0.04**	**-0.12**	**0.33**	**0.10**	**0.33**	**0.48**
NO_2	0.08	0.30	0.52	0.51	0.15	-0.01	0.32	0.54	0.52	**0.12**	**0.02**	**0.49**	**0.32**	**0.56**	**0.50**
O_3	0.19	-0.05	-0.43	-0.45	0.04	0.36	-0.09	-0.46	-0.46	**0.07**	**0.33**	**-0.35**	**-0.09**	**-0.48**	**-0.45**
SO_2	0.31	0.29	0.48	0.44	0.36	0.18	0.28	0.48	0.44	**0.34**	**0.18**	**0.48**	**0.30**	**0.43**	**0.43**
$ACSM\_SO_4$	0.81	0.38	0.20	0.10	0.80	0.66	0.30	0.16	0.06	**0.82**	**0.63**	**0.27**	**0.38**	**0.10**	**0.04**
$ACSM\_NO_3$	0.33	0.45	0.52	0.48	0.36	0.23	0.45	0.52	0.47	**0.33**	**0.26**	**0.51**	**0.45**	**0.55**	**0.45**
R_{MS}															
HOA	0.20	0.47	0.62	0.93	0.33	0.11	0.75	0.71	0.81	**0.28**	**0.11**	**0.66**	**0.86**	**0.74**	**0.75**
LV-OOA	0.96	0.95	0.80	0.23	0.96	0.93	0.74	0.64	0.62	**0.96**	**0.93**	**0.67**	**0.31**	**0.59**	**0.66**
SV-OOA	0.83	0.94	0.92	0.61	0.89	0.77	0.89	0.84	0.86	**0.87**	**0.77**	**0.85**	**0.59**	**0.80**	**0.87**
91fac	0.66	0.87	0.88	0.83	0.76	0.56	0.92	0.86	0.90	**0.73**	**0.56**	**0.83**	**0.82**	**0.87**	**0.87**
IEPOX-OA	0.86	0.89	0.85	0.53	0.95	0.74	0.85	0.79	0.66	**0.93**	**0.76**	**0.77**	**0.60**	**0.80**	**0.66**
BBOA	0.61	0.70	0.76	0.46	0.71	0.51	0.77	0.76	0.55	**0.68**	**0.52**	**0.73**	**0.55**	**0.75**	**0.54**
COA	0.28	0.57	0.66	0.88	0.43	0.17	0.87	0.75	0.77	**0.38**	**0.18**	**0.67**	**0.92**	**0.86**	**0.70**
O:C ratio	0.94	0.64	0.44	0.08	0.73	1.14	0.33	0.29	0.34	**0.78**	**1.14**	**0.35**	**0.08**	**0.23**	**0.39**
Mass fraction	0.52	0.19	0.17	0.11	0.27	0.33	0.14	0.14	0.12	**0.25**	**0.35**	**0.12**	**0.09**	**0.10**	**0.10**

Table S3-8. Diagnostic plots for PMF analysis of summer 2014.

# of factors	4 factors	5 factors	6 factors
Q/Qexp	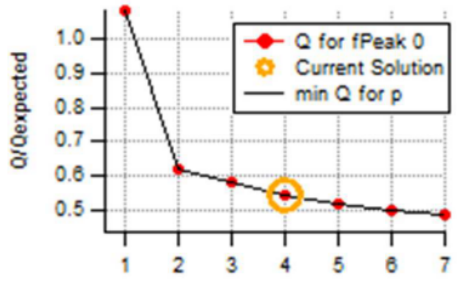	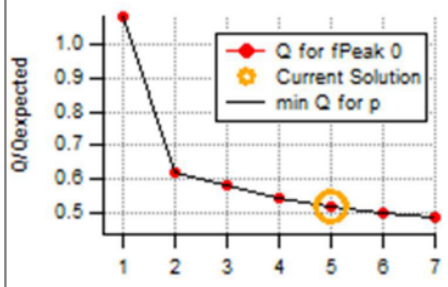	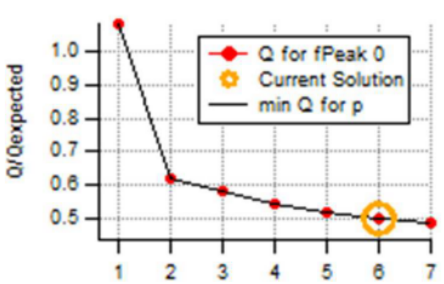
R TS&MS	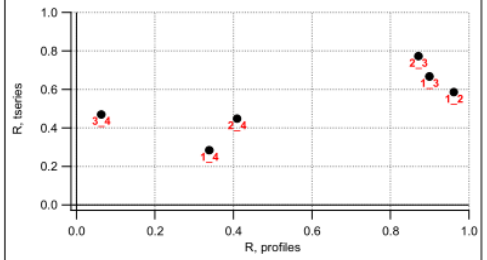	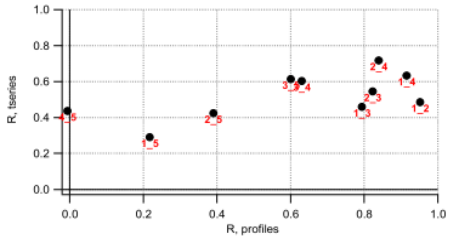	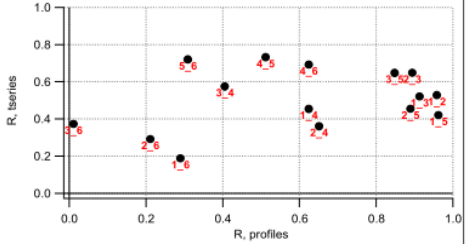
SEED	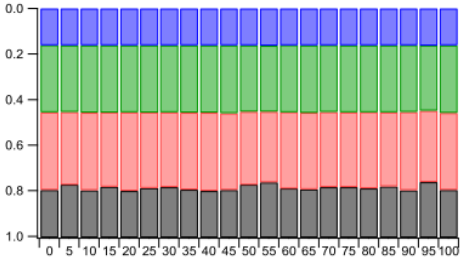	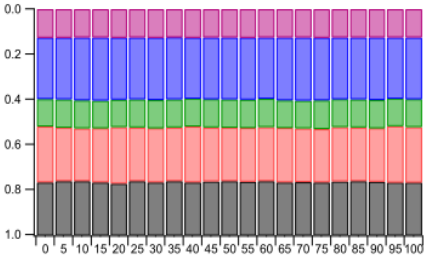	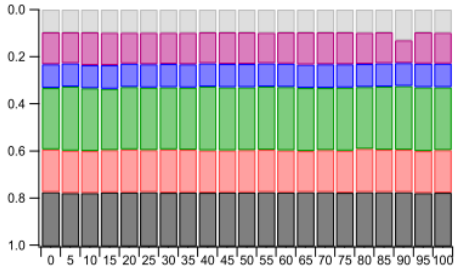

Table S3-9. Person correlation (R) of PMF analysis of summer 2014 factors with collocated measurement and reference mass spectra.

					Optimum solution										
# of factors	4-factor				5-factor					6-factor					
Assigned factor	IEPOX-OA	SV-OOA	LV-OOA	HOA	**IEPOX-OA**	**SV-OOA**	**91fac**	**LV-OOA**	**HOA**	SV-OOA	IEPOX-OA	LV-OOA	91fac or COA	Splitting	HOA
R_{TS}															
CO	0.24	0.35	0.38	0.80	**0.20**	**0.34**	**0.60**	**0.35**	**0.78**	0.19	0.19	0.32	0.65	0.60	0.78
SO_2	0.22	0.14	0.18	0.37	**0.20**	**0.11**	**0.21**	**0.17**	**0.39**	0.03	0.21	0.16	0.24	0.31	0.39
NH_3	0.13	0.23	0.27	0.43	**0.10**	**0.22**	**0.42**	**0.24**	**0.39**	0.20	0.08	0.23	0.41	0.29	0.42
HNO_3	0.26	0.24	0.38	-0.01	**0.27**	**0.15**	**0.20**	**0.37**	**-0.03**	0.22	0.24	0.41	0.13	0.09	-0.02
NO_x	0.07	0.19	0.16	0.71	**0.04**	**0.23**	**0.39**	**0.15**	**0.71**	0.07	0.04	0.10	0.47	0.49	0.71
NO	0.01	0.11	0.09	0.61	**-0.01**	**0.13**	**0.25**	**0.10**	**0.63**	-0.01	-0.01	0.05	0.32	0.41	0.63
NO_2	0.12	0.23	0.19	0.61	**0.08**	**0.26**	**0.43**	**0.16**	**0.59**	0.14	0.09	0.12	0.49	0.44	0.59
NO_y	0.09	0.22	0.19	0.72	**0.05**	**0.25**	**0.41**	**0.17**	**0.72**	0.10	0.06	0.13	0.49	0.51	0.72
O_3	0.13	0.23	0.27	0.43	**0.10**	**0.22**	**0.42**	**0.24**	**0.39**	0.20	0.08	0.23	0.41	0.29	0.42
ACSM_SO_4	0.71	0.44	0.54	0.12	**0.72**	**0.30**	**0.26**	**0.50**	**0.16**	0.32	0.73	0.54	0.22	0.35	0.14
ACSM_NO_3	0.50	0.72	0.67	0.64	**0.48**	**0.68**	**0.54**	**0.68**	**0.65**	0.50	0.49	0.62	0.62	0.80	0.60
ACSM_NH_4	0.66	0.52	0.59	0.27	**0.67**	**0.40**	**0.35**	**0.55**	**0.29**	0.37	0.67	0.57	0.34	0.46	0.27
R_{MS}															
HOA	0.34	0.40	0.06	0.95	**0.26**	**0.42**	**0.72**	**0.06**	**0.92**	0.37	0.28	0.08	0.76	0.35	0.94
LV-OOA	0.95	0.95	0.91	0.25	**0.97**	**0.94**	**0.81**	**0.91**	**0.20**	0.96	0.95	0.92	0.64	0.88	0.18
SV-OOA	0.88	0.93	0.73	0.64	**0.86**	**0.93**	**0.94**	**0.73**	**0.60**	0.92	0.86	0.75	0.81	0.87	0.58
IEPOX-OA	0.96	0.92	0.69	0.54	**0.94**	**0.93**	**0.85**	**0.70**	**0.50**	0.91	0.96	0.72	0.77	0.82	0.46
BBOA	0.73	0.73	0.47	0.47	**0.68**	**0.74**	**0.73**	**0.47**	**0.42**	0.70	0.71	0.49	0.72	0.64	0.38
Levoglucosan	0.71	0.64	0.40	0.44	**0.65**	**0.65**	**0.67**	**0.40**	**0.40**	0.61	0.70	0.42	0.67	0.54	0.37
91fac	0.76	0.80	0.50	0.86	**0.71**	**0.81**	**0.95**	**0.49**	**0.82**	0.79	0.72	0.52	0.89	0.72	0.81
COA	0.46	0.48	0.13	0.92	**0.37**	**0.50**	**0.82**	**0.12**	**0.86**	0.44	0.41	0.15	0.90	0.39	0.86
$R_{tracers}$ (n=27)															
*cis*_pinonic acid	0.13	0.02	0.09	0.10	**0.13**	**0.05**	**0.10**	**0.11**	**0.03**	0.10	0.14	0.11	0.09	0.04	0.08
IEPOX tracers	0.90	0.68	0.64	0.55	**0.90**	**0.60**	**0.66**	**0.59**	**0.23**	0.69	0.90	0.62	0.58	0.57	0.60
Levoglucosan	0.23	0.45	0.48	0.50	**0.22**	**0.44**	**0.56**	**0.49**	**0.19**	0.36	0.21	0.47	0.57	0.46	0.44
2,3-Dihydroy-4-oxopentanoic acid	0.57	0.59	0.61	0.50	**0.57**	**0.54**	**0.61**	**0.60**	**0.28**	0.54	0.56	0.61	0.57	0.54	0.49
O:C ratio	0.70	0.71	1.17	0.09	**0.81**	**0.69**	**0.43**	**1.18**	**0.08**	0.80	0.73	1.19	0.27	0.62	0.08
Mass fraction	0.21	0.34	0.29	0.16	**0.24**	**0.25**	**0.12**	**0.27**	**0.12**	0.23	0.18	0.26	0.10	0.14	0.10

Table S3-10. The comparison of PMF and ME-2 factor solutions for summer, 2014.

	PMF					ME-2									
	5-factor solution					5-factor solution					6-factor solution				
Assigned factor	HOA	IEPOX-OA	LV-OOA	91fac	SV-OOA	HOA	BBOA	IEPOX-OA	LV-OOA	SV-OOA	HOA	BBOA	IEPOX-OA	LV-OOA	91fac	SV-OOA
Constrained						*a = 0.3*	*a = 0.3*				*a = 0.3*	*a = 0.3*				
R_{TS}																
CO	0.78	0.20	0.35	0.60	0.34	0.73	0.46	0.07	0.33	0.58	0.55	0.51	0.23	0.30	0.75	0.46
HNO_3	-0.03	0.27	0.37	0.20	0.15	0.06	0.00	0.16	0.39	0.18	0.03	0.04	0.21	0.42	0.00	0.17
NO_x	0.71	0.04	0.15	0.39	0.23	0.36	0.30	0.02	0.21	0.36	0.40	0.32	0.09	0.23	0.34	0.33
NO_y	0.72	0.05	0.17	0.41	0.25	0.67	0.30	0.03	0.11	0.43	0.41	0.33	0.11	0.06	0.71	0.32
NO	0.63	-0.01	0.10	0.25	0.13	0.68	0.32	0.01	0.14	0.46	0.43	0.34	0.13	0.10	0.72	0.35
NO_2	0.59	0.08	0.16	0.43	0.26	0.61	0.17	0.09	0.08	0.35	0.31	0.19	0.06	0.03	0.66	0.22
O_3	0.39	0.10	0.24	0.42	0.22	0.54	0.38	0.04	0.13	0.42	0.42	0.41	0.14	0.10	0.57	0.34
SO_2	0.39	0.20	0.17	0.21	0.11	0.37	-0.20	0.06	0.30	0.03	-0.16	-0.21	0.04	0.36	-0.33	0.01
SO_4	0.16	0.72	0.50	0.26	0.30	0.39	0.15	0.11	0.20	0.22	0.14	0.23	0.23	0.16	0.43	0.09
NO_3	0.65	0.48	0.68	0.54	0.68	0.54	0.27	0.37	0.65	0.75	0.27	0.33	0.52	0.58	0.68	0.64
R_{MS}																
HOA	0.92	0.26	0.06	0.72	0.42	0.98	0.68	0.37	0.15	0.62	0.95	0.65	0.35	0.13	0.98	0.39
BBOA	0.42	0.68	0.47	0.73	0.74	0.79	0.95	0.71	0.46	0.77	0.74	0.93	0.70	0.42	0.71	0.67
91fac	0.82	0.71	0.49	0.95	0.81	0.87	0.88	0.77	0.56	0.91	0.88	0.82	0.76	0.54	0.80	0.79
SV-OOA	0.60	0.86	0.73	0.94	0.93	0.68	0.83	0.90	0.77	0.97	0.66	0.73	0.89	0.75	0.58	0.91
LV-OOA	0.20	0.97	0.91	0.81	0.94	0.32	0.70	0.97	0.94	0.90	0.29	0.57	0.97	0.93	0.19	0.96
IEPOX-OA	0.50	0.94	0.70	0.85	0.93	0.57	0.86	0.95	0.80	0.86	0.53	0.82	0.95	0.76	0.45	0.89
$R_{tracter}$																
IEPOX_SOA	0.23	0.90	0.59	0.66	0.60	0.68	0.45	0.89	0.67	0.45	0.41	0.57	0.92	0.65	0.63	0.40
Levoglucosan	0.19	0.22	0.49	0.56	0.44	0.12	0.38	0.07	0.30	0.31	0.40	0.38	0.13	0.32	0.18	0.31
O:C ratio	0.08	0.81	1.18	0.43	0.69	0.13	0.27	0.76	1.06	0.55	0.13	0.18	0.76	1.12	0.09	0.77
Mass fraction of OA	0.12	0.24	0.27	0.12	0.25	0.14	0.05	0.19	0.26	0.36	0.05	0.02	0.29	0.27	0.11	0.26

Table S3-11. Diagnostic plots for PMF analysis of subfall-1, 2014.

# of factors	4 factors	5 factors	6 factors
Q/Qexp	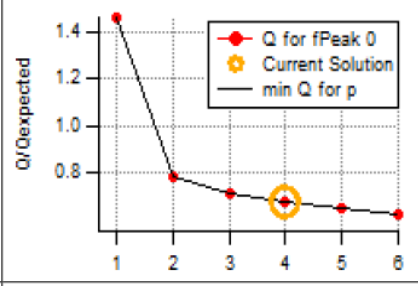	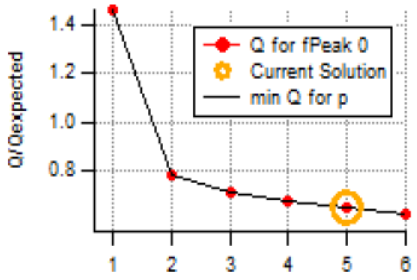	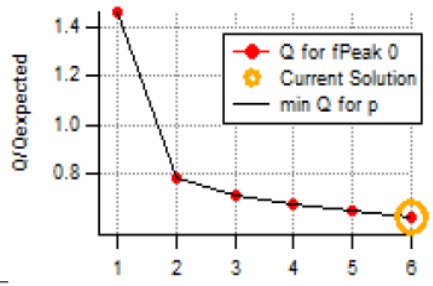
R TS&MS	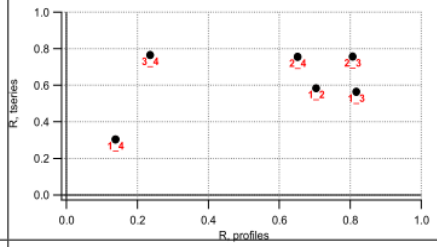	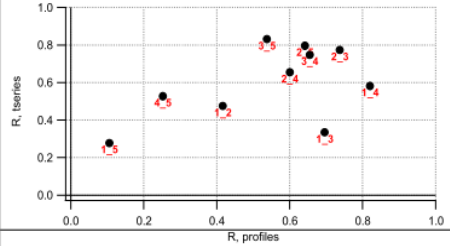	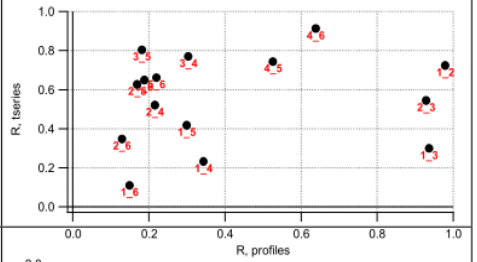
SEED	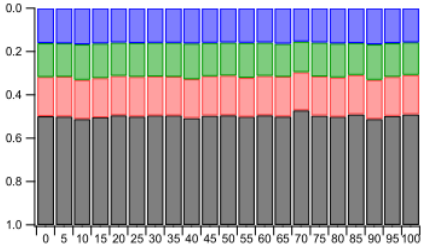	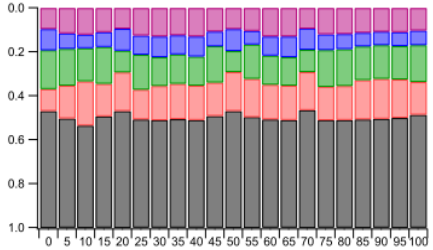	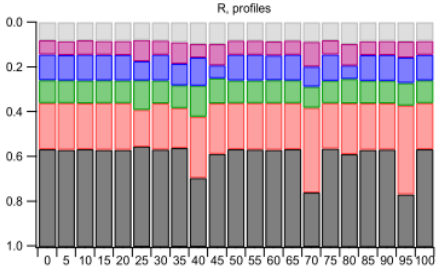

Table S3-12. Person correlation (R) of PMF analysis of subfall-1, 2014 factors with collocated measurement and reference mass spectra.

	Optimum solution														
# of factors	**4-factor**				5-factor					6-factor					
Assigned factor	**LV-OOA**	**SV-OOA**	**IEPOX-OA**	**HOA**	LV-OOA	91Fac	SV-OOA	BBOA	HOA	SV-OOA	LV-OOA	IEPOX-OA	COA	BBOA	HOA
R_{TS}															
CO	**-0.41**	**0.20**	**0.38**	**0.46**	-0.42	0.20	0.43	0.33	0.38	-0.42	-0.35	0.37	0.37	0.36	0.49
SO_2	**-0.21**	**0.30**	**0.40**	**0.27**	-0.20	0.18	0.40	0.38	0.13	-0.23	-0.15	0.40	0.33	0.37	0.26
NH_3	**0.33**	**0.38**	**0.18**	**0.36**	0.31	0.50	0.18	0.19	0.46	0.30	0.34	0.10	0.35	0.24	0.38
HNO_3	**-0.58**	**-0.62**	**-0.68**	**-0.66**	-0.58	-0.59	-0.67	-0.66	-0.61	0.05	-0.61	-0.67	-0.66	-0.65	-0.64
NO_x	**0.37**	**0.73**	**0.72**	**0.66**	0.28	0.83	0.68	0.74	0.56	-0.11	0.48	0.64	0.74	0.76	0.65
NO	**0.33**	**0.34**	**0.29**	**0.19**	0.21	0.55	0.22	0.35	0.08	0.20	0.22	0.18	0.30	0.39	0.18
NO_2	**0.37**	**0.87**	**0.86**	**0.85**	0.34	0.88	0.85	0.86	0.78	-0.24	0.59	0.83	0.89	0.87	0.84
NO_y	**0.32**	**0.71**	**0.70**	**0.63**	0.22	0.82	0.66	0.73	0.52	-0.09	0.42	0.62	0.71	0.75	0.62
O_3	**0.34**	**-0.55**	**-0.70**	**-0.73**	0.37	-0.59	-0.70	-0.70	-0.58	0.27	0.31	-0.63	-0.64	-0.75	-0.77
ACSM_SO_4	**0.52**	**0.22**	**0.22**	**0.10**	0.52	0.17	0.11	0.25	0.12	0.40	0.53	0.18	0.15	0.22	0.06
ACSM_NO_3	**0.34**	**0.39**	**0.46**	**0.41**	0.31	0.46	0.39	0.48	0.37	0.27	0.36	0.36	0.41	0.50	0.38
ACSM_NH_4	**0.49**	**0.28**	**0.25**	**0.17**	0.49	0.25	0.16	0.27	0.18	0.41	0.49	0.21	0.21	0.25	0.13
R_{MS}															
HOA	**0.22**	**0.78**	**0.39**	**0.89**	0.24	0.79	0.78	0.30	0.82	0.31	0.24	0.35	0.90	0.30	0.80
LV-OOA	**0.96**	**0.76**	**0.87**	**0.14**	0.97	0.47	0.74	0.81	0.08	0.97	0.95	0.94	0.31	0.26	0.08
SV-OOA	**0.85**	**0.94**	**0.84**	**0.53**	0.86	0.75	0.91	0.79	0.46	0.90	0.85	0.87	0.66	0.38	0.45
91fac	**0.68**	**0.97**	**0.76**	**0.75**	0.70	0.85	0.96	0.65	0.65	0.77	0.69	0.77	0.87	0.45	0.64
IEPOX-OA	**0.85**	**0.85**	**0.90**	**0.39**	0.87	0.71	0.81	0.84	0.29	0.91	0.84	0.86	0.62	0.57	0.29
BBOA	**0.67**	**0.82**	**0.85**	**0.41**	0.67	0.74	0.77	0.82	0.32	0.74	0.65	0.70	0.62	0.66	0.33
COA	**0.30**	**0.85**	**0.55**	**0.78**	0.32	0.83	0.86	0.40	0.67	0.27	0.42	0.86	0.94	0.39	0.62
$R_{tracers}$															
cis _Pinonic acid	**0.26**	**0.23**	**0.04**	**0.29**	0.26	0.27	0.24	0.05	0.32	0.15	0.26	0.09	0.27	0.01	0.37
IEPOX tracers	**0.81**	**0.92**	**0.96**	**0.99**	0.79	0.94	0.99	0.91	0.98	0.71	0.85	0.98	0.97	0.94	0.98
Levoglucosan	**0.58**	**0.68**	**0.94**	**0.89**	0.54	0.75	0.91	0.93	0.84	0.46	0.63	0.93	0.81	0.94	0.86
2,3-Dihydroy-4-oxopentanoic acid	**0.92**	**0.83**	**0.83**	**0.74**	0.92	0.76	0.79	0.82	0.74	0.84	0.92	0.81	0.72	0.73	0.56
O:C ratio	**0.95**	**0.36**	**0.41**	**0.08**	0.93	0.17	0.35	0.41	0.08	0.83	0.92	0.69	0.08	0.08	0.08
Mass fraction	**0.50**	**0.18**	**0.16**	**0.16**	0.53	0.10	0.18	0.10	0.10	0.44	0.21	0.10	0.12	0.06	0.08

Table S3-13. The comparison of PMF and ME-2 factor solutions for subfall-1, 2014.

	PMF				ME-2				
	4-factor solution				5-factor solution				
Assigned factor	HOA	IEPOX-OA	SV-OOA	LV-OOA	HOA	BBOA	91fac	SV-OOA	LV-OOA
Constrained					*a = 0.3*	*a = 0.3*			
R_{TS}									
CO	0.46	0.38	0.20	-0.41	0.22	0.51	0.42	0.22	0.40
HNO_3	-0.66	-0.68	-0.62	-0.58	0.06	0.07	0.05	0.13	0.03
NH3	0.36	0.18	0.38	0.33	0.09	0.03	0.22	0.19	0.45
NO_x	0.66	0.72	0.73	0.37	0.26	0.34	0.40	0.26	0.36
NO_y	0.63	0.70	0.71	0.32	0.26	0.34	0.41	0.27	0.37
NO	0.19	0.29	0.34	0.33	0.26	0.39	0.40	0.25	0.33
NO_2	0.85	0.86	0.87	0.37	0.20	0.14	0.34	0.23	0.35
O_3	-0.73	-0.70	-0.55	0.34	-0.21	-0.26	-0.30	-0.31	0.19
SO_2	0.27	0.40	0.30	-0.21	0.31	0.16	0.37	0.27	0.27
SO_4	0.10	0.22	0.22	0.52	0.08	0.03	0.12	0.26	0.51
NO_3	0.41	0.46	0.39	0.34	0.32	0.37	0.40	0.47	0.32
R_{MS}									
HOA	0.89	0.39	0.78	0.22	0.99	0.66	0.89	0.78	0.27
BBOA	0.41	0.85	0.82	0.67	0.75	0.95	0.88	0.84	0.57
91fac	0.75	0.76	0.97	0.68	0.84	0.80	0.94	0.84	0.70
SV-OOA	0.53	0.84	0.94	0.85	0.68	0.80	0.82	0.86	0.86
LV-OOA	0.14	0.87	0.76	0.96	0.34	0.69	0.54	0.65	0.97
IEPOX-OA	0.39	0.90	0.85	0.85	0.51	0.81	0.72	0.73	0.87
$R_{tracter}$									
IEPOX_SOA	0.99	0.96	0.92	0.81	0.95	0.84	0.98	0.96	0.83
Levoglucosan	0.89	0.94	0.68	0.58	0.80	0.95	0.87	0.81	0.74
O:C ratio	0.08	0.41	0.36	0.95	0.18	0.27	0.21	0.35	0.92
Mass fraction of OA	0.16	0.16	0.18	0.50	0.14	0.08	0.24	0.17	0.37

Table S3-14. Diagnostic plots for PMF analysis of subfall-2, 2014.

# of factors	4 factors	5 factors	6 factors
Q/Qexp	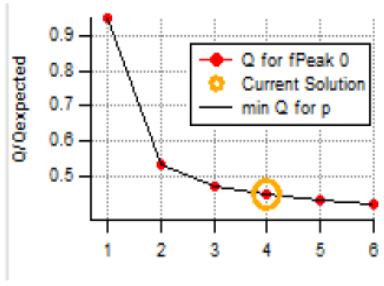	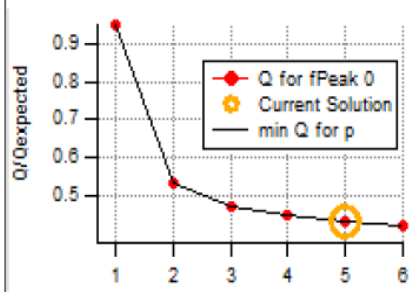	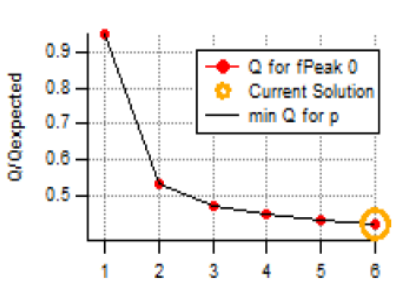
R TS&MS	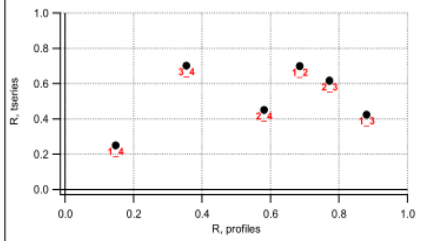	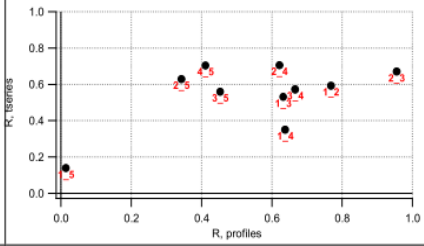	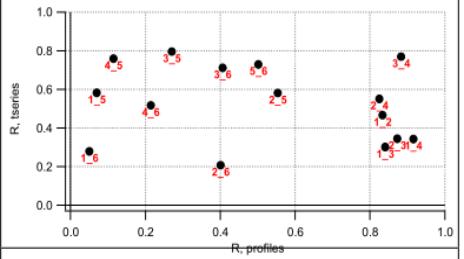
SEED	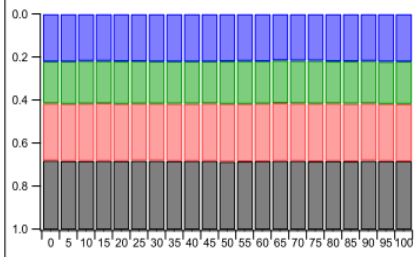	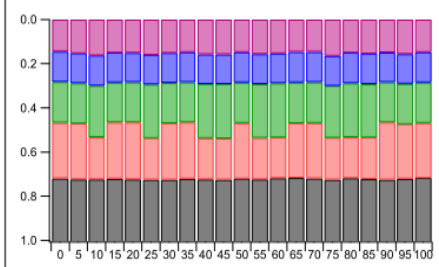	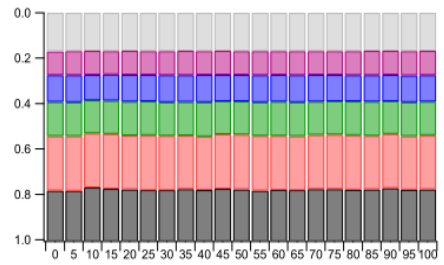

Table S3-15. Person correlation (R) of PMF analysis of subfall-2, 2014 factors with collocated measurement and reference mass spectra.

	Optimum solution														
# of factor	4-factor				5-factor					6-factor					
Assigned factor	**LV-OOA**	**SV-OOA**	**BBOA**	**HOA**	LV-OOA	IEPOX-OA	91fac	BBOA	HOA	LV-OOA	SV-OOA	BBOA	91fac	IEPOX-OA	HOA
R_{TS}															
CO	**0.18**	**0.39**	**0.78**	**0.88**	0.09	0.62	0.48	0.82	0.87	0.19	0.15	0.82	0.60	0.73	0.87
SO_2	**0.04**	**0.26**	**0.60**	**0.69**	0.00	0.42	0.35	0.62	0.68	-0.01	0.11	0.63	0.46	0.54	0.68
NH_3	**0.13**	**0.19**	**0.38**	**0.41**	0.17	0.23	0.29	0.38	0.40	0.13	0.11	0.37	0.38	0.33	0.40
NO_x	**0.04**	**0.25**	**0.62**	**0.76**	0.03	0.39	0.40	0.64	0.75	0.01	0.10	0.65	0.51	0.53	0.74
NO	**0.03**	**0.27**	**0.68**	**0.86**	-0.04	0.50	0.37	0.71	0.86	-0.01	0.09	0.73	0.47	0.62	0.85
NO_2	**0.06**	**0.23**	**0.56**	**0.65**	0.11	0.29	0.42	0.57	0.64	0.04	0.10	0.56	0.55	0.44	0.63
NO_y	**0.04**	**0.30**	**0.72**	**0.89**	0.00	0.50	0.44	0.75	0.88	0.00	0.12	0.77	0.56	0.65	0.88
O_3	**0.08**	**-0.06**	**-0.43**	**-0.53**	0.01	-0.11	-0.27	-0.46	-0.52	0.06	0.05	-0.45	-0.41	-0.28	-0.51
ACSM_SO_4	**0.35**	**-0.04**	**0.08**	**0.04**	0.36	0.08	-0.08	0.09	0.04	0.43	-0.05	0.09	0.04	0.09	0.03
ACSM_NO_3	**0.41**	**0.24**	**0.28**	**0.22**	0.46	0.26	0.27	0.28	0.21	0.43	0.21	0.28	0.31	0.27	0.21
ACSM_NH_4	**0.22**	**-0.09**	**-0.01**	**-0.03**	0.26	-0.03	-0.10	0.01	-0.03	0.30	-0.08	0.01	-0.02	-0.03	-0.04
R_{MS}															
HOA	**0.15**	**0.63**	**0.40**	**0.90**	0.12	0.54	0.67	0.52	0.84	0.12	0.50	0.48	0.31	0.58	0.90
LV-OOA	**0.95**	**0.79**	**0.93**	**0.22**	0.94	0.87	0.79	0.72	0.09	0.94	0.91	0.89	0.92	0.28	0.15
SV-OOA	**0.80**	**0.92**	**0.88**	**0.60**	0.78	0.93	0.93	0.76	0.46	0.78	0.95	0.89	0.84	0.50	0.54
91fac	**0.61**	**0.87**	**0.80**	**0.80**	0.58	0.84	0.91	0.76	0.69	0.58	0.85	0.82	0.74	0.63	0.77
IEPOX-OA	**0.82**	**0.86**	**0.91**	**0.46**	0.79	0.88	0.87	0.75	0.32	0.79	0.91	0.88	0.82	0.54	0.42
BBOA	**0.62**	**0.82**	**0.81**	**0.50**	0.59	0.81	0.84	0.76	0.36	0.59	0.82	0.82	0.67	0.53	0.45
COA	**0.23**	**0.68**	**0.54**	**0.83**	0.20	0.58	0.75	0.67	0.74	0.20	0.57	0.58	0.45	0.55	0.82
$R_{tracers}$															
cis _Pinonic acid	**0.38**	**0.30**	**0.49**	**0.47**	0.41	0.36	0.40	0.50	0.47	0.40	0.23	0.52	0.46	0.37	0.47
IEPOX tracers	**0.95**	**1.00**	**0.93**	**0.95**	0.86	1.00	0.96	0.92	0.95	0.91	0.99	0.92	0.84	0.98	0.95
Levoglucosan	**0.72**	**0.69**	**0.88**	**0.84**	0.73	0.72	0.82	0.88	0.84	0.72	0.61	0.89	0.87	0.75	0.83
2,3-Dihydroy-4-oxopentanoic acid	**0.96**	**0.98**	**0.88**	**0.91**	0.88	0.98	0.93	0.87	0.92	0.93	0.98	0.87	0.81	0.97	0.92
O:C ratio	**1.05**	**0.43**	**0.49**	**0.12**	1.13	0.52	0.40	0.32	0.08	1.13	0.64	0.50	0.63	0.08	0.08
Mass fraction	**0.32**	**0.26**	**0.20**	**0.22**	0.28	0.25	0.18	0.14	0.15	0.23	0.24	0.15	0.12	0.11	0.17

Table S3-16. Diagnostic plots for PMF analysis of winter 2015.

# of factors	3 factors	4 factors	5 factors
Q/Qexp	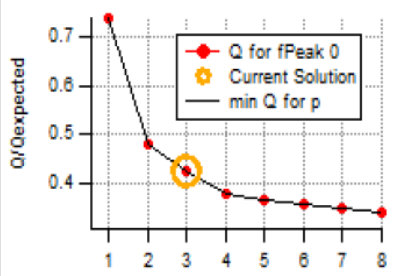	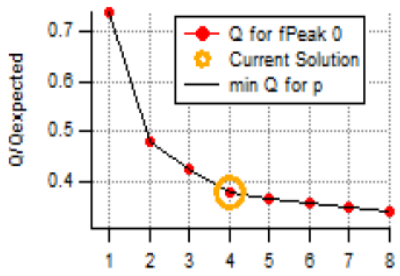	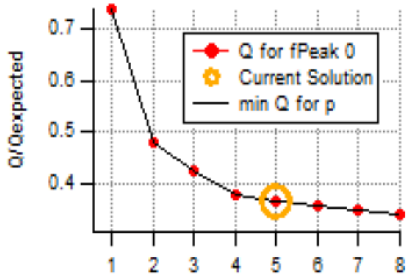
R TS&MS	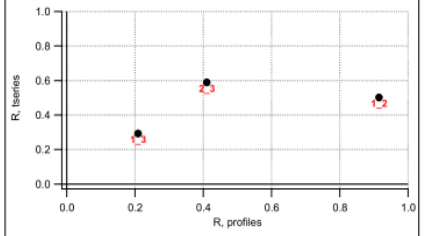	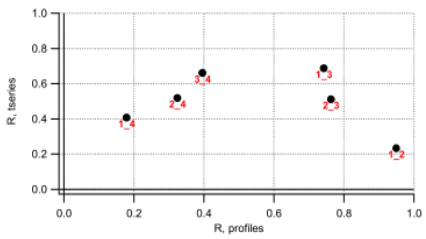	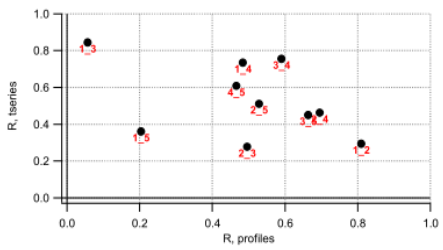
SEED	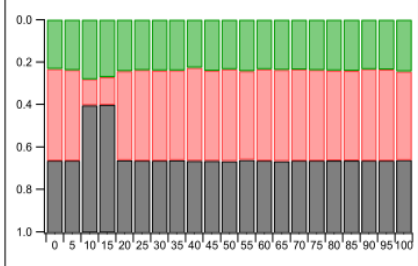	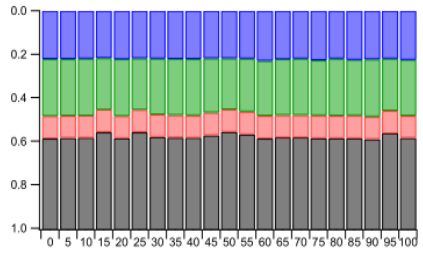	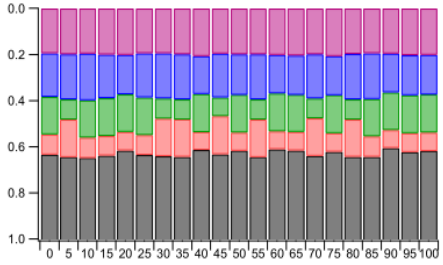

Table S3-17. Person correlation (R) of PMF analysis of winter 2015 factors with collocated measurement and reference mass spectra.

				Optimum solution								
# of factors	3 factors			4 factors				5 factors				
Assigned factor	LV-OOA	BBOA	HOA	**LV-OOA**	**SV-OOA**	**BBOA**	**HOA**	LV-OOA	SV-OOA	91fac	BBOA	HOA
R_{TS}												
CO	0.11	0.56	0.76	**0.24**	**0.47**	**0.60**	**0.75**	0.28	0.44	0.36	0.61	0.78
SO_2	-0.07	0.24	0.63	**0.01**	**0.32**	**0.28**	**0.60**	0.00	0.32	0.15	0.28	0.64
NO_x	-0.03	0.39	0.76	**0.09**	**0.38**	**0.43**	**0.73**	0.10	0.37	0.25	0.44	0.78
NO	-0.09	0.30	0.65	**0.02**	**0.28**	**0.34**	**0.63**	0.03	0.27	0.16	0.35	0.67
NO_2	0.10	0.47	0.72	**0.21**	**0.45**	**0.50**	**0.70**	0.21	0.44	0.35	0.50	0.72
NO_y	0.03	0.43	0.77	**0.15**	**0.42**	**0.47**	**0.75**	0.15	0.40	0.29	0.48	0.79
O_3	0.13	-0.15	-0.37	**0.07**	**-0.18**	**-0.19**	**-0.34**	0.03	-0.17	0.02	-0.22	-0.39
ACSM_SO_4	0.33	-0.01	0.09	**0.16**	**0.20**	**0.00**	**0.07**	0.22	0.20	0.01	0.00	0.08
ACSM_NO_3	0.50	0.38	0.29	**0.49**	**0.27**	**0.37**	**0.30**	0.55	0.25	0.36	0.38	0.29
ACSM_NH_4	0.30	0.03	0.04	**0.20**	**0.09**	**0.02**	**0.03**	0.25	0.09	0.04	0.03	0.04
R_{MS}												
HOA	0.19	0.42	0.91	**0.20**	**0.35**	**0.47**	**0.91**	0.07	0.47	0.77	0.52	0.90
LV-OOA	0.96	0.95	0.26	**0.96**	**0.93**	**0.83**	**0.21**	0.92	0.90	0.34	0.62	0.27
SV-OOA	0.82	0.92	0.63	**0.84**	**0.87**	**0.85**	**0.60**	0.74	0.90	0.64	0.70	0.63
91fac	0.65	0.84	0.82	**0.67**	**0.74**	**0.83**	**0.80**	0.52	0.80	0.78	0.77	0.81
IEPOX-OA	0.84	0.95	0.49	**0.85**	**0.86**	**0.93**	**0.45**	0.74	0.87	0.62	0.83	0.47
BBOA	0.56	0.80	0.41	**0.57**	**0.61**	**0.91**	**0.37**	0.48	0.67	0.59	0.90	0.39
COA	0.27	0.53	0.85	**0.28**	**0.41**	**0.61**	**0.83**	0.15	0.52	0.76	0.67	0.82
$R_{tracers}$												
cis- Pinoic acid	0.10	0.53	0.38	**0.27**	**0.15**	**0.54**	**0.42**	0.27	0.14	0.38	0.55	0.39
IEPOX tracers	0.58	0.57	0.37	**0.66**	**0.16**	**0.52**	**0.42**	0.56	0.16	0.72	0.48	0.34
Levoglucosan	0.47	0.81	0.75	**0.61**	**0.46**	**0.83**	**0.78**	0.66	0.44	0.64	0.86	0.77
2-MG	0.75	0.84	0.65	**0.83**	**0.44**	**0.82**	**0.70**	0.83	0.41	0.83	0.82	0.64
2,3-Dihydroy-4-oxopentanoic acid	0.41	0.54	0.40	**0.55**	**0.09**	**0.50**	**0.45**	0.45	0.08	0.62	0.48	0.38
O:C ratio	1.03	0.55	0.13	**0.98**	**0.64**	**0.46**	**0.15**	1.31	0.53	0.08	0.23	0.15
Mass fraction	0.34	0.43	0.23	**0.42**	**0.10**	**0.26**	**0.22**	0.38	0.09	0.16	0.19	0.19

Table S3-18. The comparison of PMF and ME-2 factor solutions for winter, 2015.

	PMF				ME-2								
	4-factor solution				4-factor solution				5-factor solution				
Assigned factor	HOA	BBOA	LV-OOA	SV-OOA	HOA	BBOA	LV-OOA	SV-OOA	HOA	BBOA	SV-OOA	LV-OOA	91fac
Constrained					*a = 0.05*	*a = 0.05*			*a = 0.05*	*a = 0.05*			
R_{TS}													
CO	0.75	0.60	0.24	0.47	0.73	0.66	0.30	0.19	0.72	0.65	0.61	0.24	0.16
NOx	0.73	0.43	0.09	0.38	0.77	0.53	0.17	0.18	0.78	0.51	0.54	0.11	0.13
NOy	0.75	0.47	0.15	0.42	0.78	0.55	0.21	0.20	0.78	0.54	0.56	0.15	0.16
O_3	-0.34	-0.19	0.07	-0.18	-0.32	-0.23	0.37	-0.08	-0.31	-0.22	-0.18	0.14	0.02
SO_4	0.07	0.00	0.16	0.20	0.00	0.19	0.47	0.22	0.03	0.20	0.26	0.49	0.29
NO_3	0.30	0.37	0.49	0.27	0.05	0.15	0.61	0.29	0.03	0.24	0.31	0.63	0.37
R_{MS}													
HOA	0.91	0.52	0.20	0.35	1.00	0.74	0.15	0.31	1.00	0.75	0.38	0.28	0.35
BBOA	0.21	0.91	0.57	0.61	0.76	1.00	0.48	0.60	0.76	1.00	0.62	0.58	0.60
LV-OOA	0.21	0.83	0.96	0.93	0.30	0.62	0.94	0.97	0.29	0.62	0.90	0.97	0.94
SV-OOA	0.60	0.85	0.84	0.87	0.68	0.80	0.77	0.88	0.67	0.81	0.83	0.86	0.86
IEPOX-OA	0.45	0.93	0.67	0.74	0.51	0.82	0.81	0.89	0.51	0.82	0.82	0.88	0.85
91Fac	0.80	0.83	0.67	0.74	0.85	0.88	0.55	0.73	0.85	0.89	0.71	0.70	0.72
$R_{tracter}$													
Levoglucosan	0.78	0.83	0.66	0.44	0.69	0.87	0.28	0.67	0.68	0.86	0.86	0.63	0.19
O:C ratio	0.15	0.46	0.98	0.64	0.15	0.22	0.89	0.75	0.15	0.22	0.47	0.95	0.65
Mass fraction of OA	0.22	0.26	0.42	0.10	0.17	0.14	0.63	0.06	0.13	0.14	0.16	0.53	0.04
OA concentration (ug m-3)	0.97	1.14	1.85	0.44	0.76	0.62	2.76	0.25	0.57	0.61	0.72	2.34	0.16

Table S3-19. Correlation (R) between subtypes of OA and LWC.

R	Yearlong (n=91)	Subsrping-1 (n=15)	Subspring-2 (n=9)	Summer (n=25)	Subfall-1 (n=15)	Subfall-2 (n=12)	Winter (n=15)
HOA	-0.17	-0.58	-0.12	-0.02	-0.25	0.76	-0.38
LV-OOA	-0.05	-0.51	0.05	-0.04	0.46	0.52	-0.31
SV-OOA	-0.12	n/a	-0.35	-0.10	0.12	0.23	-0.25
BBOA	-0.08	-0.65	0.15	-0.10	0.22	0.61	-0.43
IEPOX-OA	-0.30	n/a	0.54	-0.07	n/a	n/a	n/a
91Fac	n/a	n/a	0.37	-0.20	0.13	n/a	n/a

Table S3-20. Correlation (R) between subtypes of OA and aerosol pH.

R	Yearlong (n=91)	Subsrping-1 (n=15)	Subspring-2 (n=9)	Summer (n=25)	Subfall-1 (n=15)	Subfall-2 (n=12)	Winter (n=15)
HOA	-0.02	0.14	-0.08	-0.15	0.32	0.18	0.41
LV-OOA	-0.27	0.13	-0.40	-0.21	-0.50	-0.02	0.27
SV-OOA	-0.09	0.00	0.19	0.00	-0.14	0.14	-0.04
BBOA	-0.12	0.08	0.06	-0.11	-0.07	-0.02	0.48
IEPOX-OA	0.00	n/a	-0.67	-0.42	n/a	n/a	n/a
91Fac	n/a	n/a	-0.26	-0.05	0.06	n/a	n/a

CHAPTER IV:
ASSESSING THE IMPACT OF ANTHROPOGENIC POLLUTION ON ISOPRENE-DERIVED SECONDARY ORGANIC AEROSOL FORMATION IN $PM_{2.5}$ COLLECTED FROM THE BIRMINGHAM, ALABAMA GROUND SITE DURING THE 2013 SOUTHERN OXIDANT AND AEROSOL STUDY[3]

4.1 Overview

In the southeastern U.S., substantial emissions of isoprene from deciduous trees undergo atmospheric oxidation to form secondary organic aerosol (SOA) that contributes to fine particulate matter ($PM_{2.5}$). Laboratory studies have revealed that anthropogenic pollutants, such as sulfur dioxide (SO_2), oxides of nitrogen (NO_x), and aerosol acidity, can enhance SOA formation from the hydroxyl radical (OH)-initiated oxidation of isoprene; however, the mechanisms by which specific pollutants enhance isoprene SOA in ambient $PM_{2.5}$ remain unclear. The primary purpose of this campaign was to examine, in greater detail, the formation mechanisms, composition, and properties of biogenic SOA, including the effects of anthropogenic emissions. This study pertains specifically to the results from the BHM ground site, where the city's ample urban emissions mix with biogenic emissions from the surrounding rural areas, creating an ideal location to investigate such interactions. The results presented here anthropogenic emissions. This study pertains specifically to the results from the BHM ground

[3] This chapter is reproduced by permission from "Assessing the Impact of Anthropogenic Pollution on Isoprene-Derived Secondary Organic Aerosol Formation in $PM_{2.5}$ Collected from the Birmingham, Alabama Ground Site during the 2013 Southern Oxidant and Aerosol Study" by Rattanavaraha, W., Chu, K., Budisulistiorini, S.H., Riva, M., Lin, Y.H., Edgerton, E.S., Baumann, K., Shaw, S.L., Guo, H., King, L., Weber, R.J., and Suratt J.D. *Atmospheric Chemistry and Physics*, 16(8), 4897-4914.

site, where the city's ample urban emissions mix with biogenic emissions from the surrounding rural areas, creating an ideal location to investigate such interactions. The results presented here focus on analysis of $PM_{2.5}$ collected on filters during the campaign by GC/EI-MS and ultra-performance liquid chromatography/electrospray ionization high-resolution quadrupole time-of-flight mass spectrometry (UPLC/ESI-HR-QTOFMS). The analysis of $PM_{2.5}$ was conducted in order to determine quantities of known isoprene SOA tracers and using collocated air quality and meteorological measurements to investigate how anthropogenic pollutants including NO_x, SO_2, aerosol acidity (pH), $PM_{2.5}$ sulfate (SO_4^{2-}), and O_3 affect isoprene SOA formation. These results, along with the results presented from similar studies during the 2013 SOAS campaign, seek to elucidate the chemical relationships between anthropogenic emissions and isoprene SOA formation in order to provide better parameterizations needed to improve the accuracy of air quality models in this region of the U.S.

4.2 Experimental Section

4.2.1 Site description and collocated data

Filter samples were collected in the summer of 2013 as part of the SOAS field campaign at the BHM ground site (33.553N, 86.815W). In addition to the SOAS campaign, the site is also part of the Southeastern Aerosol Research and Characterization Study (SEARCH) (Figure S4-1 of the Supplement), an observation and monitoring program initiated in 1998. SEARCH and this site are described elsewhere in detail (Hansen et al., 2003; Edgerton et al., 2006). The BHM site is surrounded by significant transportation and industrial sources of PM. West of BHM are US-31 and I-65 highways. To the north, northeast and southwest of BHM several coking ovens and an iron pipe foundry are located (Hansen et al., 2003).

4.2.2 High-Volume filter sampling and analysis methods

4.2.2.1 High-Volume filter sampling

From June 1 – July 16, 2013, $PM_{2.5}$ samples were collected onto Tissuquartz^{TM} Filters (8 x 10 in, Pall Life Sciences) using high-volume $PM_{2.5}$ samplers (Tisch Environmental) operated at 1 m^3 min^{-1} at ambient temperature described in detail elsewhere (Budisulistiorini et al. 2015; Riva et al., 2016). All quartz filters were pre-baked prior to collection. The procedure consisted of baking filters at 550 °C for 18 hours followed by cooling to 25 °C over 12 hours.

The sampling schedule is given in Table 1. Either two or four samples were collected per day. The regular schedule consisted of two samples per day, one during the day, the second at night, each collected for 11 hours. On intensive sampling days, four samples were collected, with the single daytime sample being subdivided into three separate periods. The intensive sampling schedule was conducted on days when high levels of isoprene, SO_4^{2-} and NO_x were forecast by the National Center for Atmospheric Research (NCAR) using the Flexible Particle dispersion model (FLEXPART) (Stohl et al., 2005) and Model for Ozone and Related Chemical Tracers (MOZART) (Emmons et al., 2010) simulations. Details of these simulations have been summarized in Budisulistiorini et al. (2015); however, these model data were only used qualitatively to determine the sampling schedule. The intensive collection frequency allowed enhanced time resolution for offline analysis to examine the effect of anthropogenic emissions on the evolution of isoprene SOA tracers throughout the day.

In total, 120 samples were collected throughout the field campaign with a field blank filter collected every 10 days to identify errors or contamination in sample collection and analysis. All filters were stored at -20 °C in the dark until extraction and analysis. In addition to filter sampling of $PM_{2.5}$, SEARCH provided a suite of additional instruments at the site that

measured meteorological and chemical variables, including temperature, relative humidity (RH), trace gases (i.e., CO, O_3, SO_2, NO_x, and NH_3), and continuous PM monitoring. The exact variables measured with their respective instrumentation are summarized in Table S1 of the Supplement.

4.2.2.2 Isoprene-derived SOA analysis by GC/EI-MS

SOA collected in the field on quartz filters was extracted and isoprene tracers quantified by GC/EI-MS with prior trimethylsilylation. A 37-mm diameter circular punch from each filter was extracted in a pre-cleaned scintillation vial with 20 mL of high-purity methanol (LCMS CHROMASOLV-grade, Sigma-Aldrich) by sonication for 45 minutes. The extracts were filtered through polytetrafluorethylene (PTFE) syringe filters (Pall Life Science, Acrodisc®, 0.2-µm pore size) to remove insoluble particles and residual quartz fibers. The filtrate was then blown dry under a gentle stream of N_2 at room temperature. The dried residues were immediately trimethylsilylated by reaction with 100 μL of BSTFA + TMCS (99:1 *v/v*, Supelco) and 50 μL of pyridine (anhydrous, 99.8 %, Sigma-Aldrich) at 70 °C for 1 hour. Trimethylsilyl derivatives of carbonyl and hydroxyl functional groups were measurable by our GC/EI-MS method. Derivatized samples were analyzed within 24 hours after trimethylsilylation using a Hewlett-Packard (HP) 5890 Series II Gas Chromatograph coupled to a HP 5971A Mass Selective Detector. The gas chromatograph was equipped with an *Econo-Cap®-EC®-5* Capillary Column (30 m x 0.25 mm i.d.; 0.25-μm film thickness) to separate trimethylsilyl derivatives before MS detection. 1 μL aliquots were injected onto the column. Operating conditions and procedures have been described elsewhere (Surratt et al., 2010).

Extraction efficiency was assessed and taken into account for the quantification of all SOA tracers. Efficiency was determined by analyzing 4 pre-baked filters spiked with 50 ppmv of

2-methyltetrols, 2-methylglyceric acid, levoglucosan, and *cis*- and *trans*-3-MeTHF-3,4-diols. Extraction efficiency was above 90% and used to correct the quantification of samples. Extracted ion chromatograms (EICs) of *m/z* 262, 219, 231, 335 were used to quantify the *cis*-/*trans*-3-MeTHF-3,4-diols, 2-methyltetrols and 2-methylglyceric acid, C_5-alkene triols, and IEPOX-dimers, respectively (Surratt et al., 2006).

2-Methyltetrols were quantified using an authentic reference standard that consisted of a mixture of racemic diasteroisomers. Similarly, 3-MeTHF-3,4-diol isomers were also quantified using authentic standards; however, 3-MeTHF-3,4-diol isomers were detected in few field samples. 2-Methylglyceric acid was also quantified using an authentic standard. Procedures for synthesis of the 2-methyltetrols, 3-MeTHF-3,4-diol isomers, and 2-methylglyceric acid have been described elsewhere (Zhang et al., 2012; Budisulistiorini et al., 2015). C_5-alkene triols and IEPOX-dimers were quantified using the average response factor of the 2-methyltetrols.

To investigate the effect of IEPOX-derived OS hydrolysis/decomposition during GC/EI-MS analysis, known concentrations (i.e., 1, 5, 10, and 25 pppv) of the authentic IEPOX-derived OS standard (Budisulistiorini et al., 2015) were directly injected into the GC/MS following trimethylsilylation. Ratios of detected 2-methyltetrols to the IEPOX-derived OS were applied to estimate the total IEPOX-derived SOA tracers in order to avoid double counting when combining the GC/MS and UPLC/ESI-HR-QTOFMS SOA tracer results.

4.2.2.3 Isoprene-derived SOA analysis by UPLC/ ESI-HR-QTOFMS

A 37-mm diameter circular punch from each quartz filter was extracted following the same procedure as described in Section 4.2.2.2 for the GC/EI-MS analysis. However, after drying, the dried residues were instead reconstituted with 150 μl of a 50:50 (*v/v*) solvent mixture of methanol (LC-MS CHROMASOVL-grade, Sigma-Aldrich) and high-purity water (Milli-Q,

18.2 MΩ). The extracts were immediately analyzed by the UPLC/ESI-HR-QTOFMS (6520 Series, Agilent) operated in the negative ion mode. Detailed operating conditions have been described elsewhere (Riva et al., 2016). Mass spectra were acquired at a mass resolution 7000-8000.

Extraction efficiency was determined by analyzing 3 pre-baked filters spiked with propyl sulfate and octyl sulfate (electronic grade, City Chemical LLC). Extraction efficiencies were in the range 86 – 95%. EICs of *m/z* 215, 333 and 199 were used to quantify the IEPOX-derived OS, IEPOX-derived dimer OS and the MAE-derived OS, respectively (Surratt et al., 2007a). EICs were generated with a ± 5 ppm tolerance. Accurate masses for all measured organosulfates were within ± 5 ppm. For simplicity, only the nominal masses are reported in the text when describing these products. IEPOX-derived OS and IEPOX-derived dimer OS were quantified by the IEPOX-derived standard synthesized in-house (Budisulistiorini et al., 2015). The MAE-derived OS was quantified using an authentic MAE-derived OS standard synthesized in-house by a procedure to be described in a forthcoming publication (^{1}H NMR trace, Figure S4-2). Although the MAE-derived OS (Gómez-González et al., 2008), which is more formally called 3-sulfooxy-2-hydroxy-2-methyl propanoic acid, has been chemically verified from the reactive uptake of MAE on wet acidic sulfate aerosol (Lin et al., 2013a), the term MAE/HMML-derived OS will be used hereafter to denote the two potential precursors (MAE and HMML) contributing to this OS derivative as recently discussed by Nguyen et al. (2015). It should be noted that Nguyen et al. (2015) provided indirect evidence for the possible existence of HMML. As a result, further work is needed to synthesize this compound to confirm its structure and likely role in SOA formation from isoprene oxidation.

EICs of of *m/z* 155, 169 and 139 were used to quantify the glyoxal-derived OS, methylglyoxal-derived OS, and the hydroxyacetone-derived OS, respectively (Surratt et al., 2007a). In addition, EICs of *m/z* 211, 260 and 305 were used to quantify other known isoprene-derived OSs (Surratt et al., 2007a). Glycolic acid sulfate synthesized in-house was used as a standard to quantify the glyoxal-derived OS (Galloway et al., 2009) and propyl sulfate, was used as a surrogate standard to quantify the remaining isoprene-derived OSs.

4.2.2.4 OC and WSOC analysis

A 1.5 cm^2 square punch from each quartz filter was analyzed for total organic carbon (OC) and elemental carbon (EC) by the thermal-optical method (Birch and Cary, 1996) on a Sunset Laboratory OC/EC instrument (Tigard, OR) at the National Exposure Research Laboratory (NERL) at the U.S. Environmental Protection Agency, Research Triangle Park, NC. The details of the instrument and analytical method have been described elsewhere (Birch and Cary, 1996). In addition to the internal calibration using methane gas, four different mass concentrations of sucrose solution were used to verify the accuracy of instrument during the analysis.

Water-soluble organic carbon (WSOC) was measured in aqueous extracts of quartz fiber filter samples using a total organic carbon (TOC) analyzer (Sievers 5310C, GE Water & Power) equipped with an inorganic carbon remover (Sievers 900). To maintain low background carbon levels, all glassware used was washed with water, soaked in 10% nitric acid, and baked at 500 ˚C for 5 h and 30 min prior to use. Samples were extracted in batches that consisted of 12-21 $PM_{2.5}$ samples and field blanks, one laboratory blank, and one spiked solution. A 17.3 cm^2 filter portion was extracted with 15 mL of purified water (> 18 MΩ, Barnstead Easypure II, Thermo Scientific) by ultra-sonication (Branson 5510). Extracts were then passed through a 0.45 μm

PTFE filter to remove insoluble particles. The TOC analyzer was calibrated using potassium hydrogen phthalate (KHP, Sigma Aldrich) and was verified daily with sucrose (Sigma Aldrich). Samples and standards were analyzed in triplicate; the reported values correspond to the average of the second and third trials. Spiked solutions yielded recoveries that averaged (± one standard deviation) 96 ± 5 % (n = 9). All ambient concentrations were field blank subtracted.

4.2.2.5 Estimation of aerosol pH by ISORROPIA

Aerosol pH was estimated using a thermodynamic model, ISORROPIA-II (Nenes et al., 1998). SO_4^{2-}, nitrate (NO_3^-), and ammonium (NH_4^+) ion concentrations measured in $PM_{2.5}$ collected from BHM, as well as relative humidity (RH), temperature and gas-phase ammonia (NH_3) were used as inputs into the model. These variables were obtained from the SEARCH network at BHM, which collected the data during the period covered by the SOAS campaign. The ISORROPIA-II model estimates particle hydronium ion concentration per unit volume of air (H^+, μg m^{-3}), aerosol liquid water content (LWC, μg m^{-3}), and aqueous aerosol mass concentration (μg m^{-3}). The model-estimated parameters were used in the following formula to calculate the aerosol pH:

$$\text{Aerosol pH} = -\log_{10} a_{H^+} = -\log_{10}\left(\frac{H^+_{air}}{LMASS} \times \rho_{aer} \times 1000\right)$$

where a_{H^+} is H^+ activity in the aqueous phase (mol L^{-1}), *LMASS* is total liquid-phase aerosol mass (μg m^{-3}) and ρ_{aer} is aerosol density. Details of the ISORROPIA-II model and its ability to predict pH, LWC, and gas-to-particle partitioning are not the focus of this study and are discussed elsewhere and (Fountoukis et al., 2009).

4.2.2.6 Estimation of nighttime NO_3

Nitrate radical (NO_3) production ($P[NO_3]$) was calculated using the following equation:

$$P[NO_3] = [NO_2][O_3]k$$

where $[NO_2]$ and $[O_3]$ correspond to the measured ambient NO_2 and O_3 concentrations (mol cm^{-3}), respectively, and *k* is the temperature-dependent rate constant (Herron and Huie, 1974; Graham and Johnston, 1978). Since no direct measure of NO_3 radical was made at this site during SOAS, $P[NO_3]$ was used as a proxy for NO_3 radicals present in the atmosphere to examine if there is any association of it with isoprene-derived SOA tracers.

4.3 Results and Discussion

4.3.1 Overview of the study

The campaign extended from June 1 through July 16, 2013. Temperature during this period ranged from a high of 32.6 °C to a low of 20.5 °C, with an average of 26.4 °C. RH varied from 37-96% throughout the campaign, with an average of 71.5%. Rainfall occurred intermittently over 2-3 day periods and averaged 0.1 inches per day. Wind analysis reveals that air masses approached largely from the south-southeast at an average wind speed of 2 m s^{-1}. Summaries of meteorological conditions as well as wind speed and direction during the course of the campaign are given in Table 2 and illustrated in Figures 4-1 and 4-2.

The average concentration of carbon monoxide (CO), a combustion byproduct, was 208.7 ppbv. The mean concentration of O_3 was significantly higher (t-test, *p-value* < 0.05) on intensive sampling days (37.0 ppbv) compared to regular sampling days (25.2 ppbv). Campaign average concentrations of NO_x, NH_3, and SO_2 were 7.8, 1.9, and 0.9 ppbv, respectively. On average, OC and WSOC levels were 7.2 (n = 120) and 4 μg m^{-3} (n = 100), respectively. The largest inorganic component of $PM_{2.5}$ was SO_4^{2-}, which averaged 2 μg m^{-3} with excursions between 0.4 and 4.9 μg m^{-3} during the campaign. NH_4^+ and NO_3^- were present at low levels, averaging 0.66 and 0.14 μg m^{-3}, respectively. Time series of gas and $PM_{2.5}$ components are shown in Figure 4-2. WSOC

accounted for 35% of OC mass (Figure S4-3a), and was smaller than that recently reported in rural areas during SOAS (Budisulistiorini et al., 2015; Hu et al., 2015), but consistent with previous observations at the BHM site (Ding et al., 2008). WSOC/OC ratios are commonly lower in urban than rural areas, as a consequence of higher primary OC emissions; thus, PM at BHM probably contains increased OC.

Diurnal variation of meteorological parameters, trace gases, and $PM_{2.5}$ components are shown in Figure S4-4 of the Supplement. Temperature dropped during nighttime, and reached a maximum in the afternoon (Figure S4-4a). Conversely, RH was low during day and high at night. High NO_x levels were found in the early morning and decreased during the course of the day (Figure S4-4c), most likely due to forming NO_x sinks (e.g., $RONO_2$, $ROONO_2$, and HNO_3) as well as possibly due to increasing planetary boundary layer (PBL) heights. O_3 reached a maximum concentration between 12 - 3 pm due to photochemistry (Figure S4-4b). SO_2 was slightly higher in the morning (Figure S4-4c), but decreased during the day most likely as a result of PBL dynamics. NH_3 remained fairly constant throughout the day (Figure S4-4c). No significant diurnal variation was found in the concentration of inorganic $PM_{2.5}$ components, including SO_4^{2-}, NO_3^-, and NH_4^+ (Figure S4-4d). Unfortunately, a measurement of isoprene could not be made at BHM during the campaign. However, the diurnal trend of isoprene levels might be similar to the data at the CTR site (Xu et al., 2015), which is only 61 miles away from BHM. Xu et al. (2015) observed the highest levels of isoprene (~ 6 ppb) at CTR in the mid-afternoon (3 pm local time) and its diurnal trend was similar to isoprene-OA measured by the Aerodyne Aerosol Mass Spectrometer (AMS) during the SOAS campaign at the CTR site.

4.3.2 Characterization of Isoprene SOA

Table 3 summarizes the mean and maximum concentrations of known isoprene-derived SOA tracers detected by GC/EI-MS and UPLC/ESI-HR-QTOFMS. Levoglucosan was also analyzed as a tracer for biomass burning. Among the isoprene-derived SOA tracers, the highest mean concentration was for 2-methyltetrols (376 ng m^{-3}), followed by the sum of C_5-alkene triols (181 ng m^{-3}) and the IEPOX-derived OS (165 ng m^{-3}). The concentrations account for 3.8%, 1.8% and 1.6%, respectively, of total OM mass. Noteworthy is that maximum concentrations of 2-methylerythritol (a 2-methyltetrol isomer; 1049 ng m^{-3}), IEPOX-derived OS (865 ng m^{-3}) and (E)-2-methylbut-3-ene-1,2,4-triol (879 ng m^{-3}) were attained during the intensive sampling period 4-7 pm local time on June 15, 2013, following five consecutive days of dry weather (Figures 4-2a and 4-2d) when high levels of isoprene, SO_4^{2-}, and NO_x were forecast.

Our investigation for the potential of OS hydrolysis/decomposition during GC/EI-MS analysis demonstrated that only 1.7% of 2-methylthreitol and 2.4% of 2-methylerythritol could be derived from the IEPOX-derived OSs. In order to accurately estimate the mass concentrations of the IEPOX-derived SOA tracers, we took this effect into account. Together, the IEPOX-derived SOA tracers, which represent SOA formation from isoprene oxidation predominantly under the low-NO_x pathway, comprised 92.45% of the total detected isoprene-derived SOA tracer mass at the BHM site. This contribution is slightly lower than observations reported at rural sites located in Yorkville, GA (97.50%) and Look Rock, Tennessee (LRK) (97%) (Lin et al., 2013b; Budisulistiorini et al., 2015).

The sum of MAE/HMML-OS and 2-MG, which represent SOA formation from isoprene oxidation predominantly under the high-NO_x pathway, contributed 3.25% of the total isoprene-derived SOA tracer mass, while the OS derivative of glycolic acid (GA sulfate) contributed

3.3%. The contribution of GA sulfate was consistent with the level of GA sulfate measured by the airborne NOAA Particle Analysis Laser Mass Spectrometer (PALMS) over the continental U.S. during the Deep Convective Clouds and Chemistry Experiment and SEAC4RS (Liao et al., 2015). However, the contribution of GA sulfate to the total OM at BHM (0.3%) is lower than aircraft-based measurements made by Liao et al. (2015) near the ground in the eastern U.S. (0.9%). GA sulfate can form from biogenic and anthropogenic emissions other than isoprene, including glyoxal, which is thought to be a primary source of GA sulfate (Galloway et al., 2009). For this reason, GA sulfate will not be further discussed in this study.

Isoprene SOA contribution to total OM was estimated by assuming the OM/OC ratio 1.6 based on recent studies (El-Zanan et al., 2009; Simon et al., 2011; Ruthenburg et al., 2014; Blanchard et al., 2015). On average, isoprene-derived SOA tracers (sum of both IEPOX- and MAE/HMML-derived SOA tracers) contributed ~7% (ranging up to ~ 20% at times) of the total particulate OM mass. The average contribution is lower than measured at other sites in the S.E. USA, including both rural LRK (Budisulistiorini et al., 2015; Hu et al., 2015) and urban Atlanta, GA (Budisulistiorini et al., 2013). The contribution of SOA tracers to OM in the current study was estimated on the basis of offline analysis of filters, while tracer estimates in the two earlier studies were based on online ACSM/AMS measurements. The low isoprene SOA/OM ratio is consistent with the low WSOC/OC reported in Section 4.3.1, suggesting a larger contribution of primary OA or hydrophobic secondary OM originating from anthropogenic emissions to the total OM at BHM. However, it should be noted that total IEPOX-derived SOA mass at BHM may actually be closer to ~14% since recent measurements by the Aerodyne ACSM at LRK indicated that tracers could only account for ~50% of the total IEPOX-derived SOA mass resolved by the ACSM (Budisulistiorini et al., 2015). Unfortunately, an Aerodyne ACSM or AMS was not

available at the BHM site to support the confirmation that IEPOX-derived SOA mass at BHM might account for 14% (on average) of the total OM mass.

Levoglucosan, a biomass-burning tracer, averaged 1% of total OM with spikes up to 8%, the same level measured for 2-methylthreitol and (E)-2-methylbut-3-ene-1,2,4-triol (Table 3). The ratio of average levoglucosan at BHM relative to CTR was 5.4, suggesting significantly more biomass burning impacting the BHM site.

IEPOX- and MAE/HMML-derived SOA tracers accounted for 18% and 0.4% of the WSOC mass, respectively (Figure S4-3b), lower than the respective contributions of 24% and 0.7% measured at LRK (Budisulistiorini et al., 2015).

Figure 4-3 shows no difference for the average day and night concentration of isoprene-derived SOA tracers, suggesting that the majority of isoprene SOA tracers are potentially long-lived and formed upwind. A recent study by Lopez-Hilfiker et al. (2016) at the CTR site during the 2013 SOAS demonstrated that isoprene-derived SOA was comprised of effectively nonvolatile material, which could allow for this type of SOA to be long-lived in the atmosphere. Although 2-MG and MAE-derived OS are known to form under high-NO_x conditions (Lin et al., 2013a), no correlation between 2-MG and MAE-derived OS with NO_x (Table 4) is observed at the BHM. This supports that isoprene SOA tracers likely formed at upwind locations and subsequently transported to the sampling site. Higher isoprene emissions during the daytime and cooler nighttime temperatures do not appear to cause any differences between daytime and nighttime isoprene-derived SOA tracer concentrations. Figures 4-4 and 4-5 show the variation of isoprene-derived SOA tracers during intensive sampling periods. The highest concentrations were usually observed in samples collected from 4 pm – 7 pm, local time; however, no statistical significance were observed between intensive periods. This observation illustrates the

importance of the higher time-resolution of the tracer data during intensive sampling periods over course of the campaign (Table S2-S6). An additional consequence of the intensive sampling periods was resolution of a significant correlation between isoprene SOA tracers and O_3 to be discussed in more detail in Section 4.3.3.2.

4.3.3 Influence of anthropogenic emissions on isoprene-derived SOA

4.3.3.1 Effects of reactive nitrogen-containing species

During the campaign, no isoprene-derived SOA tracers, including MAE/HMML-derived OS and 2-MG, correlated with NO_x or NO_y ($r^2 = 0$, n = 120). This is inconsistent with the current understanding of SOA formation from isoprene oxidation pathways under high-NO_x conditions, which proceeds through uptake of MAE (Lin et al., 2013a), and, as recently suggested, HMML (Nguyen et al., 2015), to yield 2-MG and its OS derivative. Plume age, as a ratio of NO_x:NO_y, in this study was highly correlated with O_3 ($r^2 = 0.79$, n = 120) which is consistent with the relative diurnal variation of NO_x, NO_y, and O_3 as discussed in Section 4.3.1. This correlation might be also explained by the photolysis of NO_2, which is abundant due to traffic at the urban ground site, resulting in formation of tropospheric O_3. A negative correlation coefficient ($r^2 = 0.22$, n = 120) between plume age and 2-MG abundance was found as a consequence of relative diurnal variations. The peak of 2-MG was observed in the afternoon after NO_x has decreased. This correlation leads to the hypothesis that the formation of 2-MG may be associated with ageing of air masses; however, further investigation is warranted. A previous study supported a major role for NO_3 in the nighttime chemistry of isoprene (Ng et al., 2008). Correlation of IEPOX- and MAE/HMML-derived SOA with nighttime NO_2, O_3, and P[NO_3] were examined in this study (Figures 4-6 and 4-7). As shown in Figure 4-6f, a moderate correlation between MAE/HMML-derived SOA and nighttime P[NO_3] ($r^2 = 0.57$, n = 40) was observed. The regression analysis

revealed a significant correlation at the 95% confidence interval (*p-value* < 0.05) (Table S7). This finding suggests that some MAE/HMML-derived SOA may form locally from the reaction of isoprene with NO_3 radical at night. A field study reported a peak isoprene mixing ratio in early evening (Starn et al., 1998) as the PBL height decreases at night. As a result, lowering PBL heights could concentrate the remaining isoprene, NO_2, and O_3 that can continue to react during the course of the evening. 2-MG formation has been reported to be NO_2-dependent via the formation and further oxidation of MPAN (Surratt et al., 2006; Chan et al., 2010). Hence, decreasing PBL may be related to nighttime MAE/HMML-derived SOA formation through isoprene oxidation by both $P[NO_3]$ and NO_2.

Although $P[NO_3]$ depends on both NO_2 and O_3 levels, O_3 correlates moderately with MAE/HMML-derived SOA tracers during day (r^2 = 0.48, n = 75), but not at night (r^2 = 0.08, n = 45). The effect of O_3 on isoprene-derived SOA formation during daytime will be discussed further in Section 4.3.3.2. NO_2 levels correlate only weakly with MAE/HMML-derived SOA tracers (r^2 = 0.26, n = 45), indicating that NO_2 levels alone do not explain the moderate correlation of $P[NO_3]$ with these tracers. To our knowledge, correlation of $P[NO_3]$ with high-NO_x SOA tracers has not been observed in previous field studies, indicating that further work is needed to examine the potential role of nighttime NO_3 radicals in forming these SOA tracers.

As shown in Figure 4-7f, IEPOX-derived SOA was weakly correlated (r^2 = 0.26, n = 40) with nighttime $P[NO_3]$. The correlation appears to be driven by the data at the low end of the scale and could therefore be misleading. However, Schwantes et al. (2015) demonstrated that NO_3-initiated oxidation of isoprene yields isoprene nitrooxy hydroperoxides (INEs) through nighttime reaction of RO_2 + HO_2, which upon further oxidation yielded isoprene nitrooxy hydroxyepoxides (INHEs). The INHEs undergo reactive uptake onto acidic sulfate aerosol to

yield SOA constituents similar to those of IEPOX-derived SOA. The present study raises the possibility that a fraction of IEPOX-derived SOA comes from NO_3-initiated oxidation of isoprene at night. The work of Ng et al. (2008), which only observed SOA as a consequence of the RO_2 + RO_2 and RO_2 + NO_3 reactions dominating the fate of the RO_2 radicals, does not explain the weak association between IEPOX-derived SOA tracers and P[NO3] we observe in this study. It is now thought that RO_2 + HO_2 should dominate the fate of RO_2 radicals in the atmosphere (Paulot et al., 2009; Schwantes et al., 2015).

4.3.3.2 Effect of O_3

During the daytime, O_3 was moderately correlated (r^2 = 0.48, n = 75) with total MAE/HMML-derived SOA (Figure 4-6b). This correlation was stronger (r^2 = 0.72, n = 30, *p-value* < 0.05, Table S7) when filters taken during regular daytime sampling periods are considered, suggesting that formation of MACR (a precursor to MAE and HMML) (Lin et al., 2013b; Nguyen et al., 2015) was enhanced by oxidation of isoprene by O_3 (Kamens et al., 1982). O_3 was not correlated (r^2 = 0.08, n = 45) with MAE/HMML-derived SOA at night (Figure 4-6e). The latter finding is consistent with the absence of photolysis to drive the production of O_3. However, residual O_3 may play an important role at night to form MAE/HMML-derived SOA via the P[NO_3] pathway discussed in Section 4.3.3.1.

O_3 was not correlated (r^2= 0.10, n = 75) with IEPOX-derived SOA during daytime (Figure 4-7b), but weakly correlated with 2-methylerythritol (r^2 = 0.25, n = 30) as shown in Table S2, especially during intensive 3 sampling periods (r^2 = 0.34, n = 15, Table S5). An important observation with regard to this result is that no correlation has been found between O_3 and 2-methyltetrols (r^2 < 0.01) in previous field studies (Lin et al., 2013b; Budisulistiorini et al., 2015). Isoprene ozonolysis yielded 2-methyltetrols in chamber studies in the presence of

acidified sulfate aerosol (Riva et al., 2016), but C_5-alkene-triols were not formed by this pathway. The greatest abundance of isoprene-derived SOA tracers in daytime samples was generally observed in intensive 3 samples; however, there was no statistical significance observed between intensive samples. The moderate correlation (r^2 = 0.34, n = 15, *p-value* < 0.05) between O_3 and the 2-methyltetrols observed in intensive 3 samples occurred when O_3 reached maximum levels, suggesting that ozonolysis of isoprene plays a role in 2-methyltetrol formation. Lack of correlation between O_3 and C_5-alkene triols during intensive 3 sampling (r^2 = 0.10, n = 15) supports this contention. Previous studies (Nguyen et al., 2010; Inomata et al., 2014) proposed that SOA formation from isoprene ozonolysis occurs from stabilized Criegee intermediates (sCIs) that can further react in the gas phase to form higher molecular weight products that subsequently partition to the aerosol phase to make SOA. Recent work by Riva et al. (2016) systematically demonstrated that isoprene ozonolysis in the presence of wet acidic aerosol yields 2-methyltetrols and organosulfates unique to this process. Notably, no C_5-alkene triols were observed, which are known to form simultaneously with 2-methyltetrols if IEPOX multiphase chemistry is involved (Lin et al., 2012). Riva et al. (2016) tentatively proposed that hydroperoxides formed in the gas phase from isoprene ozonolysis potentially partition to wet acidic sulfate aerosols and hydrolyze to yield 2-methyltetrols as well as the unique set of organosulfates observed (Riva et al., 2016). Additional work using authentic hydroperoxide standards is needed to validate this tentative hypothesis.

4.3.3.3 Effect of particle SO_4^{2-}

SO_4^{2-} was moderately correlated with IEPOX-derived SOA (r^2 = 0.36, n = 117) and MAE/HMML-derived SOA (r^2 = 0.33, n = 117) at the 95% confidence interval as shown in Table S7. The strength of the correlations was consistent with studies at other sites across the

Southeastern U.S. (Budisulistiorini et al., 2013; Lin et al., 2013b; Budisulistiorini et al., 2015; Xu et al., 2015). Aerosol surface area provided by acidic SO_4^{2-} has been demonstrated to control the uptake of isoprene-derived epoxides (Lin et al., 2012; Gaston et al., 2014; Nguyen et al., 2014; Riedel et al., 2016).

Furthermore, SO_4^{2-} is proposed to enhance IEPOX-derived SOA formation by providing particle water (H_2O_{ptcl}) required for IEPOX uptake (Xu et al., 2015). Aerosol SO_4^{2-} also promotes acid-catalyzed ring-opening reactions of IEPOX by H^+, proton donors such as NH_4^+, and nucleophiles (e.g., H_2O, SO_4^{2-}, or NO_3^-) (Surratt et al., 2010; Nguyen et al., 2014). Since SO_4^{2-} tends to drive both particle water and acidity (Fountoukis and Nenes, 2007), the extent to which each influences isoprene SOA formation during field studies remains unclear. Multivariate linear regression analysis on SOAS data from the CTR site and the SCAPE dataset revealed a statistically significant positive linear relationship between SO_4^{2-} and the isoprene (IEPOX)-OA factor resolved by positive matrix factorization (PMF). On the basis of this analysis the abundance of SO_4^{2-} was concluded to control directly the isoprene SOA formation over broad areas of the Southeastern U.S. (Xu et al., 2015), consistent with previous reports (Lin et al., 2013; Budisulistiorini et al., 2013; Budisulistiorini et al., 2015). Another potential pathway for SO_4^{2-} levels to enhance isoprene SOA formation is through salting-in effects, which the solubility of polar organic compounds would be increased in aqueous solution with increasing salt concentration (Xu et al., 2015). However, systematic investigations of this effect are lacking and further studies are warranted.

4.3.3.4 Effect of aerosol acidity

The aerosol at BHM was acidic throughout the SOAS campaign (pH range 1.60 – 1.94, average 1.76) in accord with a study by Guo et. al. (2014) that found aerosol pH ranging from 0 – 2 throughout the southeastern U.S. However, no correlation of pH with isoprene SOA formation was observed at BHM, also consistent with previous findings using the thermodynamic models to estimate aerosol acidity in many field sites across the southeastern U.S. region, including Yorkville, GA (YRK) (Lin et al., 2013b), Jefferson Street, GA (JST) (Budisulistiorini et al., 2013), and LRK (Budisulistiorini et al., 2015). However, it is important to point out that the lack of correlation between SOA tracers and acidity may stem from the small variations in aerosol acidity and the fact that aerosols are very acidic throughout the campaign. Gaston et al. (2014) and Riedel et al. (2015) recently demonstrated that an aerosol pH < 2 at atmospherically-relevant aerosol surface areas would allow reactive uptake of IEPOX onto acidic (wet) sulfate aerosol surfaces to be competitive with other loss processes (e.g., deposition and reaction of IEPOX with OH). In fact, it was estimated that under such conditions IEPOX would have a lifetime of ~ 5 hr. The constant presence of acidic aerosol has also been observed at other field sites in the southeastern U.S. (Budisulistiorini et al., 2013; Budisulistiorini et al., 2015; Xu et al., 2015), supporting a conclusion that acidity is not the limiting variable in forming isoprene SOA.

4.3.4 Comparison among different sampling sites during 2013 SOAS campaign

Table 5 summarizes the mean concentration and contribution of each isoprene SOA tracer at BHM, CTR, and LRK. BHM is an industrial-residential area, LRK and CTR are rural areas, although LRK is influenced by a diurnal upslope/downslope cycle of air from an urban locality (Knoxville) (Tanner et al., 2005). IEPOX-derived SOA (isoprene SOA produced under low-NO_x

conditions) was predominant at all three sites during the SOAS campaign, while MAE/HMML-derived SOA (isoprene SOA produced under high-NO_x conditions) constituted a minor contribution. The average ratio of 2-methyltetrols to C_5-alkene triols at BHM was 2.2, nearly double that of CTR (1.3) and LRK (1.1). Although 2-methyltetrols and C_5-alkene triols are considered to form readily from the acid-catalyzed reactive uptake and multiphase chemistry of IEPOX (Edney et al., 2005; Surratt et al., 2006), Riva et al. (2016) recently demonstrated that only 2-methyltetrols can be formed via isoprene ozonolysis in the presence of acidic sulfate aerosol. The detailed mechanism explaining isoprene ozonolysis is still unclear, but acid-catalyzed heterogeneous reaction with organic peroxides or H_2O_2 was considered to be possible routes for 2-methyltetrol formation. The higher levels of the 2-methyltetrols observed at the urban BHM site indicates a likely competition between the IEPOX uptake and ozonolysis pathways. Together, these findings suggest that urban O_3 may play an important role in forming the 2-methyltetrols observed at BHM. There were notable trends found among the three sites: (1) average C_5-alkene triol concentrations were higher at CTR (214.1 ng m^{-3}) than at BHM (169.7 ng m^{-3}) and LRK (144.4 ng m^{-3}); (2) average isomeric 3-MeTHF-diol concentrations were lower at CTR (0.2 ng m^{-3}) than the BHM (15.4 ng m^{-3}) or LRK (4.4 ng m^{-3}) sites. Except for the 2-methyltetrols, reasons for the differences observed for the other tracers between sites remains unclear and warrant future investigations.

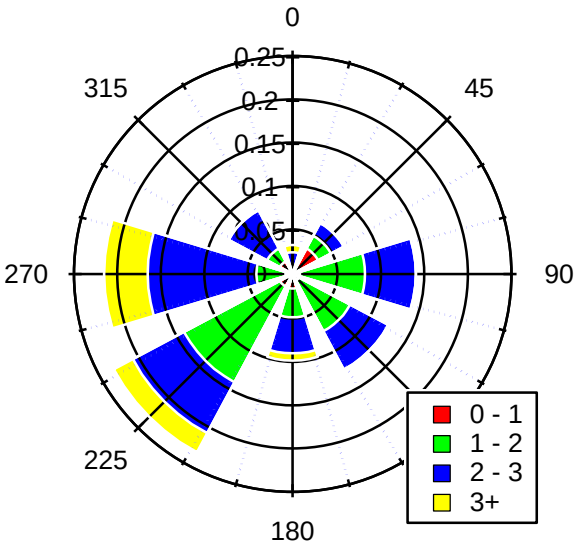

Figure 4-1. Wind rose illustrating wind direction during the campaign at the BHM site. Bars indicate direction of incoming wind, with 0 degrees set to geographic north. Length of bar size indicates frequency with color segments indicating the wind speed in m s^{-1}.

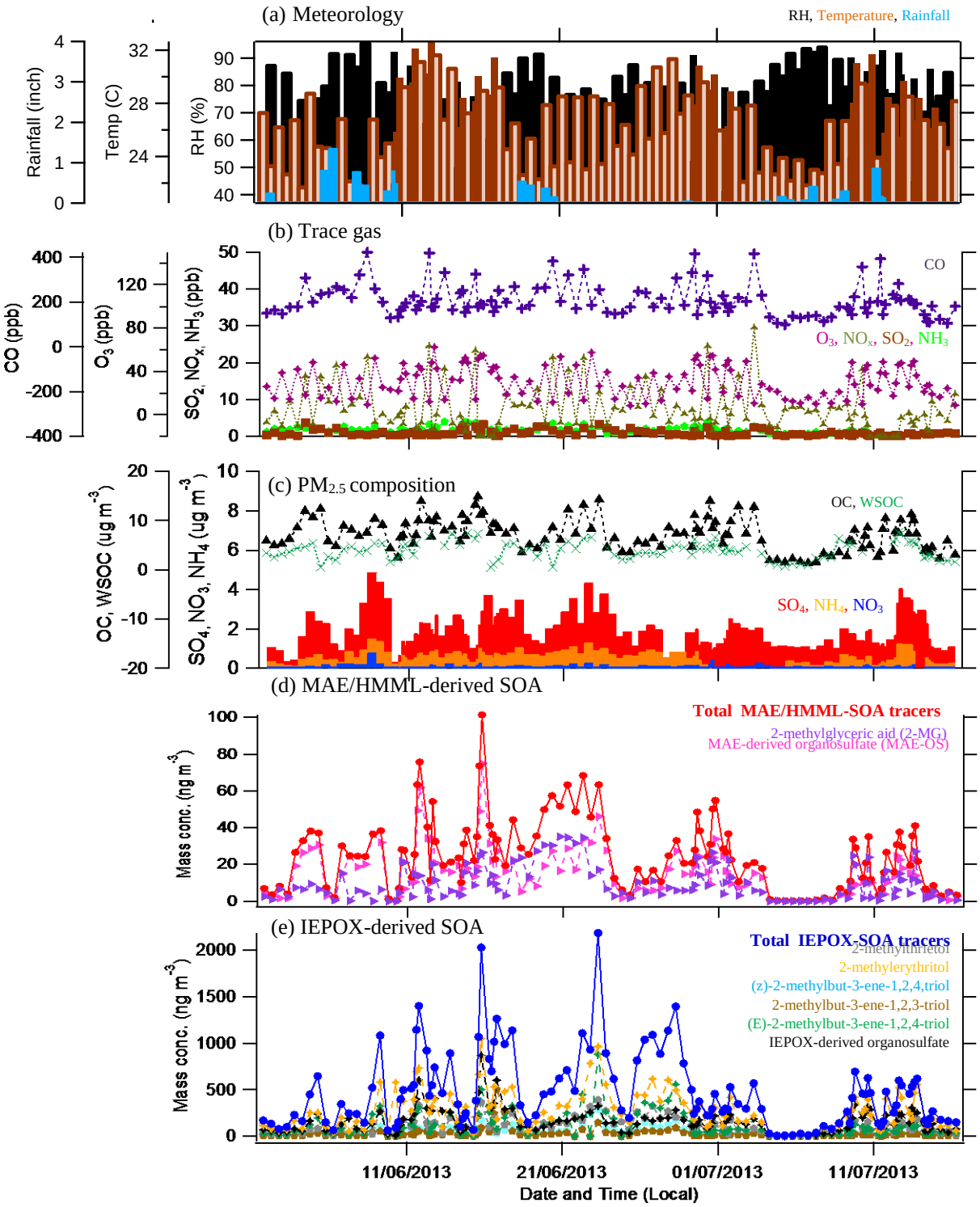

Figure 4-2. Time series of (a) meteorological data, (b) trace gases, (c) PM2.5 constituents, (d) MAE/HMML-derived SOA tracers and (e) IEPOX-derived SOA tracers during the 2013 SOAS campaign at the BHM site.

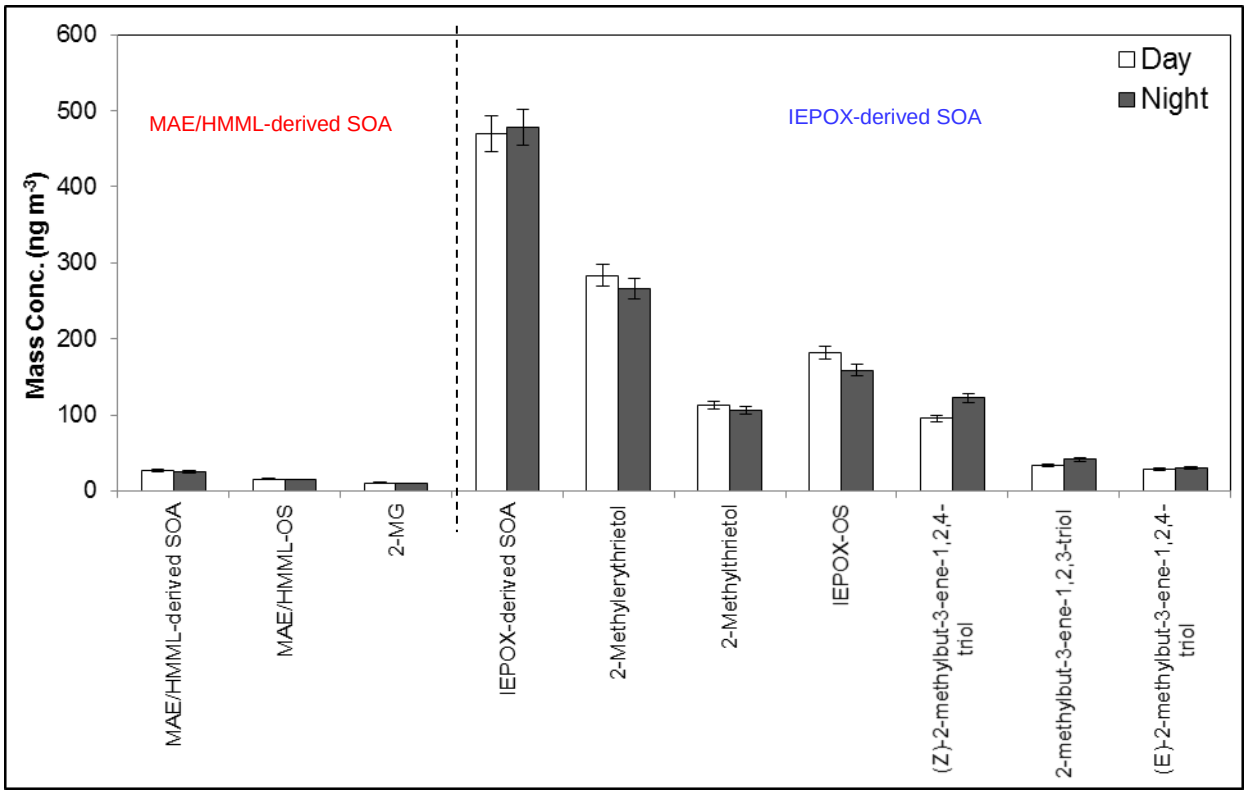

Figure 4-3. The bar chart shows average daytime and nighttime concentrations of isoprene-derived SOA tracers with 95% confident interval. No significant variation between daytime and nighttime was observed.

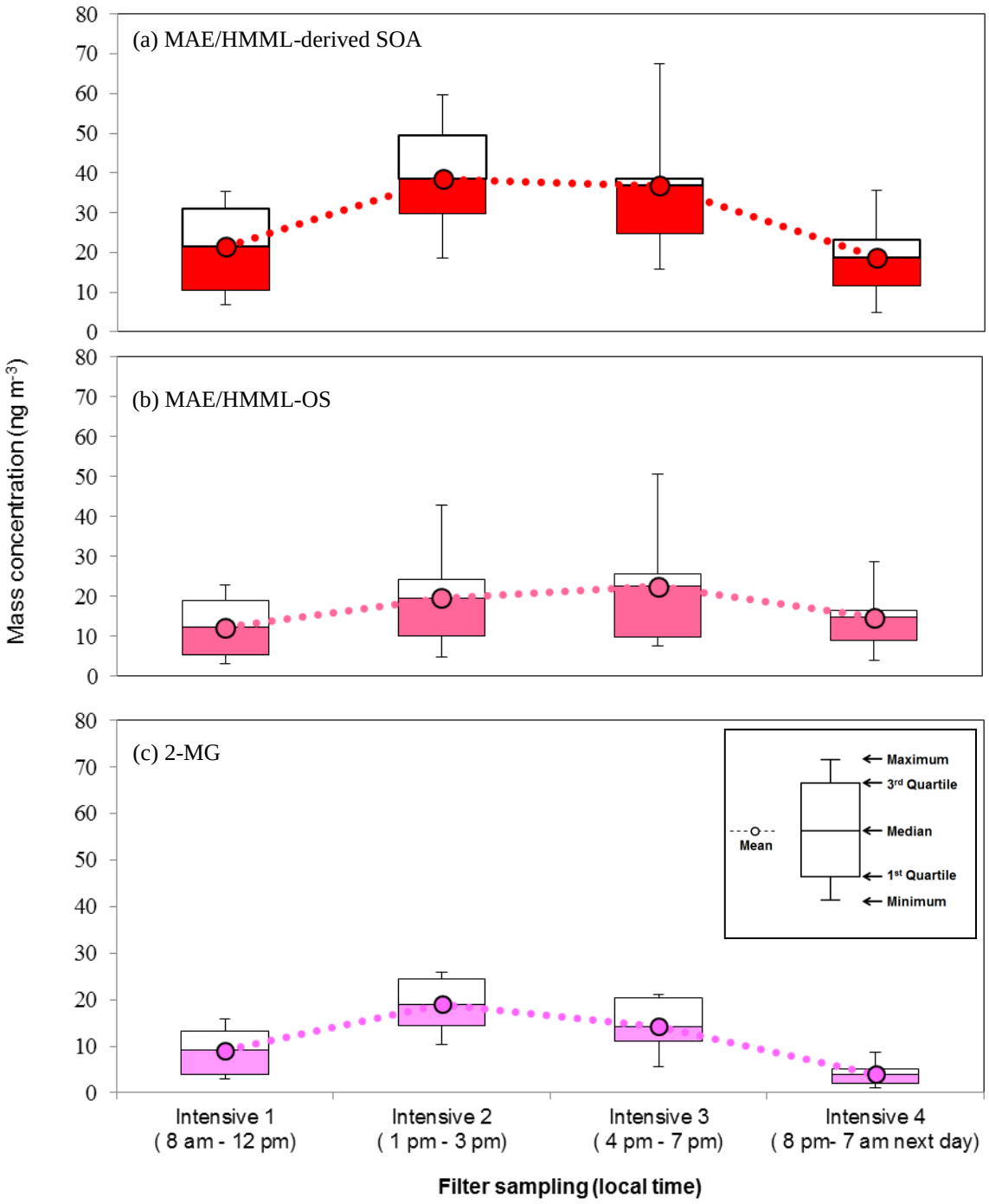

Figure 4-4. The box-and-whisker plot (n = 15) of (a) MAE/HMML-derived SOA, (b) MAE/HMML-OS, and (c) 2-MG. These demonstrate that the statistical distribution of SOA abundance during each intensive sampling period. No significant variation amongst intensive samples was observed.

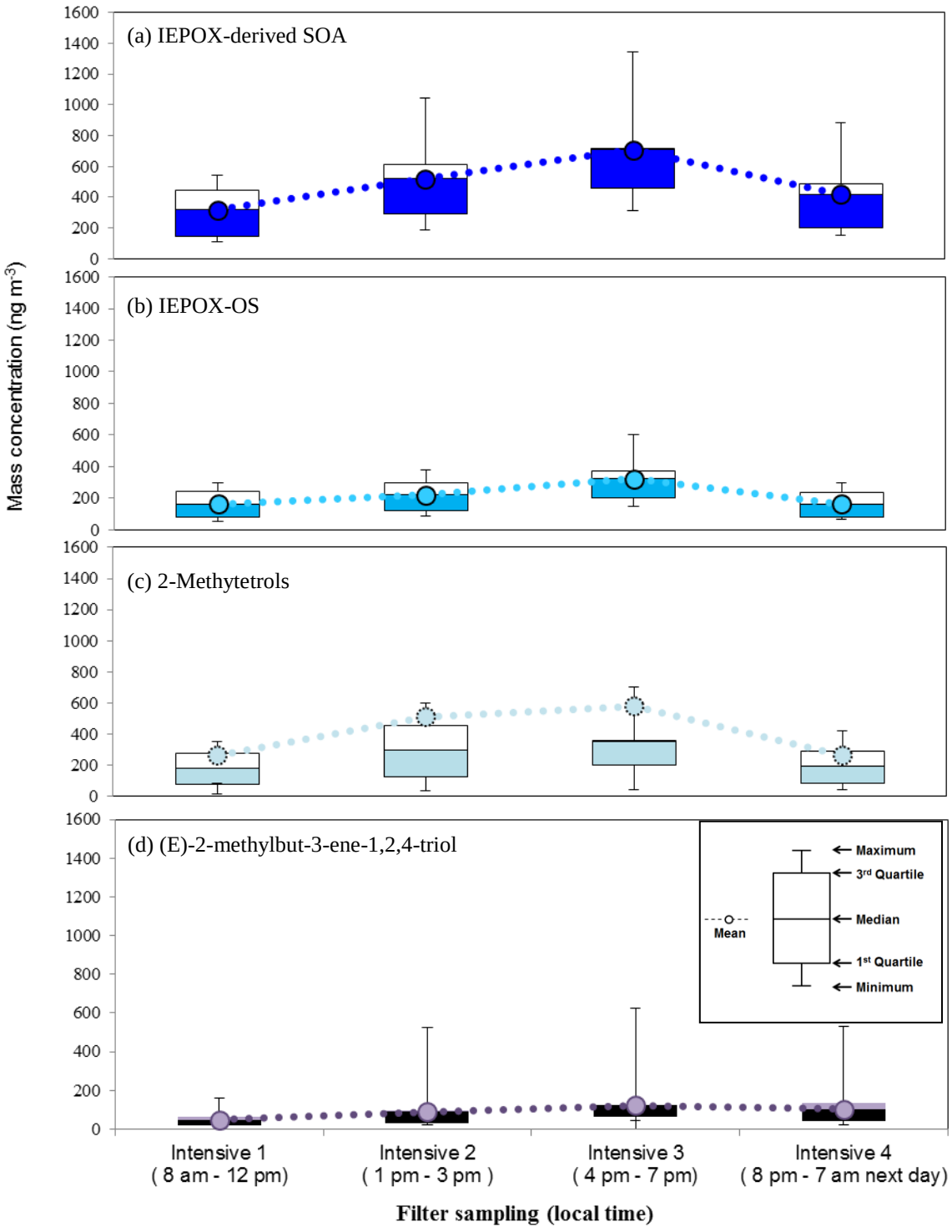

Figure 4-5. The box-and-whisker plot (n = 15) of (a) IEPOX-derived SOA, (b) IEPOX-OS, (c) 2-methyltetrols, and (d) (E)-2-methylbut-3-ene-1,2,4-triol. These demonstrate that the statistical distribution of SOA abundance during each intensive sampling period. No significant variation amongst intensive samples was observed.

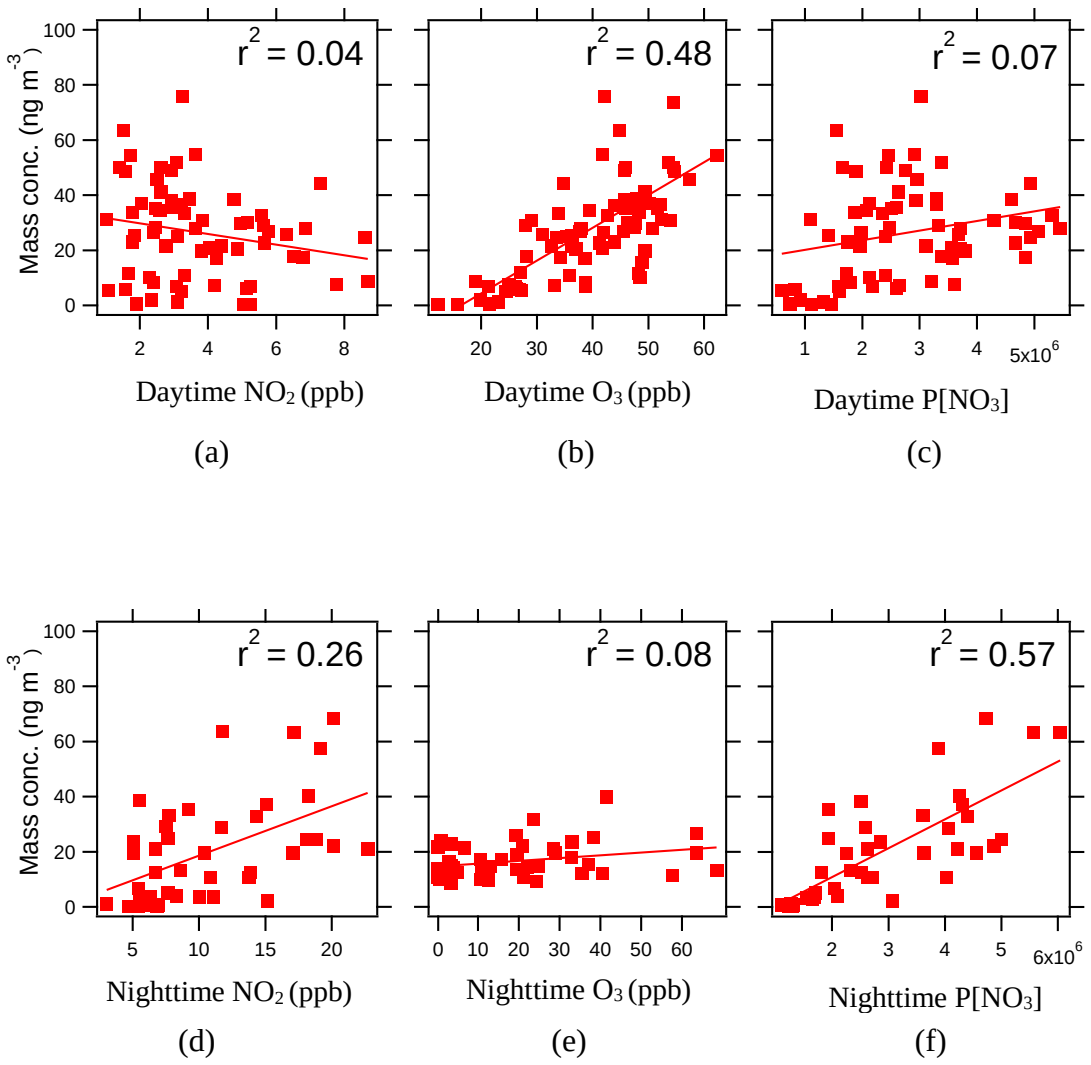

Figure 4-6. Correlation of MAE/HMML-derived SOA tracers with (a) daytime NO_2, (b) daytime O_3, (c) daytime $P[NO_3]$, (d) nighttime NO_2, (e) nighttime O_3, and (f) nighttime $P[NO_3]$. Nighttime $P[NO_3]$ correlation suggests that NO_3 radical chemistry could explain some fraction of the MAE/HMML-derived SOA tracer concentrations.

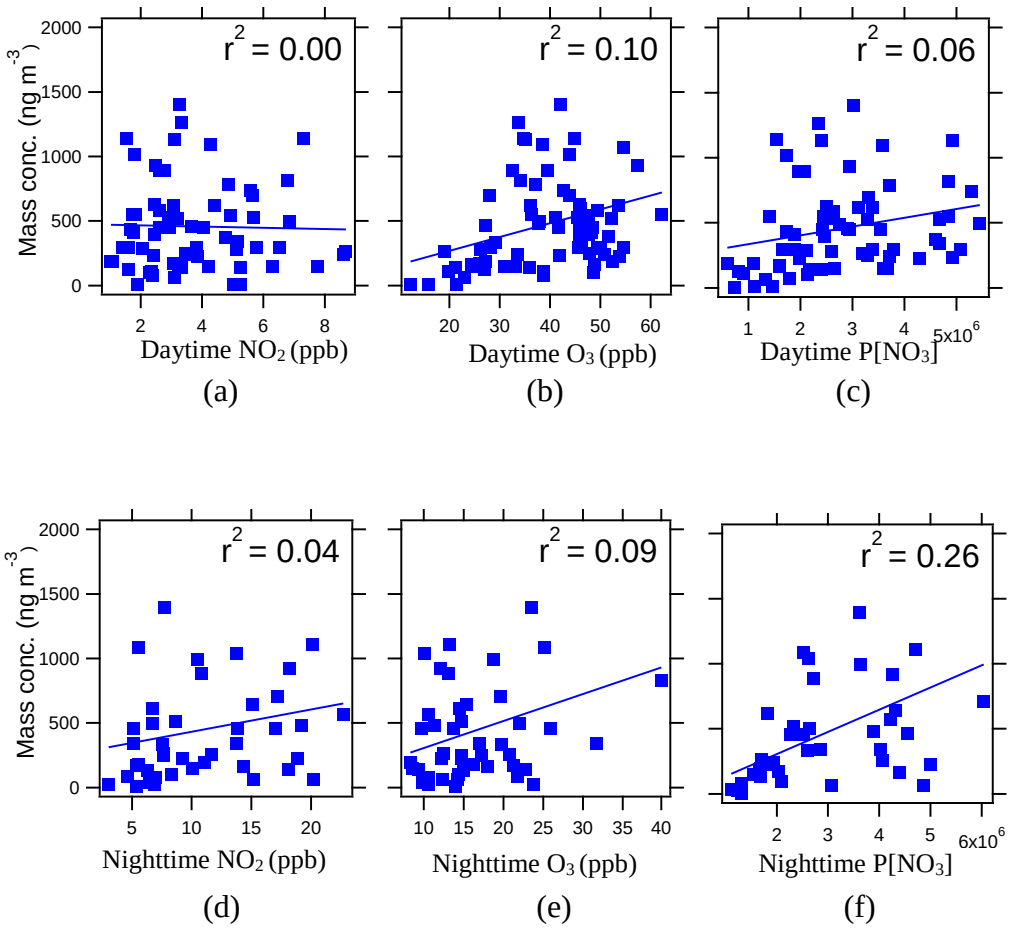

Figure 4-7. Correlation of IEPOX-derived SOA tracers with (a) daytime NO_2, (b) daytime O_3, (c) daytime $P[NO_3]$, (d) nighttime NO_2, (e) nighttime O_3, and (f) nighttime $P[NO_3]$. Nighttime $P[NO_3]$ correlation suggests that NO3 radical chemistry could explain some fraction of the IEPOX-derived SOA tracer concentrations. The contribution of nighttime $P[NO_3]$ to IEPOX-derived SOA would be smaller than MAE/HMML-derived SOA due to the weaker correlation.

Table 4-1. Sampling schedule during SOAS at the BHM ground site.

No. of samples/ day	Sampling schedule	Dates
2 (regular)	Day: 8 am – 7 pm Night: 8 pm – 7 am next day	June 1 – June 9 June 13, June 17 – June 28, July 2- July 9, July 15
4 (intensive)	Intensive 1: 8 am – 12 pm, Intensive 2: 1 pm – 3 pm, Intensive 3: 4 pm – 7 pm, Intensive 4: 8 pm – 7 am next day	June 10 – June 12, June 14 – June 16, June 29 – June 30, July 1, July 9 – July 14

Table 4-2. Summary of collocated measurements of meteorological variables, gaseous species, and $PM_{2.5}$ constituents.

Category	Condition	Average	SD	Minimum	Maximum
Meteorology	Rainfall (in)	0.1	0.2	0.0	1.4
	Temp (°C)	26.4	3.0	20.5	32.7
	RH (%)	71.5	15.0	36.9	96.1
	BP (mbar)	994.2	3.9	984.2	1002.4
	SR (W m^{-2})	303.7	274.5	7.0	885.0
Trace gas (ppbv)	O_3	31.1	14.8	8.3	62.2
	CO	208.7	72.0	99.6	422.9
	SO_2	0.9	0.8	0.1	3.7
	NO	1.3	1.2	0.1	7.0
	NO_2	6.6	5.1	1.0	22.7
	NO_x	7.8	6.0	1.3	29.7
	NO_y	9.1	5.8	2.2	30.4
	HNO_3	0.3	0.2	0.1	1.0
	NH_3	1.9	0.8	0.7	4.0
$PM_{2.5}$ (μg m^{-3})	OC	7.2	3.2	1.4	14.9
	EC	0.6	0.5	0.1	2.7
	WSOC	4.0	1.8	0.5	7.5
	SO_4^{2-}	2.0	0.9	0.4	4.9
	NO_3^-	0.1	0.1	0.0	0.8
	NH_4^+	0.7	0.3	0.2	1.2
	Aerosol pH	1.8	0.1	1.6	1.9

Table 4-3. Summary of isoprene-derived SOA tracers measured by GC/EI-MS and UPLC/ESI-HR-QTOFMS.

SOA tracers	*m/z*	Frequency of detection (%)[a]	Max concentration (ng/m^3)	Mean concentration (ng/m^3)	Isoprene SOA Mass fraction (%)[b]	% of total OM[c]
Measured by GC/EI-MS						
2-methylerythritol[d]	219	99.2	1048.9	269.0	33.8	2.7
2-methylthreitol[d]	219	100.0	388.9	107.3	13.5	1.1
(E)-2-methylbut-3-ene-1,2,4-triol[e]	231	96.7	878.9	112.7	14.2	1.1
(Z)-2-methylbut-3-ene-1,2,4-triol[e]	231	95.8	287.8	38.9	4.9	0.4
2-methylbut-3-ene-1,2,3-triol[e]	231	94.2	503.3	28.9	3.6	0.3
2-methylglyceric acid[d]	219	93.3	35.0	10.8	1.4	0.1
cis-3-MeTHF-3,4-diol[d]	262	22.5	98.9	6.9	0.9	0.1
trans-3-MeTHF-3,4-diol[d]	262	10.0	137.6	8.6	1.1	0.1
IEPOX-derived dimer[e]	333	10.0	2.2	0.0	0.0	0.0
Levoglucosan[d]	204	100.0	922.6	98.7	-	1.0
Measured by UPLC/ESI-HR-QTOFMS						
IEPOX-derived OSs						
$C_5H_{11}O_7S^-$ [d]	215	100.0	864.9	164.5	20.7	1.6
$C_{10}H_{21}O_{10}S^-$[f]	333	1.7	0.3	0.0	0.0	0.0
MAE-derived OS[d]						
$C_4H_7O_7S^-$	199	100.0	35.7	7.2	1.9	0.1
GA sulfate[d]						
$C_2H_3O_6S^-$	155	100.0	75.2	26.2	3.3	0.3
Methylglyoxal-derived OS[g]						
$C_3H_5O_6S^-$	169	97.5	10.5	2.7	0.3	0.0
Isoprene-derived OSs[g]						
$C_5H_7O_7S^-$	211	97.5	5.2	1.4	0.2	0.0
$C_5H_{10}NO_9S^-$	260	90.0	3.9	0.3	0.0	0.0
$C_5H_9N_2O_{11}S^-$	305	5.0	3.3	2.9	0.4	0.0
Hydroxyacetone-derived OS[g]						
$C_2H_3O_5S^-$	139	30.8	2.6	0.2	0.0	0.0

[a] Total filters = 120

[b] Mass fraction is the contribution of each species among total known isoprene-derived SOA mass detected by GC/EI MS and UPLC/ESI-HR-QTOFMS

[c] OM/OC = 1.6

[d] OA tracers quantified by authentic standards

[e] SOA tracers quantified by 2-methyltetrols as a surrogate standard

[f] SOA tracer quantified by IEPOX-derived OS (*m/z* 215) as a surrogate standard

[g] SOA tracers quantified by propyl sulfate as a surrogate standard

Table 4-4. Overall correlation (r^2) of isoprene-derived SOA tracers and collocated measurements at BHM during 2013 SOAS campaign.

SOA tracers	CO	O_3	NO_x	NO_y	SO_2	NH_3	SO_4	NO_3	NH_4	OC	WSOC	pH
MAE/HMML-derived SOA tracers*	**0.07**	**0.26**	**0.00**	**0.01**	**0.06**	**0.11**	**0.33**	**0.01**	**0.18**	**0.47**	**0.20**	**0.00**
2-methylglyceric acid	0.01	0.26	0.01	0.00	0.01	0.07	0.10	0.00	0.06	0.19	0.02	0.00
MAE-derived OS	0.10	0.14	0.00	0.02	0.07	0.09	0.38	0.01	0.18	0.32	0.23	0.01
IEPOX-derived SOA tracers**	**0.04**	**0.05**	**0.00**	**0.01**	**0.05**	**0.01**	**0.36**	**0.00**	**0.21**	**0.24**	**0.12**	**0.00**
2-methylerythritol	0.00	0.16	0.03	0.02	0.01	0.00	0.30	0.02	0.18	0.18	0.19	0.00
2-methylthreitol	0.00	0.13	0.02	0.03	0.02	0.00	0.20	0.01	0.16	0.17	0.15	0.00
(E)-2-methylbut-3-ene-1,2,4-triol	0.07	0.00	0.02	0.01	0.07	0.00	0.15	0.00	0.19	0.11	0.04	0.00
(Z)-2-methylbut-3-ene-1,2,4-triol	0.04	0.00	0.00	0.00	0.06	0.00	0.28	0.00	0.20	0.04	0.00	0.00
2-methylbut-3-ene-1,2,3-triol	0.02	0.00	0.03	0.00	0.00	0.02	0.32	0.01	0.03	0.17	0.04	0.00
IEPOX-derived OS	0.02	0.14	0.03	0.00	0.00	0.00	0.27	0.00	0.16	0.29	0.29	0.00
IEPOX dimer	0.00	0.00	0.00	0.00	0.00	0.00	0.00	0.00	0.00	0.00	0.00	0.00
Other isoprene SOA tracers												
GA sulfate												
$C_2H_3O_6S^-$	0.30	0.23	0.01	0.00	0.08	0.09	0.27	0.00	0.19	0.38	0.18	0.00
Methylglyoxal-derived OS												
$C_3H_5O_6S^-$	0.14	0.04	0.02	0.03	0.03	0.07	0.31	0.02	0.25	0.21	0.24	0.00
Isoprene-derived OSs												
$C_5H_7O_7S^-$	0.01	0.23	0.03	0.01	0.00	0.02	0.21	0.00	0.16	0.31	013	0.00
$C_5H_{10}NO_9S^-$	0.17	0.00	0.12	0.14	0.10	0.14	0.31	0.16	0.23	0.20	0.07	0.00
$C_5H_9N_2O_{11}S^-$ ***	0.32	0.71	0.66	0.58	0.42	0.02	0.68	0.50	0.42	0.00	0.50	0.00
Hydroxyacetone-derived OS												
$C_2H_3O_5S^-$	0.02	0.10	0.08	0.07	0.05	0.00	0.00	0.03	0.00	0.01	0.01	0.00
Other tracer												
Levoglucosan	0.00	0.09	0.02	0.01	0.02	0.00	0.00	0.02	0.00	0.08	0.04	0.01

* Summed tracers for MAE/HMML-derived SOA

** Summed tracers for IEPOX-derived SOA

***Found only in 6 of 120 filters

The correlations in this table are positive.

Table 4-5. Summary of isoprene-derived SOA tracers from the three SOAS ground sites: BHM, CTR, and LRK.

SOA tracers	Urban		Rural			
	BHM		CTR		LRK	
	Mean (ng m^{-3})	Average fraction of detected tracers (%)	Mean (ng m^{-3})	Average fraction of detected tracers (%)	Mean (ng m^{-3})	Average fraction of detected tracers (%)
MAE/HMML derived SOA						
MAE/HMML-derived OS	7.2	1.1	10.2	1.3	8.2	1.8
2-methylglyceric acid	10.4	1.7	5.1	0.7	7.5	1.6
IEPOX derived SOA						
IEPOX-derived OS	164.5	24.3	207.1	26.8	139.2	30.3
IEPOX-derived dimer OS	0.04	0.00	0.7	0.1	1.1	0.2
2-methylerythritol	266.7	37.9	204.8	26.5	120.7	26.3
2-methylthreitol	107.3	15.8	73.7	9.5	42.4	9.2
(E)-2-methylbut-3-ene-1,2,4-triol	109.0	12.3	137.3	17.8	98.8	21.5
(Z)-2-methylbut-3-ene-1,2,4-triol	37.3	4.1	50.7	6.6	29.1	6.1
2-methylbut-3-ene-1,2,3-triol	23.4	2.5	26.1	3.4	16.5	3.6
trans-3-MeTHF-3,4-diol	8.6	1.0	0.0	0.0	2.7	0.6
cis-3-MeTHF-3,4-diol	6.8	1.0	0.2	0.0	1.7	0.4

4.4 Supporting Information

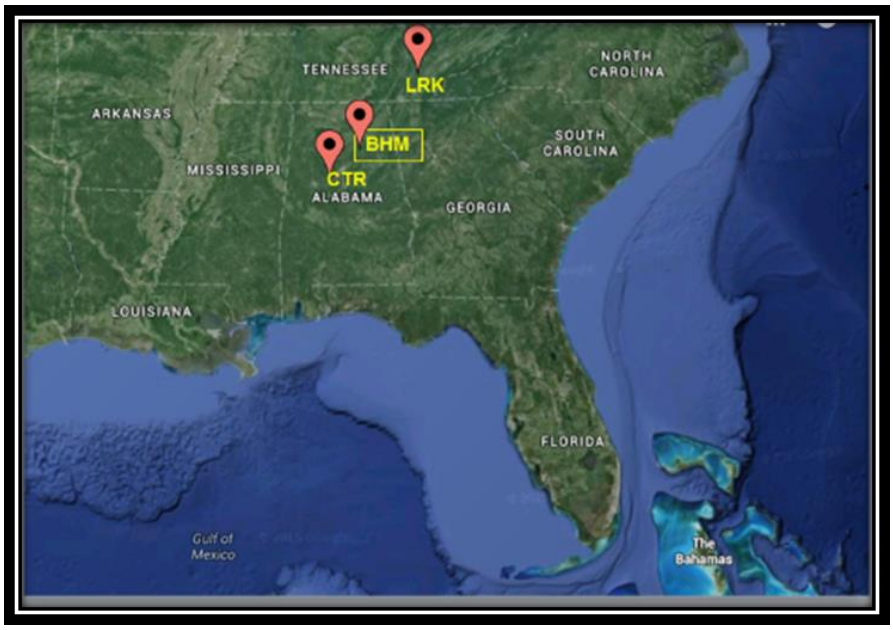

Figure S4-1. The locations of the three sampling sites during 2013 SOAS: BHM, CTR, and LRK. BHM was the focused site in this study.

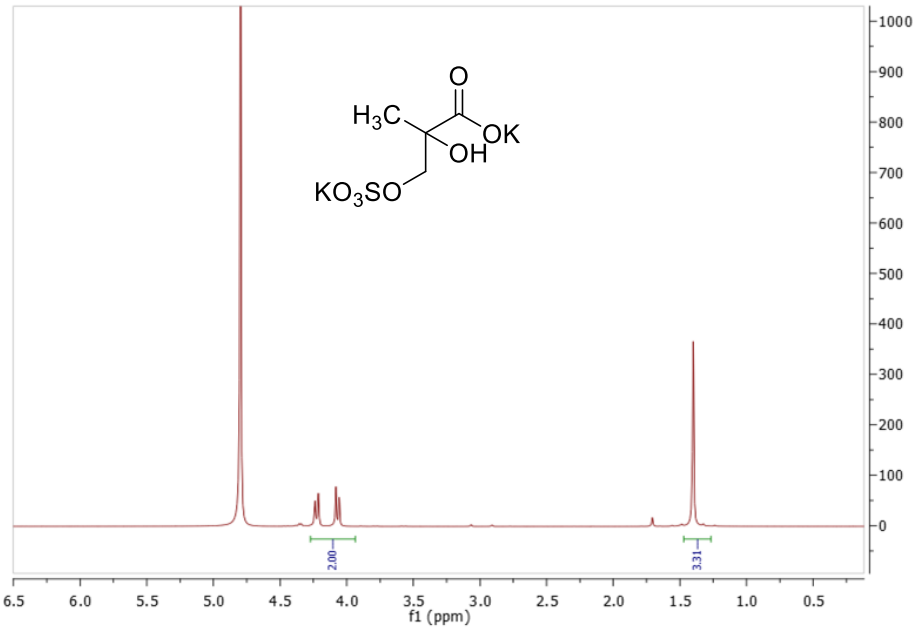

Figure S4-2. ^{1}H NMR (400 MHz, D_2O) of the MAE/HMML-derived OS.

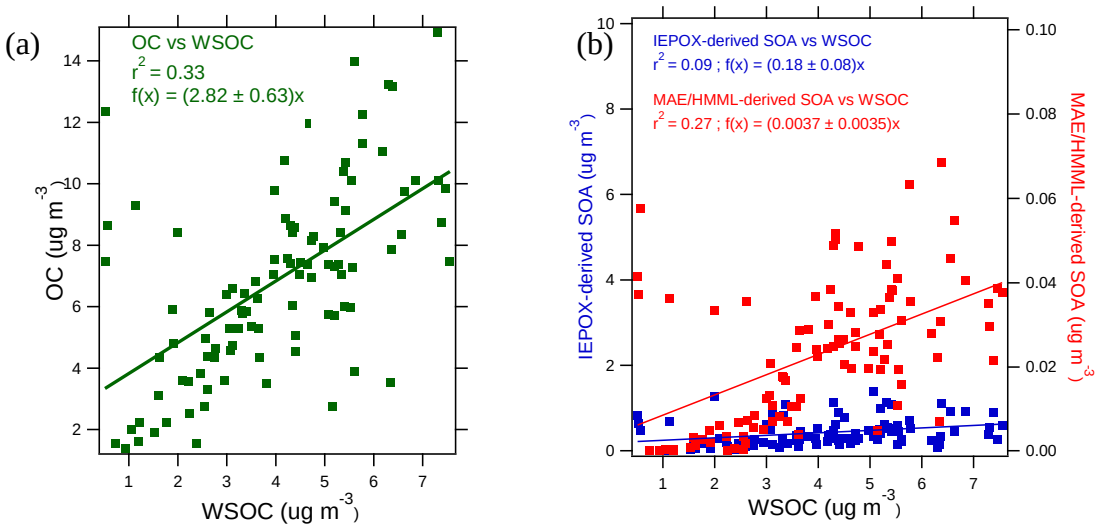

Figure S4-3. (a) Comparison of organic carbon (OC) and water soluble organic carbon (WSOC), suggesting that 35% of OC at BHM was WSOC. (b) Comparison of IEPOX- and MAE/HMML-derived SOA tracers with WSOC, indicating that IEPOX- and MAE/HMML-derived SOA tracers explained 18 and 0.4% of the WSOC, respectively.

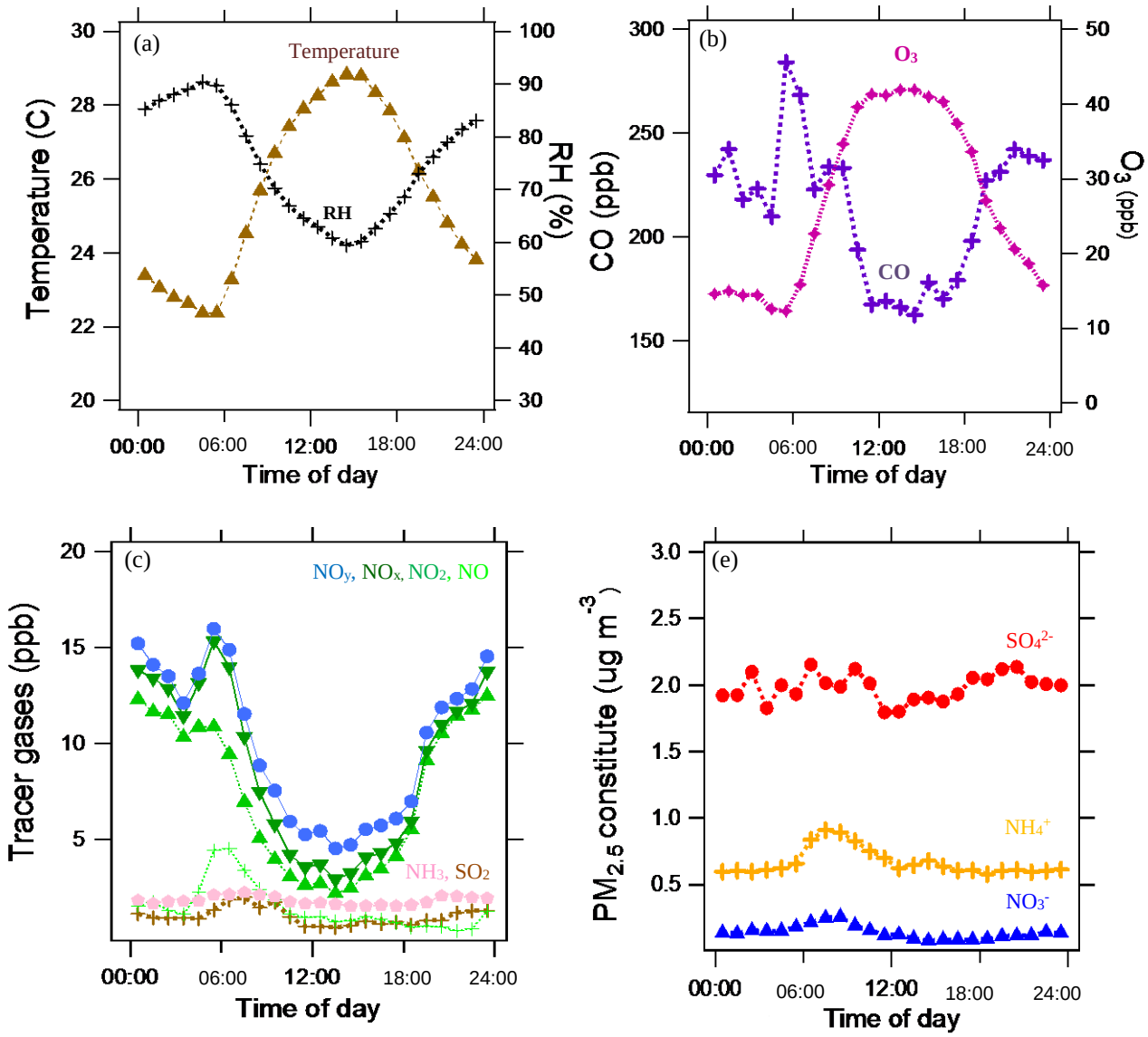

Figure S4-4. Diurnal variations of (a) meteorology, (b) O_3 and CO, (c) NO_y, NO, NO_2, and NO_x, and (d) $PM_{2.5}$ constituents at BHM during the 2013 SOAS campaign. High temperature and low RH were observed at 2-4 pm local time. O_3 reached its maximum, while CO dropped to its minimum in early afternoon. NO_x and NO_y were high during early morning hours and declined in the afternoon due to photochemical processes. No significant diurnal variation was observed for NH_3, SO_2, SO_4^{2-}, NH_4^+, and NO_3^-.

Table S4-1. Instrumentation and time resolution of collocated measurements at BHM.

Category	Variable	Analyzer/Sensor	Time Resolution (Interval, average) (minutes)
Meteorology	Wind Speed/Direction	RMYoung 81000 sonic	5, 60
	T/RH/BP	Paroscientific Met4A	5, 60
	T/RH	Vaisala	5, 60
	PAR	Licor	5, 60
	Precipitation	ETI-NOAH IV	5, 60
	Aerosol/cloud layers	JenOptik CHM 15k ceilometer	5, 60
	Surface wetness	Vaisala (SWS2)	5, 60
Trace Gases	O_3	Thermo 49i	5, 60
	CO	Thermo 48i	5, 60
	SO_2	Thermo 43i	5, 60
	NO	Thermo 42i	5, 60
	NO_2	Photolysis/Thermo 49i	5, 60
	HNO_3	Continuous denuder diff/Thermo 42i	5, 60
	NO_y	Cat. reduction/Thermo 42i	5, 60
	NH_3	Continuous denuder diff/Thermo 42i	5, 60
Continuous PM	$PM_{2.5}$ Mass	TEOM	60
	PMcoarse Mass	Dichotomous TEOM	60
	$PM_{2.5}$ SO_4	Cat. reduction/Thermo 43i	60
	$PM_{2.5}$ NO_3	Cat. reduction/Thermo 42i	60
	$PM_{2.5}$ NH_4	Cat. oxidation/Thermo 42i	60
	$PM_{2.5}$ TC/EC	Sunset	60
	Dry Babs (880 nm)	Radiance Research M903	5, 60
	Dry Bsp (530 nm)	Magee 2ch. Aeth	5, 60
	Ambient Bsp (530 nm)	Optec NGN-2a	5, 60
Filter-Based PM	$PM_{2.5}$ Mass	gravimetry	1440, daily
	$PM_{2.5}$ ions	IC	1440, 1 in 3 days
	$PM_{2.5}$ major/minor elements	XRF	1440, daily
	$PM_{2.5}$ water-soluble metals	ICPMS	1440, 1 in 3 days
	$PM_{2.5}$ OC/EC	TOR	1440, 1 in 3 days
	PM_{coarse} Mass	gravimetry	1440, 1 in 3 days
	PM_{coarse} ions	IC	1440, 1 in 3 days
	PM_{coarse} major/minor elements	XRF	1440, 1 in 3 days
	PM_{coarse} water-soluble metals	ICPMS	1440, 1 in 3 days
Hi-Vol Based PM	$PM_{2.5}$ OC/EC	TOR	23-hr, daily
	$PM_{2.5}$ ions	IC	23-hr, daily
	$PM_{2.5}$ (other)	Various	11-hr, daily

Table S4-2. Correlation (r^2) of isoprene-derived SOA tracers and collocated measurements during regular day sampling (8 am – 7 pm).

SOA tracers	CO	O_3	NO_x	NO_y	SO_2	NH_3	SO_4	NO_3	NH_4	OC	WSOC	pH
MAE/HMML-derived SOA tracers	**0.31**	**0.72**	**0.04**	**0.00**	**0.20**	**0.34**	**0.51**	**0.10**	**0.53**	**0.44**	**0.48**	**0.01**
2-methylglyceric acid	0.14	0.44	0.01	0.00	0.09	0.15	0.19	0.03	0.27	0.09	0.12	0.00
MAE-derived OS	0.28	0.60	0.04	0.00	0.14	0.31	0.66	0.14	0.56	0.58	0.52	0.01
IEPOX-derived SOA tracers	**0.09**	**0.26**	**0.01**	**0.01**	**0.08**	**0.12**	**0.41**	**0.04**	**0.41**	**0.31**	**0.32**	**0.01**
2-methylerythritol	0.04	0.30	0.03	0.00	0.05	0.04	0.31	0.00	0.31	0.24	0.30	0.01
2-methylthreitol	0.02	0.20	0.02	0.00	0.06	0.03	0.21	0.00	0.23	0.13	0.19	0.00
(E)-2-methylbut-3-ene-1,2,4-triol	0.05	0.24	0.02	0.00	0.03	0.05	0.33	0.02	0.32	0.22	0.27	0.00
(Z)-2-methylbut-3-ene-1,2,4-triol	0.10	0.11	0.00	0.01	0.09	0.17	0.34	0.10	0.32	0.24	0.16	0.01
2-methylbut-3-ene-1,2,3-triol	0.11	0.11	0.00	0.01	0.09	0.18	0.36	0.10	0.34	0.25	0.17	0.01
IEPOX-derived OS	0.17	0.41	0.01	0.01	0.08	0.19	0.47	0.07	0.50	0.53	0.59	0.01
IEPOX dimer	0.00	0.00	0.00	0.00	0.00	0.00	0.00	0.00	0.00	0.00	0.00	0.00
Other isoprene SOA tracers												
GA sulfate												
$C_2H_3O_6S^-$	0.22	0.20	0.00	0.00	0.07	0.19	0.49	0.20	0.39	0.33	0.21	0.01
Methylglyoxal-derived OS												
$C_3H_5O_6S^-$	0.25	0.40	0.01	0.01	0.11	0.11	0.57	0.05	0.46	0.41	0.47	0.01
Isoprene-derived OSs												
$C_5H_7O_7S^-$	0.13	0.34	0.01	0.01	0.02	0.17	0.35	0.11	0.40	0.21	0.28	0.00
$C_5H_{10}NO_9S^-$	0.02	0.37	0.12	0.06	0.00	0.01	0.48	0.12	0.38	0.18	0.12	0.11
$C_5H_9N_2O_{11}S^-$ *	0.25	0.56	0.48	0.40	0.15	0.40	0.52	0.28	0.24	0.57	0.46	0.00
Hydroxyacetone-derived OS												
$C_2H_3O_5S^-$	0.42	0.73	0.06	0.16	0.00	0.18	0.55	0.23	0.71	0.57	0.66	0.00
Other tracer												
Levoglucosan	0.26	0.34	0.00	0.00	0.09	0.21	0.44	0.10	0.47	0.22	0.25	0.01

* Found only in 6 of 120 filters

The correlations in this table are positive.

Table S4-3. Correlation (r^2) of isoprene-derived SOA tracers and collocated measurements during intensive 1 sampling (8 am – 11 am).

SOA tracers	CO	O_3	NO_x	NO_y	SO_2	NH_3	SO_4	NO_3	NH_4	OC	WSOC	pH
MAE/HMML-derived SOA tracers	**0.00**	**0.20**	**0.04**	**0.16**	**0.01**	**0.07**	**0.35**	**0.25**	**0.46**	**0.47**	**0.16**	**0.18**
2-methylglyceric acid	0.03	0.22	0.05	0.10	0.00	0.07	0.00	0.43	0.11	0.46	0.07	0.08
MAE-derived OS	0.01	0.09	0.02	0.12	0.01	0.03	0.72	0.06	0.62	0.26	0.08	0.18
IEPOX-derived SOA tracers	**0.11**	**0.04**	**0.05**	**0.00**	**0.06**	**0.26**	**0.30**	**0.00**	**0.16**	**0.04**	**0.02**	**0.03**
2-methylerythritol	0.15	0.01	0.02	0.00	0.16	0.52	0.22	0.03	0.18	0.00	0.00	0.15
2-methylthreitol	0.04	0.00	0.00	0.00	0.10	0.19	0.13	0.02	0.16	0.00	0.02	0.13
(E)-2-methylbut-3-ene-1,2,4-triol	0.12	0.03	0.06	0.01	0.01	0.27	0.23	0.00	0.09	0.11	0.05	0.00
(Z)-2-methylbut-3-ene-1,2,4-triol	0.13	0.02	0.05	0.01	0.03	0.32	0.28	0.00	0.08	0.09	0.05	0.00
2-methylbut-3-ene-1,2,3-triol	0.07	0.02	0.02	0.00	0.02	0.26	0.22	0.01	0.03	0.04	0.28	0.01
IEPOX-derived OS	0.09	0.07	0.07	0.00	0.05	0.19	0.30	0.00	0.17	0.04	0.00	0.02
IEPOX dimer	0.00	0.00	0.00	0.00	0.00	0.00	0.00	0.00	0.00	0.00	0.00	0.00
Other isoprene SOA tracers												
GA sulfate												
$C_2H_3O_6S^-$	0.00	0.19	0.03	0.01	0.01	0.03	0.37	0.02	0.44	0.25	0.11	0.00
Methylglyoxal-derived OS												
$C_3H_5O_6S^-$	0.05	0.05	0.18	0.28	0.02	0.00	0.01	0.11	0.24	0.09	0.56	0.03
Isoprene-derived OSs												
$C_5H_7O_7S^-$	0.09	0.15	0.00	0.20	0.05	0.02	0.36	0.12	0.25	0.40	0.00	0.02
$C_5H_{10}NO_9S^-$	0.00	0.05	0.02	0.06	0.06	0.04	0.38	0.00	0.23	0.17	0.18	0.37
$C_5H_9N_2O_{11}S^-$ *	0.00	0.00	0.00	0.00	0.00	0.21	0.00	0.00	0.00	0.00	0.00	0.00
Hydroxyacetone-derived OS												
$C_2H_3O_5S^-$	0.25	0.67	0.71	0.65	0.21	0.21	0.03	0.26	0.12	0.50	0.00	0.70
Other tracer												
Levoglucosan	0.03	0.07	0.02	0.00	0.07	0.07	0.08	0.11	0.01	0.03	0.02	0.24

* Found only in 6 of 120 filters

The correlations in this table are positive.

Table S4-4. Correlation (r^2) of isoprene-derived SOA tracers and collocated measurements during intensive 2 sampling (12 pm – 3 pm).

SOA tracers	CO	O_3	NO_x	NO_y	SO_2	NH_3	SO_4	NO_3	NH_4	OC	WSOC	pH
MAE/HMML-derived SOA tracers	**0.13**	**0.42**	**0.0**	**0.12**	**0.04**	**0.01**	**0.14**	**0.05**	**0.29**	**0.55**	**0.19**	**0.00**
2-methylglyceric acid	0.01	0.47	0.25	0.32	0.00	0.04	0.00	0.05	0.04	0.17	0.07	005
MAE-derived OS	0.15	0.20	0.04	0.01	0.06	0.00	0.18	0.15	0.31	0.49	0.24	0.03
IEPOX-derived SOA tracers	**0.22**	**0.00**	**0.04**	**0.08**	**0.00**	**0.21**	**0.34**	**0.32**	**0.37**	**0.46**	**0.81**	**0.02**
2-methylerythritol	0.41	0.00	0.13	0.14	0.01	0.16	0.48	0.24	0.50	0.42	0.77	0.01
2-methylthreitol	0.29	0.00	0.03	0.07	0.00	0.07	0.22	0.41	0.39	0.32	0.70	0.02
(E)-2-methylbut-3-ene-1,2,4-triol	0.17	0.00	0.04	0.07	0.01	0.17	0.30	0.31	0.29	0.44	0.61	0.02
(Z)-2-methylbut-3-ene-1,2,4-triol	0.21	0.00	0.05	0.07	0.01	0.17	0.33	0.29	0.31	0.45	0.64	0.01
2-methylbut-3-ene-1,2,3-triol	0.03	0.02	0.00	0.02	0.03	0.07	0.13	0.21	0.06	0.09	0.62	0.03
IEPOX-derived OS	0.19	0.02	0.11	0.21	0.00	0.32	0.43	0.16	0.39	0.52	0.58	0.00
IEPOX dimer	0.00	0.00	0.00	0.00	0.00	0.00	0.00	0.00	0.00	0.00	0.00	0.00
Other isoprene SOA tracers												
GA sulfate												
$C_2H_3O_6S^-$	0.24	0.23	0.00	0.08	0.00	0.06	0.32	0.23	0.46	0.46	0.48	0.00
Methylglyoxal-derived OS												
$C_3H_5O_6S^-$	0.27	0.28	0.01	0.02	0.01	0.06	0.29	0.00	0.29	0.33	0.43	0.03
Isoprene-derived OSs												
$C_5H_7O_7S^-$	0.14	0.02	0.06	0.07	0.03	0.06	0.16	0.00	0.18	0.18	0.09	0.00
$C_5H_{10}NO_9S^-$	0.00	0.15	0.07	0.05	0.21	0.34	0.03	0.05	0.00	0.06	0.00	0.18
$C_5H_9N_2O_{11}S^-$ *	0.00	0.00	0.00	0.00	0.00	0.00	0.00	0.00	0.00	0.00	0.00	0.00
Hydroxyacetone-derived OS												
$C_2H_3O_5S^-$	0.09	0.40	0.01	0.01	0.10	0.05	0.04	0.07	0.10	0.07	0.62	0.01
Other tracer												
Levoglucosan	0.03	0.00	0.22	0.13	0.00	0.01	0.03	0.17	0.00	0.02	0.00	0.07

* Found only in 6 of 120 filters

The correlations in this table are positive.

Table S4-5. Correlation (r^2) of isoprene-derived SOA tracers and collocated measurements during intensive 3 sampling (4 pm – 7 pm).

SOA tracers	CO	O_3	NO_x	NO_y	SO_2	NH_3	SO_4	NO_3	NH_4	OC	WSOC	pH
MAE/HMML-derived SOA tracers	**0.01**	**0.47**	**0.45**	**0.39**	**0.47**	**0.00**	**0.19**	**0.10**	**0.12**	**0.54**	**0.23**	**0.15**
2-methylglyceric acid	0.12	0.37	0.03	0.17	0.25	0.00	0.00	0.05	0.02	0.34	0.50	0.15
MAE-derived OS	0.00	0.37	0.44	0.39	0.41	0.01	0.25	0.09	0.13	0.45	0.04	0.10
IEPOX-derived SOA tracers	**0.10**	**0.15**	**0.18**	**0.14**	**0.50**	**0.17**	**0.47**	**0.00**	**0.18**	**0.31**	**0.24**	**0.03**
2-methylerythritol	0.03	0.34	0.08	0.04	0.58	0.12	0.34	0.01	0.14	0.42	0.22	0.00
2-methylthreitol	0.04	0.32	0.03	0.01	0.43	0.17	0.25	0.03	0.14	0.54	0.21	0.01
(E)-2-methylbut-3-ene-1,2,4-triol	0.00	0.21	0.05	0.02	0.70	0.13	0.33	0.00	0.12	0.38	0.01	0.02
(Z)-2-methylbut-3-ene-1,2,4-triol	0.00	0.21	0.09	0.05	0.77	0.14	0.41	0.00	0.13	0.27	0.01	0.01
2-methylbut-3-ene-1,2,3-triol	0.54	0.00	0.12	0.13	0.00	0.01	0.18	0.04	0.06	0.00	0.33	0.02
IEPOX-derived OS	0.15	0.10	0.17	0.12	0.42	0.16	0.41	0.00	0.15	0.24	0.29	0.03
IEPOX dimer	0.00	0.00	0.00	0.00	0.00	0.00	0.00	0.00	0.00	0.00	0.00	0.00
Other isoprene SOA tracers												
GA sulfate												
$C_2H_3O_6S^-$	0.20	0.28	0.43	0.32	0.02	0.00	0.19	0.16	0.30	0.55	0.01	0.21
Methylglyoxal-derived OS												
$C_3H_5O_6S^-$	0.26	0.16	0.01	0.01	0.10	0.12	0.57	0.34	0.60	0.03	0.00	0.02
Isoprene-derived OSs												
$C_5H_7O_7S^-$	0.06	0.18	0.19	0.13	0.12	0.14	0.45	0.02	0.35	0.55	0.02	0.00
$C_5H_{10}NO_9S^-$	0.06	0.45	0.00	0.03	0.80	0.05	0.44	0.03	0.18	0.27	0.15	0.00
$C_5H_9N_2O_{11}S^-$ *	0.00	0.00	0.00	0.00	0.00	0.00	0.00	0.00	0.00	0.00	0.00	0.00
Hydroxyacetone-derived OS												
$C_2H_3O_5S^-$	0.49	0.01	0.10	0.20	0.13	0.05	0.44	0.24	0.11	0.06	0.29	0.10
Other tracer												
Levoglucosan	0.00	0.01	0.02	0.04	0.00	0.06	0.00	0.02	0.00	0.20	0.01	0.04

* Found only in 6 of 120 filters

The correlations in this table are positive.

Table S4-6. Correlation (r^2) of isoprene-derived SOA tracers and collocated measurements during intensive 4 and regular nighttime (8 pm – 7 am next day).

SOA tracers	CO	O_3	NO_x	NO_y	SO_2	NH_3	SO_4	NO_3	NH_4	OC	WSOC	pH
MAE/HMML-derived SOA tracers	**0.35**	**0.08**	**0.18**	**0.21**	**0.17**	**0.39**	**0.48**	**0.15**	**0.42**	**0.53**	**0.15**	**0.01**
2-methylglyceric acid	0.18	0.00	0.13	0.10	0.12	0.18	0.17	0.05	0.22	0.17	0.01	0.04
MAE-derived OS	0.35	0.14	0.15	0.17	0.11	0.32	0.51	0.17	0.36	0.58	0.20	0.00
IEPOX-derived SOA tracers	**0.10**	**0.10**	**0.02**	**0.03**	**0.08**	**0.10**	**0.37**	**0.02**	**0.30**	**0.27**	**0.15**	**0.00**
2-methylerythritol	0.02	0.12	0.00	0.00	0.05	0.01	0.23	0.00	0.20	0.14	0.09	0.00
2-methylthreitol	0.06	0.09	0.00	0.01	0.09	0.05	0.38	0.01	0.30	0.21	0.15	0.00
(E)-2-methylbut-3-ene-1,2,4-triol	0.09	0.08	0.02	0.03	0.10	0.10	0.35	0.03	0.28	0.26	0.11	0.00
(Z)-2-methylbut-3-ene-1,2,4-triol	0.07	0.07	0.01	0.02	0.10	0.07	0.32	0.02	0.27	0.22	0.08	0.00
2-methylbut-3-ene-1,2,3-triol	0.02	0.05	0.00	0.01	0.03	0.02	0.18	0.01	0.16	0.15	0.09	0.00
IEPOX-derived OS	0.17	0.10	0.08	0.10	0.01	0.16	0.27	0.03	0.21	0.31	0.14	0.01
IEPOX dimer	0.00	0.00	0.00	0.00	0.00	0.00	0.00	0.00	0.00	0.00	0.00	0.00
Other isoprene SOA tracers												
GA sulfate												
$C_2H_3O_6S^-$	0.12	0.22	0.02	0.04	0.04	0.14	0.28	0.01	0.15	0.31	0.26	0.01
Methylglyoxal-derived OS												
$C_3H_5O_6S^-$	0.16	0.05	0.03	0.05	0.00	0.18	0.19	0.01	0.17	0.26	0.24	0.00
Isoprene-derived OSs												
$C_5H_7O_7S^-$	0.12	0.15	0.01	0.02	0.02	0.09	0.22	0.01	0.11	0.17	0.12	0.00
$C_5H_{10}NO_9S^-$	0.20	0.00	0.11	0.12	0.08	0.21	0.39	0.18	0.33	0.30	0.09	0.00
$C_5H_9N_2O_{11}S^-$ *	0.00	0.00	0.00	0.00	0.00	0.00	0.00	0.00	0.00	0.00	0.00	0.00
Hydroxyacetone-derived OS												
$C_2H_3O_5S^-$	0.89	0.09	0.83	0.89	0.30	0.83	0.00	0.00	0.17	0.40	0.59	0.01
Other tracer												
Levoglucosan	0.23	0.00	0.22	0.24	0.08	0.21	0.13	0.01	0.18	0.25	0.11	0.00

* Found only in 6 of 120 filters

The correlations in this table are positive.

Table S4-7. Regression and correlation (r^2) analysis at the 95% confidence interval.

	Variables		Regression Statistics					*p-value*
	Y	x	Number of observations	Multiple r	r^2	Adjusted r^2	Standard error	
Nighttime: MAE/HMML-derived SOA vs $P[NO_3]$	MAE/HMML - derived SOA	$P[NO_3]$	40	0.7532	0.5673	0.5559	12.5098	2.05E-08
Nighttime: IEPOX-derived SOA vs $P[NO_3]$	IEPOX-derived SOA	$P[NO_3]$	40	0.5086	0.2587	0.2392	393.7399	8.05E-04
Regular day sampling: MAE/HMML-derived SOA vs O_3	MAE/HMML - derived SOA	O_3	30	0.8457	0.7153	0.7051	8.9517	4.00E-09
Daytime: 2-methyltetrols vs O_3	2-methyltetrols	O_3	64	0.3610	0.1303	0.1163	254.4175	3.39E-03
Intensive 3: MAE/HMML-derived SOA vs O_3	MAE/HMML - derived SOA	O_3	15	0.6844	0.4683	0.4274	18.3128	4.89E-03
Intensive 3: 2-methyltetrols vs O_3	2-methyltetrols	O_3	15	0.5844	0.3415	0.2908	259.0249	2.22E-02
MAE/HMML-derived SOA vs SO_4	MAE/HMML - derived SOA	SO_4	117	0.5779	0.3340	0.3282	15.8648	8.96E-12
IEPOX-derived SOA vs SO_4	IEPOX-derived SOA	SO_4	117	0.6027	0.3632	0.3577	310.4400	6.51E-13

CHAPTER V:
CONCLUSIONS

The characteristics and sources of NR-PM_1 were investigated at CTR (a rural site) during 2015/2016 using the Aerodyne ACSM for a 1-year sampling period. ME-2 analysis was applied to this yearlong dataset. HOA, BBOA, IEPOX-OA and 91Fac were constrained using an *a*-value approach to provide a priori information of target profiles to eliminate the low signal-to-noise of the ACSM data due to low concentrations of substances in rural air. To our knowledge, the SOA (IEPOX-OA and 91Fac) were constrained with ME-2 for the first time in this study. The comparison between ME-2 with and without SOA constrained yielded near-identical solutions, but provided the best correlations between resolved factors and collocated measurements, reference mass spectra and SOA tracers. Therefore, the SOA constrained is appropriate to apply in yearlong ME-2 analysis at CTR. The yearlong ME-2 results were divided into seasonal periods using the Old Farmer's Almanac to observe temporal variations. ACSM measurements demonstrated that NR-PM_1 was highest in summer (5.9 $\pm$ 2.9 μg m^{-3}) and lowest in winter 1.8 $\pm$ 1.3 μg m^{-3}). OA was the most dominant mass fraction (74% on average) of NR-PM_1. HOA was resolved at CTR in all seasons at comparable levels (0.14 – 0.41 μg m^{-3}), likely influenced by long-distance transportation. BBOA was highest in winter (0.39 $\pm$ 1.10 µg m^{-3}) and likely associated with the local prescribed burns. The detailed analysis of BBOA during prescribed burn events suggests that the ACSM can clearly resolve BBOA contributions to total OA mass. IEPOX-OA was highest (0.81 $\pm$ 0.50 µg m^{-3}) in summer and lowest (0.11 $\pm$

0.08 μg m^{-3}) in winter. The average diurnal profile of IEPOX-OA increased between 1 – 3 PM local time, consistent with the local formation of IEPOX-derived SOA. 91Fac had a similar diurnal profile to IEPOX-OA. The sum of LV-OOA and SV-OOA contributed the largest mass fraction (49% on average) of OA; however, it remains unclear where these factors are derived from.

The characteristics and sources of ambient NR-PM_1 were also investigated at JST (an urban site) during 2014/2015 using the Aerodyne ACSM for a 1-year sampling period. Seasonal PMF analyses clearly resolved sources of OA. Spring and fall datasets were separated into finer periods in order to carefully investigate non-homogeneous emission sources during transitioning periods (spring to summer versus fall to winter). ME-2 analysis was applied in some cases to aid in identifying OA subtypes. SOA components were constrained with ME-2 in yearlong analysis in order to investigate the presence of IEPOX-OA throughout the year, but SOA components were not constrained with ME-2 in seasonal analysis. ACSM measurements demonstrated that NR-PM_1 was highest in summer (16.7 $\pm$ 8.4 μg m^{-3}) and lowest in winter (8.0 $\pm$ 5.7 μg m^{-3}). OA was the most dominant mass fraction of NR-PM_1 in all seasons, averaging 55.5 – 73.6%. When PMF and ME-2 were both applied for source apportionment of OA, they yielded similar types and abundances of OA in colder seasons. However, ME-2 resolved more factors in warmer seasons, which could be influenced by mix sources and oxidation processes of OA. HOA from primary emissions was observed in all seasons, averaging 5 – 22% of total OA mass. BBOA was observed all year, with highest contributions to total OA in late fall (20%) and lowest in summer (2%). BBOA correlated well with levoglucosan (R = 0.78 – 0.88) in colder seasons, likely supporting that fresh BBOA can be more easily resolved during colder seasons. IEPOX-OA was observed in warmer seasons, averaging 25– 29% of the total OA mass. IEPOX-OA had a

consistent temporal variation with 91Fac OA. The highest contribution of IEPOX-OA (29%) to total OA mass was observed during summer. Moderate correlation between IEPOX-OA and aerosol pH in late spring (R = -0.67) and summer (R = -0.42) was observed from this study, suggesting an enhancement of IEPOX-OA under acidic conditions. The sum of LV-OOA and SV-OOA contributed the largest mass fraction (46 – 70%) of OA during all seasons; however, it remains unclear where these factors are derived from. Further work is needed to resolve whether known factors like BBOA, HOA or even the isoprene-derived SOA types (IEPOX-OA and 91Fac) eventually contribute to LV-OOA due to atmospheric aging or multiphase chemical processes.

HOA is higher at JST than CTR. BBOA is strongly correlated with levoglucosan at JST, which suggests fresh biomass burning influences, whereas weak correlations between BBOA and levoglucosan at CTR was observed and suggests the possible influences of aged biomass burning. Biogenic SOA factors (IEPOX-OA and 91Fac) are present at CTR and JST with higher concentrations in warmer seasons. It is clear that even in urban areas of the southeastern U.S., IEPOX-OA is major fraction of OA.

Chapter IV examined isoprene-derived SOA tracers in $PM_{2.5}$ samples collected at the BHM ground site during the 2013 SOAS campaign and revealed the complexity and potential multitude of chemical pathways leading to isoprene SOA formation. Isoprene-derived SOA tracers contributed up to ~20% (~7% on average) of total OM mass. IEPOX-derived SOA tracers were responsible for 92.45% of the total quantified isoprene SOA tracer mass, with 2-methyltetrols being the major component (47%). Differences in the relative contributions of IEPOX- and MAE/HMML-derived SOA tracers at BHM and the rural CTR and LRK sites (Budisulistiorini et al., 2015) during the 2013 SOAS campaign support suggestions that

anthropogenic emissions affect isoprene SOA formation. The correlation between 2-methyltetrols and O_3 at BHM is in accord with work by Riva et al. (2016), demonstrating a potential role of O_3 in generating isoprene-derived SOA in addition to the currently accepted IEPOX multiphase pathway.

At BHM, the statistical correlation of particulate SO_4^{2-} with IEPOX- ($r^2 = 0.36$, n = 117, $p < 0.05$) and MAE-derived SOA tracers ($r^2 = 0.33$, n = 117, $p < 0.05$) suggests that SO_4^{2-} plays a role in isoprene SOA formation. Although none of isoprene-derived SOA tracers correlated with gas-phase NO_x and NO_y, MAE/HMML-derived SOA tracers correlated with nighttime P[NO_3] ($r^2 = 0.57$, n = 40), indicating that NO_3 may affect local MAE/HMML-derived SOA formation. Nighttime P[NO_3] was weakly correlated ($r^2 = 0.26$, n = 40) with IEPOX-derived SOA tracers, lending some support to recent work by Schwantes et al. (2015) showing that isoprene + NO_3 yields INHEs that can by undergo reactive uptake to yield IEPOX tracers and contribute to IEPOX-derived SOA tracer loadings. The correlation of daytime O_3 with MAE/HMML-derived SOA and with 2-methyltetrols offers a new insight into influences on isoprene SOA formation. Notably, O_3 has not been reported to correlate with isoprene-derived SOA tracers in previous field studies (Lin et al., 2013b; Budisulistiorini et al., 2015). In this study, the strong correlation ($r^2 = 0.72$, n = 30) at the 95% confidence interval of O_3 with MAE/HMML-derived SOA tracers during the regular daytime sampling schedule indicates that O_3 likely oxidizes some isoprene to MACR as precursor of 2-MG at BHM. The weak correlation ($r^2 = 0.16$, n = 75) between O_3 and 2-methyltetrols early in the day as well as the better correlation ($r^2 = 0.34$, n = 15) later in the day (intensive 3, 4-7 PM local time) are consistent with recent laboratory studies demonstrating that 2-methyltetrols can be formed via isoprene ozonolysis in the presence of acidified sulfate aerosol (Riva et al., 2016).

Although urban O_3 and nighttime $P[NO_3]$ may have a role in local formation of MAE/HMML- and IEPOX-derived SOA tracers at BHM, this does not appear to explain the majority of the SOA tracers, since no significant day-night variation of the entire group of tracers was observed during the campaign. The majority of IEPOX-derived SOA was likely formed when isoprene SOA precursors (IEPOX) were generated upwind and transported to the BHM site. Wind directions during the campaign are consistent with long-range transport of isoprene SOA precursors from southwest of the site, which is covered by forested areas. The absence of a correlation of aerosol acidity with MAE/HMML- and IEPOX-derived SOA tracers indicates that acidity is not the limiting variable that controls formation of these compounds. Because the aerosols are acidic (campaign average aerosol pH of 1.8), the lack of correlation between SOA tracers and acidity may stem from the nearly invariant aerosol acidity throughout the campaign. Hence, despite laboratory studies demonstrating that aerosol acidity can enhance isoprene SOA formation (Surratt et al., 2007; Surratt et al., 2010; Lin et al., 2012), the effect may not be significant in the southeastern U.S. during the summer months due to the constant acidity of aerosols. Future work should examine how well current models can predict the isoprene SOA levels observed during this study, especially in the presence of fresh urban emissions. Furthermore, explicit models are now available to predict the isoprene SOA tracers measured here (McNeill et al., 2012; Pye et al., 2013), which will allow the modeling community to test the current parameterizations that are used to capture the enhancing effect of anthropogenic pollutants on isoprene-derived SOA formation. In addition, the significant correlations of isoprene-derived SOA tracers with $P[NO_3]$ observed during this study indicate a need to better understand nighttime chemistry of isoprene. Lastly, although O_3 appears to have an enhancing effect on isoprene-derived SOA tracers, the intermediates are unknown. Hydroperoxides

suggested by Riva et al. (2016) may be key, but chamber experiments with authentic precursors are needed to test this hypothesis.

REFERENCES

Aiken, A.C., Decarlo, P.F., Kroll, J.H., Worsnop, D.R., Huffman, J.A., Docherty, K.S., Ulbrich, I.M., Mohr, C., Kimmel, J.R., Sueper, D., 2008. O/C and OM/OC ratios of primary, secondary, and ambient organic aerosols with high-resolution time-of-flight aerosol mass spectrometry. Environ. Sci. Technol. 42, 4478-4485.

Aiken, A., Salcedo, D., Cubison, M.J., Huffman, J., DeCarlo, P., Ulbrich, I.M., Docherty, K.S., Sueper, D., Kimmel, J., Worsnop, D.R., 2009. Mexico City aerosol analysis during MILAGRO using high resolution aerosol mass spectrometry at the urban supersite (T0)– Part 1: Fine particle composition and organic source apportionment. Atmos. Chem. Phys.9, 6633-6653.

Alfarra, M.R., Coe, H., Allan, J.D., Bower, K.N., Boudries, H., Canagaratna, M.R., Jimenez, J.L., Jayne, J.T., Garforth, A.A., Li, S.M. and Worsnop, D.R., 2004. Characterization of urban and rural organic particulate in the lower Fraser valley using two aerodyne aerosol mass spectrometers. Atmos Environ, 38(34), 5745-5758.

Alfarra, M.R., Prevot, A.S., Szidat, S., Sandradewi, J., Weimer, S., Lanz, V.A., Schreiber, D., Mohr, M., Baltensperger, U., 2007. Identification of the mass spectral signature of organic aerosols from wood burning emissions. Environ. Sci. Technol. 41, 5770-5777.

Allan, J.D., Jimenez, J.L., Williams, P.I., Alfarra, M.R., Bower, K.N., Jayne, J.T., Coe, H., Worsnop, D.R., 2003. Quantitative sampling using an Aerodyne aerosol mass spectrometer 1. Techniques of data interpretation and error analysis. J. Geophys. Res. Atmos. 108, 4090.

Birch, M. E., and Cary, R. A., 1996. Elemental carbon-based method for occupational monitoring of particulate diesel exhaust: methodology and exposure issues, Analyst. 121, 1183-1190.

Blanchard, C. L., Hidy, G. M., Shaw, S., Baumann, K., and Edgerton, E. S., 2015. Effects of emission reductions on organic aerosol in the southeastern United States, Atmos. Chem. Phys. Discuss. 15, 17051-17092, doi:10.5194/acpd-15-17051-2015.

Boucher, O., Randall, D., Artaxo, P., Bretherton, C., Feingold, G., Forster, P., Kerminen, V.-M., Kondo, Y., Liao, H., and Lohmann, U., 2013. Clouds and aerosols, in: Climate change 2013: the physical science basis. Contribution of Working Group I to the Fifth Assessment Report of the Intergovernmental Panel on Climate Change, Cambridge University Press, 571-657.

Boyd, C.M., Sanchez, J., Xu, L., Eugene, A.J., Nah, T., Tuet, W.Y., Guzman, M.I., Ng, N.L., 2015. Secondary organic aerosol formation from the β-pinene+ NO 3 system: effect of humidity and peroxy radical fate. Atmos. Chem. Phys. 15(13), 7497-7522.

Budisulistiorini, S.H., Canagaratna, M.R., Croteau, P.L., Marth, W.J., Baumann, K., Edgerton, E.S., Shaw, S.L., Knipping, E.M., Worsnop, D.R., Jayne, J.T., 2013. Real-time continuous characterization of secondary organic aerosol derived from isoprene epoxydiols in downtown Atlanta, Georgia, using the Aerodyne Aerosol Chemical Speciation Monitor. Environ. Sci. Technol. 47, 5686-5694.

Budisulistiorini, S., Canagaratna, M.R., Croteau, P.L., Baumann, K., Edgerton, E.S., Kollman, M.S., Ng, N.L., Verma, V., Shaw, S.L., Knipping, E.M. and Worsnop, D.R., 2014. Intercomparison of an Aerosol Chemical Speciation Monitor (ACSM) with ambient fine aerosol measurements in downtown Atlanta, Georgia. Atmos. Meas. Tech. 7(7), 1929-1941.

Budisulistiorini, S.H., Li, X., Bairai, S.T., Renfro, J., Liu, Y., Liu, Y.J., McKinney, K.A., Martin, S.T., McNeill, V.F., Pye, H.O.T. and Nenes, A., 2015. Examining the effects of anthropogenic emissions on isoprene-derived secondary organic aerosol formation during the 2013 Southern Oxidant and Aerosol Study (SOAS) at the Look Rock, Tennessee ground site. Atmos. Chem. Phys. 15(15), 8871-8888.

Budisulistiorini, S. H., Baumann, K., Edgerton, E. S., Bairai, S. T., Mueller, S., Shaw, S. L., Knipping, E. M., Gold, A., and Surratt, J. D., 2016. Seasonal characterization of submicron aerosol chemical composition and organic aerosol sources in the southeastern United States: Atlanta, Georgia,and Look Rock, Tennessee. Atmos. Chem. Phys. 16, 5171-5189.

Canagaratna, M.R., Jayne, J.T., Ghertner, D.A., Herndon, S., Shi, Q., Jimenez, J.L., Silva, P.J., Williams, P., Lanni, T., Drewnick, F., 2004. Chase studies of particulate emissions from in-use New York City vehicles. Aerosol Sci. Tech. 38, 555-573.

Canagaratna, M., Jimenez, J., Kroll, J., Chen, Q., Kessler, S., Massoli, P., Hildebrandt Ruiz, L., Fortner, E., Williams, L., Wilson, K., 2015. Elemental ratio measurements of organic compounds using aerosol mass spectrometry: characterization, improved calibration, and implications. Atmos. Chem. Phys. 15, 253-272.

Canonaco, F., Crippa, M., Slowik, J.G., Baltensperger, U. and Prévôt, A.S.H., 2013. SoFi, an IGOR-based interface for the efficient use of the generalized multilinear engine (ME-2) for the source apportionment: ME-2 application to aerosol mass spectrometer data. Atmos. Meas. Tech. 6(12), 3649-3661.

Carlton, A., Wiedinmyer, C., and Kroll, J., 2009. A review of Secondary Organic Aerosol (SOA) formation from isoprene, Atmos. Chem. Phys. 9, 4987-5005.

Carlton, A. G., Bhave, P. V., Napelenok, S. L., Edney, E. O., Sarwar, G., Pinder, R. W., Pouliot, G. A., and Houyoux, M., 2010a. Model representation of secondary organic aerosol in CMAQv4. 7, Environ. Sci. Technol., 44, 8553-8560.

Carlton, A. G., Pinder, R. W., Bhave, P. V., and Pouliot, G. A., 2010b. To what extent can biogenic SOA be controlled?, Environ. Sci. Technol., 44, 3376-3380.

Chan, A., Chan, M., Surratt, J., Chhabra, P., Loza, C., Crounse, J., Yee, L., Flagan, R., Wennberg, P., and Seinfeld, J., 2010. Role of aldehyde chemistry and NOx concentrations in secondary organic aerosol formation, Atmos. Chem. Phys, 10, 7169-7188.

Chen, Q., Farmer, D.K., Rizzo, L.V., Pauliquevis, T., Kuwata, M., Karl, T.G., Guenther, A., Allan, J.D., Coe, H., Andreae, M.O. and Pöschl, U., 2015. Submicron particle mass concentrations and sources in the Amazonian wet season (AMAZE-08). Atmos. Chem. Phys, 15(7), 3687-3701.

Claeys, M., Graham, B., Vas, G., Wang, W., Vermeylen, R., Pashynska, V., Cafmeyer, J., Guyon, P., Andreae, M. O., and Artaxo, P., 2004. Formation of secondary organic aerosols through photooxidation of isoprene, Science. 303, 1173-1176.

Crippa, M., Canonaco, F., Lanz, V., Äijälä, M., Allan, J., Carbone, S., Capes, G., Ceburnis, D., Dall'Osto, M., Day, D., 2014. Organic aerosol components derived from 25 AMS data sets across Europe using a consistent ME-2 based source apportionment approach. Atmos. Chem. Phys. 14, 6159-6176.

DeCarlo, P., Ulbrich, I., Crounse, J., Foy, B.d., Dunlea, E., Aiken, A., Knapp, D., Weinheimer, A., Campos, T., Wennberg, P., 2010. Investigation of the sources and processing of organic aerosol over the Central Mexican Plateau from aircraft measurements during MILAGRO. Atmos. Chem. Phys. 10, 5257-5280.

Ding, X., Zheng, M., Yu, L., Zhang, X., Weber, R. J., Yan, B., Russell, A. G., Edgerton, E. S., and Wang, X., 2008. Spatial and seasonal trends in biogenic secondary organic aerosol tracers and water-soluble organic carbon in the southeastern United States, Environ. Sci. Technol. 42, 5171-5176.

Edgerton, E.S., Hartsell, B.E., Saylor, R.D., Jansen, J.J., Hansen, D.A., Hidy, G.M., 2006. The Southeastern Aerosol Research and Characterization Study, part 3: Continuous measurements of fine particulate matter mass and composition. J.Air Waste Manag. Assoc. 56, 1325-1341.

Edney, E. O., Kleindienst, T. E., Jaoui, M., Lewandowski, M., Offenberg, J. H., Wang, W., Claeys, M., 2005. Formation of 2-methyl tetrols and 2-methylglyceric acid in secondary organic aerosol from laboratory irradiated isoprene/NOX/SO 2/air mixtures and their detection in ambient PM 2.5 samples collected in the eastern United States. Atmos. Environ. 39(29), 5281-5289.

El-Zanan, H. S., Zielinska, B., Mazzoleni, L. R., and Hansen, D. A., 2009. Analytical determination of the aerosol organic mass-to-organic carbon ratio, J.Air Waste Manag.Assoc. 59, 58-69.

Emmons, L. K., Walters, S., Hess, P. G., Lamarque, J. F., Pfister, G. G., Fillmore, D., Granier, C., Guenther, A., Kinnison, D., Laepple, T., Orlando, J., Tie, X., Tyndall, G., Wiedinmyer, C., Baughcum, S. L., and Kloster, S., 2010. Description and evaluation of the Model for Ozone and Related chemical Tracers, version 4 (MOZART-4), Geosci. Model Dev., 3, 43-67, 10.5194/gmd-3-43-2010.

Foley, K., Roselle, S., Appel, K., Bhave, P., Pleim, J., Otte, T., Mathur, R., Sarwar, G., Young, J., and Gilliam, R., 2010. Incremental testing of the Community Multiscale Air Quality (CMAQ) modeling system version 4.7, Geosci. Model Dev. 3, 205-226.

Forster, P., Ramaswamy, V., Artaxo, P., Berntsen, T., Betts, R., Fahey, D.W., Haywood, J., Lean, J., Lowe, D.C., Myhre, G., 2007. Changes in atmospheric constituents and in radiative forcing. Chapter 2, Climate Change 2007. The Physical Science Basis.

Fountoukis, C., Nenes, A., 2007. ISORROPIA II: a computationally efficient thermodynamic equilibrium model for K^+– Ca^{2+}– Mg^{2+}– NH^{4+}– Na^+ –SO_4^{2-} – NO_3^- – Cl^- – H_2O aerosols. Atmos. Chem. Phys. 7, 4639-4659.

Fountoukis, C., Nenes, A., Sullivan, A., Weber, R., Reken, T. V., Fischer, M., Matias, E., Moya, M., Farmer, D., and Cohen, R., 2009. Thermodynamic characterization of Mexico City aerosol during MILAGRO 2006, Atmos. Chem. Phys, 9, 2141-2156.

Fröhlich, R., Cubison, M.J., Slowik, J.G., Bukowiecki, N., Canonaco, F., Croteau, P.L., Gysel, M., Henne, S., Herrmann, E., Jayne, J.T. and Steinbacher, M., 2015. Fourteen months of on-line measurements of the non-refractory submicron aerosol at the Jungfraujoch (3580 m asl)–chemical composition, origins and organic aerosol sources. Atmos. Chem. Phys. 15(19), 11373-11398.

Galloway, M. M., Chhabra, P. S., Chan, A. W. H., Surratt, J. D., Flagan, R. C., Seinfeld, J. H., and Keutsch, F. N., 2009. Glyoxal uptake on ammonium sulphate seed aerosol: reaction products and reversibility of uptake under dark and irradiated conditions, Atmos. Chem. Phys., 9, 3331-3345, 10.5194/acp-9-3331-2009.

Gómez-González, Y., Surratt, J. D., Cuyckens, F., Szmigielski, R., Vermeylen, R., Jaoui, M., Lewandowski, M., Offenberg, J. H., Kleindienst, T. E., Edney, E. O., Blockhuys, F., Van Alsenoy, C., Maenhaut, W., and Claeys, M., 2008. Characterization of organosulfates from the photooxidation of isoprene and unsaturated fatty acids in ambient aerosol using liquid chromatography/(-) electrosprayionization massspectrometry, J.MassSpectrom. 43,371–382.

Graham, R. A., and Johnston, H. S., 1978. The photochemistry of the nitrate radical and the kinetics of the nitrogen pentoxide-ozone system, J.Phys. Chem. 82, 254-268.

Grieshop, A., P., Logue, J., M., Donahue., J., M., and Robinson, A., L., 2009. Laboratory investigation of photochemical oxidation of organic aerosol from wood fires 1 : measurement and simulation of organic aerosol evolution, Atmos. Chem. Phys. 9, 1263-1277.

Groblicki, P.J., Wolff, G.T., Countess, R.J., 1981. Visibility-reducing species in the Denver "brown cloud"—I. Relationships between extinction and chemical composition. Atmos. Environ.15, 2473-2484.

Guenther, A., Karl, T., Harley, P., Wiedinmyer, C., Palmer, P. I., and Geron, C., 2006. Estimates of global terrestrial isoprene emissions using MEGAN (Model of Emissions of Gases and Aerosols from Nature). Atmos. Chem. Phys. 6, 3181-3210.

Guenther, A. B., Jiang, X., Heald, C. L., Sakulyanontvittaya, T., Duhl, T., Emmons, L. K., and Wang, X., 2012. The Model of Emissions of Gases and Aerosols from Nature version 2.1 (MEGAN2.1): an extended and updated framework for modeling biogenic emissions, Geosci Model Dev, 5, 1471-1492.

Guo, H., Xu, L., Bougiatioti, A., Cerully, K.M., Capps, S.L., Hite Jr, J., Carlton, A., Lee, S., Bergin, M., Ng, N., 2015. Fine-particle water and pH in the southeastern United States. Atmos. Chem. Phys. 15, 5211-5228.

Hallquist, M., Wenger, J.C., Baltensperger, U., Rudich, Y., Simpson, D., Claeys, M., Dommen, J., Donahue, N.M., George, C., Goldstein, A.H. and Hamilton, J.F., 2009. The formation, properties and impact of secondary organic aerosol: current and emerging issues. Atmos. Chem. Phys. 9(14), 5155-5236.

Hansen, D.A., Edgerton, E.S., Hartsell, B.E., Jansen, J.J., Kandasamy, N., Hidy, G.M., Blanchard, C.L., 2003. The Southeastern aerosol research and characterization study: part 1—overview. J.Air Waste Manag.Assoc. 53, 1460-1471.

Henze, D. K., Seinfeld, J. H., and Shindell, D. T., 2009. Inverse modeling and mapping US air quality influences of inorganic PM 2.5 precursor emissions using the adjoint of GEOS-Chem, Atmos. Chem. Phys., 9, 5877-5903.

Herron, J. T., and Huie, R. E., 1974. Rate constants for the reactions of ozone with ethene and propene, from 235.0 to 362.0. deg. K, J.Phys. Chem, 78, 2085-2088.

Hu, W. W., Campuzano-Jost, P., Palm, B. B., Day, D. A., Ortega, A. M., Hayes, P. L., Krechmer, J. E., Chen, Q., Kuwata, M., Liu, Y. J., de Sá, S. S., McKinney, K., Martin, S. T., Hu, M., Budisulistiorini, S. H., Riva, M., Surratt, J. D., St. Clair, J. M., Isaacman-Van Wertz, G., Yee, L. D., Goldstein, A. H., Carbone, S., Brito, J., Artaxo, P., de Gouw, J. A., Koss, A., Wisthaler, A., Mikoviny, T., Karl, T., Kaser, L., Jud, W., Hansel, A., Docherty, K. S., Alexander, M. L., Robinson, N. H., Coe, H., Allan, J. D., Canagaratna, M. R., Paulot, F., and Jimenez, J. L., 2015. Characterization of a real-time tracer for isoprene

epoxydiols-derived secondary organic aerosol (IEPOX-SOA) from aerosol mass spectrometer measurements. Atmos. Chem. Phys. 15, 11807-11833.

Huang, X.-F., Xue, L., Tian, X.-D., Shao, W.-W., Sun, T.-L., Gong, Z.-H., Ju, W.-W., Jiang, B., Hu, M., He, L.-Y., 2013. Highly time-resolved carbonaceous aerosol characterization in Yangtze River Delta of China: composition, mixing state and secondary formation. Atmos. Environ. 64, 200-207.

Inomata, Satoshi, Kei Sato, Jun Hirokawa, Yosuke Sakamoto, Hiroshi Tanimoto, Motonori Okumura, Susumu Tohno, and Takashi Imamura., 2014. Analysis of secondary organic aerosols from ozonolysis of isoprene by proton transfer reaction mass spectrometry. Atmos Environ., 97, 397-405.

Jimenez, J.L., Jayne, J.T., Shi, Q., Kolb, C.E., Worsnop, D.R., Yourshaw, I., Seinfeld, J.H., Flagan, R.C., Zhang, X., Smith, K.A. and Morris, J.W., 2003. Ambient aerosol sampling using the aerodyne aerosol mass spectrometer. J. Geophys Res. 108, 8425.

Kamens, R., Gery, M., Jeffries, H., Jackson, M., and Cole, E., 1982. Ozone-isoprene reactions: product formation and aerosol potential, Int. J. Chem. Kinet., 14, 955-975.

Kanakidou, M., Seinfeld, J.H., Pandis, S.N., Barnes, I., Dentener, F.J., Facchini, M.C., Van Dingenen, R., Ervens, B., Nenes, A., Nielsen, C.J., Swietlicki, E., Putaud, J.P., Balkanski, Y., Fuzzi, S., Horth, J., Moortgat, G.K., Winterhalter, R., Myhre, C.E.L., Tsigaridis, K., Vignati, E., Stephanou, E.G., Wilson, J., 2005. Organic aerosol and global climate modelling: a review. Atmos. Chem. Phys. 5, 1053-1123.

Karambelas, A., Pye, H. O., Budisulistiorini, S. H., Surratt, J. D., and Pinder, R. W.; 2014. Contribution of isoprene epoxydiol to urban organic aerosol: evidence from modeling and measurements, Environ. Sci. Technol. Lett., 1, 278-283.

Kessler, S.H., Smith, J.D., Che, D.L., Worsnop, D.R., Wilson, K.R., Kroll, J.H., 2010. Chemical sinks of organic aerosol: Kinetics and products of the heterogeneous oxidation of erythritol and levoglucosan. Envi. Sci. Tech. 44(18), 7005-7010.

Krechmer, J.E., Coggon, M.M., Massoli, P., Nguyen, T.B., Crounse, J.D., Hu, W., Day, D.A., Tyndall, G.S., Henze, D.K., Rivera-Rios, J.C. and Nowak, J.B., 2015. Formation of low volatility organic compounds and secondary organic aerosol from isoprene hydroxyhydroperoxide low-NO oxidation. Environ. Sci. Technol. 49(17), 10330-10339.

Kroll, J. H., Ng, N. L., Murphy, S. M., Flagan, R. C., and Seinfeld, J. H. 2005. Secondary organic aerosol formation from isoprene photooxidation under high-NOx conditions, Geophys. Res. Lett. 32.

Kroll, J. H., Ng, N. L., Murphy, S. M., Flagan, R. C., and Seinfeld, J. H., 2006. Secondary Organic Aerosol Formation from Isoprene Photooxidation, Environ. Sci. Technol. 40, 1869-1877, 10.1021/es0524301.

Lanz, V.A., Alfarra, M.R., Baltensperger, U., Buchmann, B., Hueglin, C., Szidat, S., Wehrli, M.N., Wacker, L., Weimer, S., Caseiro, A., 2007. Source attribution of submicron organic aerosols during wintertime inversions by advanced factor analysis of aerosol mass spectra. Environ. Sci. Technol. 42, 214-220.

Liao, J., Froyd, K. D., Murphy, D. M., Keutsch, F. N., Yu, G., Wennberg, P. O., St Clair, J. M., Crounse, J. D., Wisthaler, A., and Mikoviny, T., 2015. Airborne measurements of organosulfates over the continental US, J.Geophys Res A., 120, 2990-3005.

Lin, Y.-H., Zhang, Z., Docherty, K.S., Zhang, H., Budisulistiorini, S.H., Rubitschun, C.L., Shaw, S.L., Knipping, E.M., Edgerton, E.S., Kleindienst, T.E., 2012. Isoprene epoxydiols as precursors to secondary organic aerosol formation: acid-catalyzed reactive uptake studies with authentic compounds. Environ. Sci. Technol. 46, 250-258.

Lin, Y.-H., Zhang, H., Pye, H.O., Zhang, Z., Marth, W.J., Park, S., Arashiro, M., Cui, T., Budisulistiorini, S.H., Sexton, K.G., 2013. Epoxide as a precursor to secondary organic aerosol formation from isoprene photooxidation in the presence of nitrogen oxides. Proc. Natl. Acad. Sci. 110, 6718-6723.

Lin, Y.-H., Budisulistiorini, S. H., Chu, K., Siejack, R. A., Zhang, H., Riva, M., Zhang, Z., Gold, A., Kautzman, K. E., and Surratt, J. D., 2014. Light-absorbing oligomer formation in secondary organic aerosol from reactive uptake of isoprene epoxydiols, Environ. Sci. Technol. 48, 12012-12021.

Liu, P.S., Deng, R., Smith, K.A., Williams, L.R., Jayne, J.T., Canagaratna, M.R., Moore, K., Onasch, T.B., Worsnop, D.R. and Deshler, T., 2007. Transmission efficiency of an aerodynamic focusing lens system: Comparison of model calculations and laboratory measurements for the Aerodyne Aerosol Mass Spectrometer. Aerosol Sci. Tech. 41(8), 721-733.

Lopez-Hilfiker, F. D., Claudia Mohr, Emma L. D'Ambro, Anna Lutz, Theran P. Riedel, Cassandra J. Gaston, Siddharth Iyer et al., 2016. Molecular Composition and Volatility of Organic Aerosol in the Southeastern US: Implications for IEPOX Derived SOA. Environ. Sci. Technol., 50, no. 5, 2200-2209.

McNeill, V. F., Woo, J. L., Kim, D. D., Schwier, A. N., Wannell, N. J., Sumner, A. J., & Barakat, J. M., 2012. Aqueous-phase secondary organic aerosol and organosulfate formation in atmospheric aerosols: a modeling study, Environ. Sci. Technol., 46(15), 8075-8081.

McNeill, V. F., 2015. Aqueous organic chemistry in the atmosphere: Sources and chemical processing of organic aerosols. Environ. Sci. Technol., 49(3), 1237-1244.

Minguillón, M., Perron, N., Querol, X., Szidat, S., Fahrni, S., Alastuey, A., Jimenez, J., Mohr, C., Ortega, A., Day, D., 2011. Fossil versus contemporary sources of fine elemental and organic carbonaceous particulate matter during the DAURE campaign in Northeast Spain. Atmos. Chem. Phys. 11, 12067-12084.

Mohr, C., Huffman, J.A., Cubison, M.J., Aiken, A.C., Docherty, K.S., Kimmel, J.R., Ulbrich, I.M., Hannigan, M., Jimenez, J.L., 2009. Characterization of primary organic aerosol emissions from meat cooking, trash burning, and motor vehicles with high-resolution aerosol mass spectrometry and comparison with ambient and chamber observations. Environ. Sci. Technol. 43, 2443-2449.

Nemitz, E., Jimenez, J.L., Huffman, J.A., Ulbrich, I.M., Canagaratna, M.R., Worsnop, D.R., Guenther, A.B., 2008. An eddy-covariance system for the measurement of surface/atmosphere exchange fluxes of submicron aerosol chemical species—first application above an urban area. Aerosol Sci. Tech. 42, 636-657.

Nenes, A., Pandis, S.N., Pilinis, C., 1998. ISORROPIA: A new thermodynamic equilibrium model for multiphase multicomponent inorganic aerosols. Aqua. Geochem. 4, 123-152.

Ng, N., Canagaratna, M., Jimenez, J., Zhang, Q., Ulbrich, I., Worsnop, D., 2010. Real-time methods for estimating organic component mass concentrations from aerosol mass spectrometer data. Environ. Sci. Technol. 45, 910-916.

Ng, N.L., Herndon, S.C., Trimborn, A., Canagaratna, M.R., Croteau, P., Onasch, T.B., Sueper, D., Worsnop, D.R., Zhang, Q., Sun, Y., 2011. An Aerosol Chemical Speciation Monitor (ACSM) for routine monitoring of the composition and mass concentrations of ambient aerosol. Aerosol Sci. Tech. 45, 780-794.

Nguyen, Tran B., Adam P. Bateman, David L. Bones, Sergey A. Nizkorodov, Julia Laskin, and Alexander Laskin., 2010. High-resolution mass spectrometry analysis of secondary organic aerosol generated by ozonolysis of isoprene. Atmos. Environ. 44. 8, 1032-1042.

Nguyen, T.B., Coggon, M.M., Bates, K.H., Zhang, X., Schwantes, R.H., Schilling, K.A., Loza, C.L., Flagan, R.C., Wennberg, P.O. and Seinfeld, J.H., 2014. Organic aerosol formation from the reactive uptake of isoprene epoxydiols (IEPOX) onto non-acidified inorganic seeds. Atmos. Chem. Phys. 14(7), 3497-3510.

Nguyen, T. B., Bates, K. H., Crounse, J. D., Schwantes, R. H., Zhang, X., Kjaergaard, H. G., Surratt, J. D., Lin, P., Laskin, A., and Seinfeld, J. H., 2015. Mechanism of the hydroxyl radical oxidation of methacryloyl peroxynitrate (MPAN) and its pathway toward secondary organic aerosol formation in the atmosphere, PCCP.17, 17914-17926.

Nozière, B., Kalberer, M., Claeys, M., Allan, J., D'Anna, B., Decesari, S., Finessi, E., Glasius, M., Grgic, I., Hamilton, J.F. and Hoffmann, T., 2015. The molecular identification of organic compounds in the atmosphere: state of the art and challenges. Chem. Rev. 115(10), 3919-3983.

Olson, C. N., Galloway, M. M., Yu, G., Hedman, C. J., Lockett, M. R., Yoon, T., and Keutsch, F. N., 2011. Hydroxycarboxylic acid-derived organosulfates: synthesis, stability, and quantification in ambient aerosol. Environ. Sci. Technol., 45(15), 6468-6474.

Paatero, P. and Tapper, U., 1994. Positive matrix factorization: A non-negative factor model with optimal utilization of error estimates of data values. Environmetrics, 5(2), 111-126.

Parworth, C., Fast, J., Mei, F., Shippert, T., Sivaraman, C., Tilp, A., Watson, T. and Zhang, Q., 2015. Long-term measurements of submicrometer aerosol chemistry at the Southern Great Plains (SGP) using an Aerosol Chemical Speciation Monitor (ACSM). Atmos. Environ. 106, 43-55.

Paulot, F., Crounse, J. D., Kjaergaard, H. G., Kürten, A., Clair, J. M. S., Seinfeld, J. H., & Wennberg, P. O., 2009. Unexpected epoxide formation in the gas-phase photooxidation of isoprene. Science. 325(5941), 730-733.

Perraud, V., Bruns, E.A., Ezell, M.J., Johnson, S.N., Yu, Y., Alexander, M.L., Zelenyuk, A., Imre, D., Chang, W.L., Dabdub, D., 2012. Nonequilibrium atmospheric secondary organic aerosol formation and growth. Proc. Natl. Acad. Sci. 109, 2836-2841.

Petit, J.-E., Favez, O., Sciare, J., Crenn, V., Sarda-Estève, R., Bonnaire, N., Močnik, G., Dupont, J.-C., Haeffelin, M., Leoz-Garziandia, E., 2015. Two years of near real-time chemical composition of submicron aerosols in the region of Paris using an Aerosol Chemical Speciation Monitor (ACSM) and a multi-wavelength Aethalometer. Atmos. Chem. Phys. 15, 2985-3005.

Pope, C. A., and Dockery, D. W., 2006. Health Effects of Fine Particulate Air Pollution: Lines that Connect, J.Air Waste Manag. Assoc., 56, 709-742.

Pye, H.O., Pinder, R.W., Piletic, I.R., Xie, Y., Capps, S.L., Lin, Y.-H., Surratt, J.D., Zhang, Z., Gold, A., Luecken, D.J., 2013. Epoxide pathways improve model predictions of isoprene markers and reveal key role of acidity in aerosol formation. Environ. Sci. Technol. 47, 11056-11064.

Ramadan, Z., Eickhout, B., Song, X.-H., Buydens, L., Hopke, P.K., 2003. Comparison of positive matrix factorization and multilinear engine for the source apportionment of particulate pollutants. Chemo. Intel. Lab. Sys. 66, 15-28.

Rattanavaraha, W., Chu, K., Budisulistiorini, S.H., Riva, M., Lin, Y.H., Edgerton, E.S., Baumann, K., Shaw, S.L., Guo, H., King, L. Weber, R.J., 2016. Assessing the impact of anthropogenic pollution on isoprene-derived secondary organic aerosol formation in PM 2.5 collected from the Birmingham, Alabama, ground site during the 2013 Southern Oxidant and Aerosol Study. Atmos. Chem. Phys. 16(8), 4897-4914.

Reyes-Villegas, E., Green, D. C., Priestman, M., Canonaco, F., Coe, H., Prévôt, A. S. H., Allan, J. D., 2016. Organic Aerosol source apportionment in London 2013 with ME-2: exploring the solution space with annual and seasonal analysis, Atmos. Chem. Phys. Discuss., doi:10.5194/acp-2016-465, in review.

Riedel, T. P., Lin, Y.-H., Budisulistiorini, S. H., Gaston, C. J., Thornton, J. A., Zhang, Z., Vizuete, W., Gold, A., and Surratt, J. D., 2015. Heterogeneous reactions of isoprene-derived epoxides: reaction probabilities and molar secondary organic aerosol yield estimates, Environ. Sci. Technol. Lett. 2, 38-42.

Ripoll, A., Minguillón, M.C., Pey, J., Jimenez, J., Day, D.A., Sosedova, Y., Canonaco, F., Prévôt, A., Querol, X., Alastuey, A., 2015. Long-term real-time chemical characterization of submicron aerosols at Montsec (southern Pyrenees, 1570 m asl). Atmos. Chem. Phys. 15, 2935-2951.

Riva, M., Budisulistiorini, S. H., Zhang, Z., Gold, A., Surratt, J. D., 2016. Chemical characterization of secondary organic aerosol constituents from isoprene ozonolysis in the presence of acidic aerosol. Atmos. Environ. 130, 5-13.

Robinson, N.H., Hamilton, J.F., Allan, J.D., Langford, B., Oram, D.E., Chen, Q., Docherty, K., Farmer, D.K., Jimenez, J.L., Ward, M.W., Hewitt, C.N., Barley, M.H., Jenkin, M.E., Rickard, A.R., Martin, S.T., McFiggans, G., Coe, H., 2011. Evidence for a significant proportion of Secondary Organic Aerosol from isoprene above a maritime tropical forest. Atmos. Chem. Phys. 11, 1039-1050.

Ruthenburg, T. C., Perlin, P. C., Liu, V., McDade, C. E., and Dillner, A. M., 2014. Determination of organic matter and organic matter to organic carbon ratios by infrared spectroscopy with application to selected sites in the IMPROVE network, Atmos. Environ. 86, 47-57.

Schindelka, J., Iinuma, Y., Hoffmann, D., & Herrmann, H., 2013. Sulfate radical-initiated formation of isoprene-derived organosulfates in atmospheric aerosols. Fara. discuss., 165, 237-259.

Schneider, J., Weimer, S., Drewnick, F., Borrmann, S., Helas, G., Gwaze, P., Schmid, O., Andreae, M., Kirchner, U., 2006. Mass spectrometric analysis and aerodynamic properties of various types of combustion-related aerosol particles. Intern. J. Mass Spec. 258, 37-49.

Schwantes, R. H., Teng, A. P., Nguyen, T. B., Coggon, M. M., Crounse, J. D., St. Clair, J. M., Zhang, X., Schilling, K. A., Seinfeld, J. H., and Wennberg, P. O., 2015. Isoprene NO_3 Oxidation Products from the RO_2+ HO_2 Pathway, J.Phys. Chem. A.

Seinfeld, J.H. and Pankow, J.F., 2003. Organic atmospheric particulate material. Annu. Rev. Phys. Chem. 54(1), 121-140.

Shalamzari, M., Ryabtsova, O., Kahnt, A., Vermeylen, R., Hérent, M.-F., Quetin-Leclercq, J., Van der Veken, P., Maenhaut, W. and Claeys, M., 2013. Mass spectrometric characterization of organosulfates related to secondary organic aerosol from isoprene. Rapid Commun. Mass Spectrom., 27: 784–794. doi:10.1002/rcm.6511.

Simon, H., Bhave, P. V., Swall, J. L., Frank, N. H., and Malm, W. C., 2011. Determining the spatial and seasonal variability in OM/OC ratios across the US using multiple regression, Atmos. Chem. Phys., 11, 2933-2949, 10.5194/acp-11-2933-2011.

Slowik, J., Brook, J., Chang, R.-W., Evans, G., Hayden, K., Jeong, C.-H., Li, S.-M., Liggio, J., Liu, P., McGuire, M., 2011. Photochemical processing of organic aerosol at nearby continental sites: contrast between urban plumes and regional aerosol. Atmos. Chem. Phys. 11, 2991-3006.

Solomon, P., Baumann, K., Edgerton, E., Tanner, R., Eatough, D., Modey, W., Maring, H., Savoie, D., Natarajan, S., Meyer, M.B., 2003. Comparison of integrated samplers for mass and composition during the 1999 Atlanta Supersites project. J.Geo. Res. A. 108.

Starn, T., Shepson, P., Bertman, S., Riemer, D., Zika, R., and Olszyna, K., 1998. Nighttime isoprene chemistry at an urban-impacted forest site, J.Geo. Res. A. (1984–2012), 103, 22437-22447.

Stohl, A., Forster, C., Frank, A., Seibert, P., and Wotawa, G., 2005. Technical note: The Lagrangian particle dispersion model FLEXPART version 6.2, Atmos. Chem. Phys., 5, 2461-2474, 10.5194/acp-5-2461-2005.

Sun, Y.-L., Zhang, Q., Schwab, J., Demerjian, K., Chen, W.-N., Bae, M.-S., Hung, H.-M., Hogrefe, O., Frank, B., Rattigan, O., 2011. Characterization of the sources and processes of organic and inorganic aerosols in New York city with a high-resolution time-of-flight aerosol mass apectrometer. Atmos. Chem. Phys. 11, 1581-1602.

Sun, Y.L., Wang, Z.F., Du, W., Zhang, Q., Wang, Q.Q., Fu, P.Q., Pan, X.L., Li, J., Jayne, J. and Worsnop, D.R., 2015. Long-term real-time measurements of aerosol particle composition in Beijing, China: seasonal variations, meteorological effects, and source analysis. Atmos. Chem. Phys. 15(17), 10149-10165.

Surratt, J.D., Murphy, S.M., Kroll, J.H., Ng, N.L., Hildebrandt, L., Sorooshian, A., Szmigielski, R., Vermeylen, R., Maenhaut, W., Claeys, M., 2006. Chemical composition of secondary organic aerosol formed from the photooxidation of isoprene. J.Phys. Chem. A. 110, 9665-9690.

Surratt, J.D., Lewandowski, M., Offenberg, J.H., Jaoui, M., Kleindienst, T.E., Edney, E.O., Seinfeld, J.H., 2007. Effect of acidity on secondary organic aerosol formation from isoprene. Environ. Sci. Technol. 41, 5363-5369.

Surratt, J. D., Chan, A. W., Eddingsaas, N. C., Chan, M., Loza, C. L., Kwan, A. J., Hersey, S. P., Flagan, R. C., Wennberg, P. O., and Seinfeld, J. H., 2010. Reactive intermediates revealed in secondary organic aerosol formation from isoprene, Proc. Natl. Acad. Sci., 107, 6640-6645.

Tanner, R. L., Bairai, S. T., Olszyna, K. J., Valente, M. L., and Valente, R. J.: Diurnal patterns in PM 2.5 mass and composition at a background, complex terrain site, Atmos. Environ., 39, 3865-3875, 2005.

Tiitta, P., Vakkari, V., Croteau, P., Beukes, J.P., Van Zyl, P.G., Josipovic, M., Venter, A.D., Jaars, K., Pienaar, J.J., Ng, N.L. and Canagaratna, M.R., 2014. Chemical composition, main sources and temporal variability of PM 1 aerosols in southern African grassland. Atmos. Chem. Phys.14(4),1909-1927.

Ulbrich, I., Canagaratna, M., Zhang, Q., Worsnop, D., Jimenez, J., 2009. Interpretation of organic components from Positive Matrix Factorization of aerosol mass spectrometric data. Atmos. Chem. Phys. 9, 2891-2918.

Wang, W., Kourtchev, I., Graham, B., Cafmeyer, J., Maenhaut, W., and Claeys, M., 2005. Characterization of oxygenated derivatives of isoprene related to 2-methyltetrols in Amazonian aerosols using trimethylsilylation and gas chromatography/ion trap mass spectrometry, Rapid Commun. Mass Spectrom. 19, 1343-1351.

Watson, J.G., 2002. Visibility: Science and regulation. J.Air Waste Manage. Assoc. 52, 628-713.

Xu, L., Guo, H., Boyd, C.M., Klein, M., Bougiatioti, A., Cerully, K.M., Hite, J.R., Isaacman-VanWertz, G., Kreisberg, N.M., Knote, C., 2015. Effects of anthropogenic emissions on aerosol formation from isoprene and monoterpenes in the southeastern United States. Proc. Natl. Acad. Sci. 112, 37-42.

Zhang, Q., Alfarra, M.R., Worsnop, D.R., Allan, J.D., Coe, H., Canagaratna, M.R., Jimenez, J.L., 2005a. Deconvolution and quantification of hydrocarbon-like and oxygenated organic aerosols based on aerosol mass spectrometry. Environ. Sci. Technol. 39, 4938-4952.

Zhang, Q., Worsnop, D., Canagaratna, M., Jimenez, J., 2005b. Hydrocarbon-like and oxygenated organic aerosols in Pittsburgh: insights into sources and processes of organic aerosols. Atmos. Chem. Phys. 5, 3289-3311.

Zhang, Q., Jimenez, J., Canagaratna, M., Allan, J., Coe, H., Ulbrich, I., Alfarra, M., Takami, A., Middlebrook, A., Sun, Y., 2007. Ubiquity and dominance of oxygenated species in organic aerosols in anthropogenically-influenced Northern Hemisphere midlatitudes. Geo. Res. Lett. 34.

Zhang, Q., Jimenez, J.L., Canagaratna, M.R., Ulbrich, I.M., Ng, N.L., Worsnop, D.R., Sun, Y., 2011. Understanding atmospheric organic aerosols via factor analysis of aerosol mass spectrometry: a review. Analy. Bio. Chem. 401, 3045-3067.

Zhang, Z., Lin, Y.-H., Zhang, H., Surratt, J., Ball, L., Gold, A., 2012. Technical Note: Synthesis of isoprene atmospheric oxidation products: isomeric epoxydiols and the rearrangement products cis-and trans-3-methyl-3, 4-dihydroxytetrahydrofuran. Atmos. Chem. Phys.12, 8529-8535.